

ANNUAL REPORT 2007

INSTITUTE OF RADIOCHEMISTRY



Wissenschaftlich-Technische Berichte
FZD-489
2008

Annual Report 2007

Institute of Radiochemistry

Editor: Prof. Dr. G. Bernhard

**Editorial staff: Dr. H. Foerstendorf
Dr. A. Richter
Dr. K. Viehweger**



**Forschungszentrum
Dresden** Rossendorf

Contact

Forschungszentrum Dresden-Rossendorf
Institut für Radiochemie

Postal Address

P.O. Box 51 01 19
D-01314 Dresden
Germany

Address for visitors

Bautzner Landstraße (SW) 128
D-01328 Dresden
Germany

Phone: ++49 (0) 351 260 3210

Fax: ++49 (0) 351 260 3553

<http://www.fzd.de/FWR>

e-mail: contact.radiochemistry@fzd.de

This report is also available at <http://www.fzd.de/FWR>

Cover picture

Uranium(VI) sulfate complexes readily undergo electrochemical reduction to monomeric uranium(IV) complexes in aqueous solution. In situ-EXAFS spectroscopy and XRD were used to study the structure of the uranium(IV) sulfate in solution and solid state. The U(IV) monomers are coordinated by sulfate in monodentate and bidentate arrangement (see p. 11 and Hennig et al. (2008) *Inorg. Chem.*, in press; Web release date: February 2nd, 2008; DOI: 10.1021/ic701880h.).

Preface

The Institute of Radiochemistry (IRC), one of the six institutes of the Forschungszentrum Dresden-Rossendorf (FZD), contributes to the research program “Environment and Safety” and performs basic and applied research in the fields of radiochemistry and radioecology. Motivation and background of our research are environmental processes relevant for the installation of nuclear waste repositories, for remediation of uranium mining and milling sites, and for radioactive contaminations caused by nuclear accidents and fallout. Because of their high radiotoxicity and long half-life the actinides are of special interest. The research is focused on a better understanding of the chemical behavior of actinides in the environment on a molecular level.

Current topics of our research work are:

- Aquatic chemistry of actinides
- Actinides in bio-systems
- Interaction of actinides with solid phases

About 80 scientists, technicians, Ph.D. and diploma students are employed in the Institute of Radiochemistry. We accomplished many new scientific results in the past year which are presented in this annual report. Among them only few can be highlighted in this preface.

We were very successful in the determination of formation pathways and structure of various actinides with bio-relevant ligands. These results contribute to a better understanding of actinide speciation during the transfer from geo- into bio-systems, especially with respect to the chemical processes on the interfaces and in bio-fluids.

Further progress was achieved in understanding the interaction of actinides with different bacterial strains and algae. We strengthened our research about the use of bacterial S-layers as templates for technical applications.

Studies about interaction of U(VI) and U(IV) with different ligands improved our knowledge about the behavior of uranium in solutions. The structure of U(VI) and U(IV) complexes in sulfate-rich waters was resolved by a combination of electrochemical and spectroscopic methods. We got new insights in the coordination chemistry of neptunium in aqueous solutions on the basis of infrared spectroscopic measurements.

In cooperation with scientists from the University of Technology Dresden, we started investigations about the extraction behavior of actinides and lanthanides with new tripodal polyamines and the interaction of uranium and other heavy metals with milk proteins.

The migration of actinides can be influenced by formation of colloids. In this year we focused our research on the sorption of U(VI) on multi-wall carbon nanotubes and the formation of U(IV) colloids under different chemical conditions and their interaction with silicate.

Furthermore, we can report that our own radiochemical experimental facilities – Radiochemical Station on Rossendorf Beamline at ESRF (ROBL), Radiochemical Station on the Free Electron IR-laser of the Rossendorf accelerator ELBE (KB FELBE), and our different laser spectroscopic systems – are continuously working on a high quantitative and qualitative level. These methods are the basis for excellent scientific results of our researchers and all other external users.

I would like to thank the visitors, German and international ones, for their interest in our research and for their participation in the institute's seminars. We would also like to thank our scientific collaborators and the visiting scientists for coming to Dresden-Rossendorf in 2007 to share their knowledge and experience with us. We continue to strongly encourage the collaborations and visits by scientists in the future. Special thanks are due to the executive board of the Forschungszentrum Dresden-Rossendorf, the Ministry of Science and Arts of the State Saxony, the Federal Ministry of Education and Research, the Federal Ministry of Economics and Technology, the Deutsche Forschungsgemeinschaft, the European Commission, and other organizations for their support.



Prof. Dr. Gert Bernhard

Contents

SCIENTIFIC CONTRIBUTIONS (PART I)

Part I: Aquatic chemistry of actinides

| | |
|--|----|
| Structural determination of U(VI)-NO ₃ complexes in acetonitrile. A combination of UV-visible and EXAFS spectroscopies with DFT calculation..... | 9 |
| A. Ikeda, C. Hennig, A. Rossberg, S. Tsushima, A. C. Scheinost, G. Bernhard | |
| Determination of the radial distribution function of UO ₂ (CO ₃) ₃ ⁴⁻ by Monte Carlo simulation of EXAFS spectra..... | 10 |
| A. Rossberg, S. Tsushima, A. C. Scheinost | |
| The coordination of U(IV) sulfate in aqueous solution..... | 11 |
| C. Hennig, J. Claußner, A. Ikeda, K. Schmeide, V. Brendler, A. C. Scheinost, W. Kraus, F. Emmerling | |
| Stoichiometry and structure of uranyl(VI) hydroxo trimeric complex..... | 12 |
| S. Tsushima, A. Rossberg, A. Ikeda, K. Müller, A. C. Scheinost | |
| Determination of the fluorescence characteristics of a U(V)-carbonate species, [U(V)O ₂ (CO ₃) ₃] ⁵⁻ at low temperature..... | 13 |
| K. Großmann, T. Arnold, A. Ikeda, R. Steudtner G. Geipel | |
| Uranium speciation – From mineral phases to mineral waters..... | 14 |
| G. Geipel | |
| The U(VI) complexation with 2,3-dihydroxynaphthalene investigated using fs-TRLFS..... | 15 |
| H. Moll, M. Glorius, M. Eilzer, G. Geipel, G. Bernhard | |
| Complexation of uranium(IV) by citric acid studied by UV-vis spectroscopy..... | 16 |
| K. Schmeide, V. Brendler | |
| TRLFS and UV-Vis studies of the uranium(VI)–citrate system at low pH value..... | 17 |
| A. Günther, R. Steudtner, K. Schmeide | |
| Comparative EXAFS studies of the complexation of U(VI) with hydroxamic acids in aqueous solution and solids..... | 18 |
| M. Glorius, H. Moll, A. Rossberg, G. Bernhard | |
| Complexation studies of UO ₂ ²⁺ with benzenesulfonic acid..... | 19 |
| C. Joseph, K. Schmeide, G. Geipel, G. Bernhard | |
| Complexation studies of uranium(VI) with 4-hydroxybenzenesulfonic acid..... | 20 |
| B. Raditzky, G. Geipel, K. Schmeide, G. Bernhard | |
| Complexation of U(VI) with aromatic acids – A combined computational and experimental study..... | 21 |
| M. Glorius, A. Moritz, J. Wiebke, H. Moll | |
| Reduction of uranium(VI) by glucose..... | 22 |
| R. Steudtner, I. Gründig, G. Geipel | |
| Fluorescence properties of glucose at low temperatures..... | 23 |
| T. Arnold, K. Großmann | |
| The influence of the temperature on the band positions of luminescence spectra..... | 24 |
| C. Götz, G. Geipel | |
| Infrared spectroscopic investigation of Np species in aqueous solution..... | 25 |
| K. Müller, H. Foerstendorf, V. Brendler | |
| Complexation of Cm(III) with hydroxamic acids investigated by TRLFS..... | 26 |
| M. Glorius, H. Moll, G. Bernhard | |
| Curium(III) complexation with pyoverdins secreted by a groundwater strain of <i>Pseudomonas fluorescens</i> | 27 |
| H. Moll, A. Johnsson, K. Pedersen, G. Bernhard | |
| Complexation of Eu(III) with urea investigated by TRLFS..... | 28 |
| A. Heller, A. Barkleit, G. Bernhard | |
| New tripodal polyamines as potential extracting agents for lanthanides and actinides..... | 29 |
| H. B. Tanh Jeazet, M. Wenzel, Ke. Gloe, G. Geipel, G. Bernhard, K. Gloe | |

| | |
|---|----|
| Novel expanded circular helicates formed by copper(II) sulfate and bis-pyridylimine ligands..... | 30 |
| H. B. Tanh Jeazet, A. Jäger, O. Kataeva, Ke. Gloe, G. Geipel, G. Bernhard, B. Büchner, K. Gloe | |
| The architecture of self-assembled silver(I) complexes with bis-pyridylimine ligands: From coordination polymers to molecular boxes | 31 |
| H. B. Tanh Jeazet, A. Jäger, A. Heine, M. Wenzel, Ke. Gloe, G. Geipel, G. Bernhard, K. Gloe | |

SCIENTIFIC CONTRIBUTIONS (PART II)

Part II: Actinides in bio-systems

| | |
|--|----|
| Uranyl complexation with lipopolysaccharide investigated by TRLFS | 35 |
| A. Barkleit, H. Moll, G. Bernhard | |
| ATR-FTIR investigation of the complexation between U(VI) and phosvitin | 36 |
| B. Li, J. Raff, H. Foerstendorf | |
| The adsorption of uranium(VI) by milk proteins | 37 |
| H. Zänker, S. Weiß, K. Schreppel, K. Gloe, T. Henle, G. Bernhard | |
| Comparison of the binding of the uranyl ion to sodium caseinate and whey proteins | 38 |
| K. Schreppel, S. Weiß, H. Zänker, K. Gloe, T. Henle, G. Bernhard | |
| Characterization of the S-layer protein of <i>Bacillus spec. B12</i> | 39 |
| K. Pollmann, U. Weinert, K. Flemming, F. Lederer, T. Raff, J. Raff | |
| Comparison of three different methods for the detection of glycosylated S-layer proteins | 40 |
| U. Weinert, M. Vogel, J. Raff | |
| Spectroscopic and microscopic studies on the interactions of <i>Paenibacillus sp. JG-TB8</i> with U(VI) | 41 |
| T. Reitz, M. Merroun, S. Selenska-Pobell | |
| Comparison of the U (VI) complexation of different S-layers by means of ATR-FTIR spectroscopy | 42 |
| B. Li, U. Weinert, H. Foerstendorf, J. Raff | |
| Spectroscopic characterization of Pt complexation and nanocluster formation on <i>Bacillus sphaericus</i> JG-A12 S-layer..... | 43 |
| U. Jankowski, K. Fahmy, C. Hennig, S. Selenska-Pobell, M. Merroun | |
| Influence of uranium on oxygen consumption in multispecies biofilms assessed with microsensors | 44 |
| E. Krawczyk-Bärsch, T. Arnold, K. Großmann, A. Wobus, S. Hofmann | |
| New experimental setup for the determination of the differences between the chemical and radiological toxicity of actinides in algae | 45 |
| Ma. Vogel, A. Günther, J. Raff | |
| Intracellular uranium accumulation in cell suspensions of rape | 46 |
| K. Viehweger, G. Geipel | |

SCIENTIFIC CONTRIBUTIONS (PART III)

Part III: Interaction of actinides with solid phases

| | |
|---|----|
| ISDA – Integrated sorption database for interactions of chemotoxic and radioactive contaminants with mineral systems in geologic formations | 49 |
| A. Richter, V. Brendler, T. Brasser, C. Scherschel, M. Veerhoff, C. Klinger | |
| Simultaneous detection of coexisting U(VI) compounds by TRLFS | 50 |
| N. Baumann | |
| TRLFS fingerprinting of aluminosilicates..... | 51 |
| V. Brendler, A. Křepelová, N. Baumann, P. Trepte | |
| Modeling of the U(VI) sorption on mineral mixtures: Synthetic and natural sandstone | 52 |
| C. Nebelung, A. Richter, V. Brendler | |
| Cesium sorption on montmorillonite and bentonite: Sorption prediction and experiments | 53 |
| C. Nebelung, V. Brendler | |

| | |
|--|----|
| Selenite reduction by mackinawite, magnetite and siderite..... | 54 |
| A. C. Scheinost, H. Funke, R. Kirsch, L. Charlet | |
| Identification of selenium redox products by EXAFS wavelet analysis | 55 |
| H. Funke, A. C. Scheinost | |
| Sorption of uranium(VI) on multiwall carbon nanotubes..... | 56 |
| A. Schierz, H. Zänker, G. Bernhard | |
| Existence of colloidal uranium(IV) in near-neutral hydrogen carbonate solutions | 57 |
| I. Dreissig, S. Weiß, H. Zänker, G. Bernhard | |
| Investigations of the interaction of colloidal U(IV) with silicate | 58 |
| S. Weiß, H. Zänker | |
| Curium(III) speciation during the precipitation process of calcium carbonate..... | 59 |
| H. Moll, G. Bernhard | |
| Simultaneous determination of beta nuclides by liquid scintillation spectrometry | 60 |
| P. Jähnigen, C. Nebelung, G. Bernhard | |
| The problem of radioactivity in process waters of geothermal plants | 61 |
| S. Gester, V. Brendler, M. Köhler, D. Degering | |

PUBLICATIONS

| | |
|--|----|
| ▶ Articles (peer-reviewed)..... | 65 |
| ▶ Abstracts, proceedings, reports..... | 67 |
| ▶ Lectures, oral presentations | 70 |
| ▶ Posters | 74 |
| ▶ Awards, research fellowships | 77 |
| ▶ Patent..... | 77 |
| ▶ Theses..... | 77 |
| ▶ Diploma..... | 78 |
| ▶ Work placements..... | 78 |

SCIENTIFIC ACTIVITIES

| | |
|---|----|
| ▶ Seminars | 81 |
| ▶ Workshops (organized by the IRC)..... | 82 |
| ▶ Teaching activities..... | 83 |

PERSONNEL

85

ACKNOWLEDGEMENTS

89

INDEX OF AUTHORS

94

Aquatic chemistry of actinides

Structural determination of U(VI)-NO₃ complexes in acetonitrile. A combination of UV-visible and EXAFS spectroscopies with DFT calculation

A. Ikeda, C. Hennig, A. Rossberg, S. Tsushima, A. C. Scheinost, G. Bernhard

The complex structure of U(VI)-NO₃ species in acetonitrile was investigated by employing UV-visible and EXAFS spectroscopy combined with DFT calculations. This multi-technique approach was found to be very powerful for determining the complex structures of individual species in a mixed chemical system.

EXAFS spectroscopy is a very powerful tool to determine the complex structure of chemical species in solution. However, the information derived from EXAFS is only the total information about the measured chemical system. This means that EXAFS cannot distinguish individual species when several different species coexist in the same system. In order to solve this problem and expand this useful spectroscopic technique to mixed chemical systems, a multi-technique approach using UV-visible and EXAFS spectroscopy and quantum chemical calculations has been employed to determine the complex structure of individual species. Here we demonstrate one example, in which this multi-technique approach is applied to the investigation of the U(VI)-NO₃ complexation system in acetonitrile.

EXPERIMENTAL. Sample solutions were prepared by dissolving UO₂(ClO₄)·nH₂O and tetrabutylammonium nitrate in acetonitrile. The prepared samples were used both for UV-visible absorption and EXAFS measurements. The EXAFS measurements were performed at the Rossendorf Beamline BM20 (ROBL), ESRF. Density Functional Theory (DFT) calculations were performed in acetonitrile at the B3LYP level using *Gaussian 03* [1]. Further details have been described in [2].

RESULTS. UV-visible spectral titration experiment was carried out and the obtained data was treated by using the program Hyperquad [3]. Figure 1 represents the calculated speciation distribution. EXAFS measurements were also performed for the same samples used for the UV-visible titration experiment. Then, spectral isolation was carried out for the measured EXAFS spectra by Iterative Target Testing (ITT) factor analysis [4] based on the above-obtained speciation distribution information, in order to extract the pure EXAFS spectra of individual species from the measured spectral mixtures. The Fourier-transforms (FTs) of the isolated EXAFS spectra are shown in Fig. 2. It is clear that the FT peaks, which are related to the coordinated nitrate ions, become larger systematically as increasing the number of nitrate coordination. The EXAFS curve fits combined with the geometry optimization and the comparison of Gibbs free energy by DFT calculations have revealed that the pure solvated- and mononitrate species have a coordination number (CN) of 5 on the uranyl equatorial plane, forming [UO₂(H₂O)₅]²⁺ and [UO₂(H₂O)₃NO₃]⁺, respectively, while the di- and trinitrate species have a CN of 6, forming [UO₂(H₂O)₂(NO₃)₂]⁰ and [UO₂(NO₃)₃]⁻, respectively. Besides, nitrate ions coordinate to the uranyl ion always with a bidentate fashion. The complex structures proposed from these results are illustrated in Fig. 3. Hence, we can conclude from these results that the present multi-technique approach is a very promising method to identify

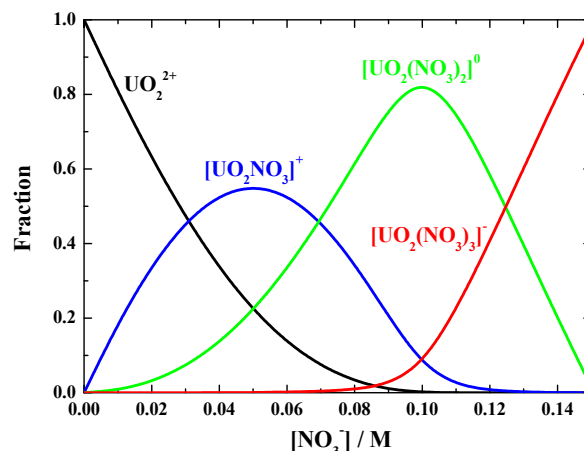


Fig. 1: Speciation distribution of U(VI)-NO₃ complexes in acetonitrile. ([U(VI)] = 0.05 M).

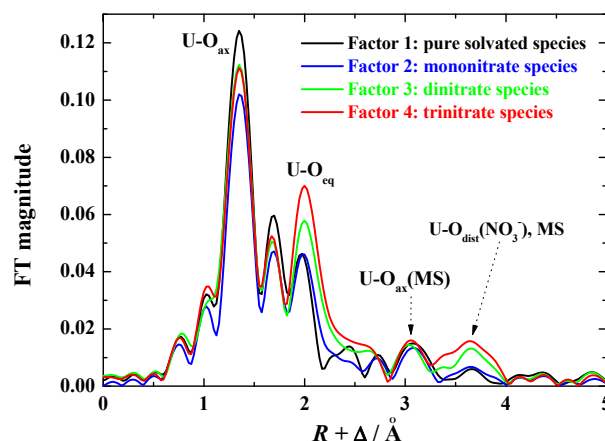


Fig. 2: Fourier-transforms of the isolated EXAFS spectra for individual solvated- and nitrate species of U(VI) in acetonitrile.

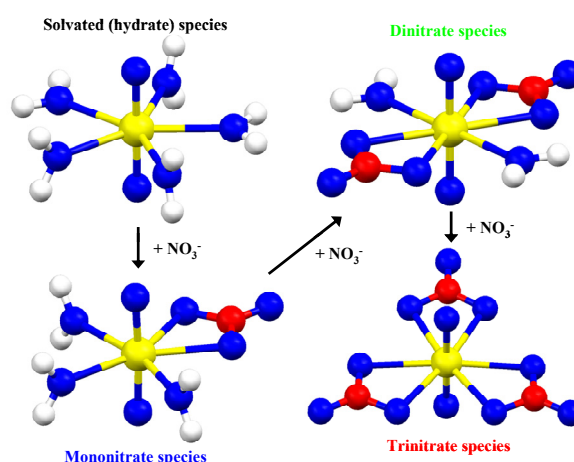


Fig. 3: Proposed complex structures of U(VI)-NO₃ species in acetonitrile.

the complex structure of individual species in the mixed chemical systems.

REFERENCES

- [1] Frisch, M. J. et al. (2004) *Gaussian 03*, Gaussian Inc.; Wallingford.
- [2] Ikeda, A. et al. (2008) *Anal. Chem.*, in press.
- [3] Gans, P. et al. (1996) *Talanta* **43**, 1739-1753.
- [4] Rossberg, A. et al. (2003) *Anal. Bioanal. Chem.* **376**, 631-638.

Determination of the radial distribution function of $\text{UO}_2(\text{CO}_3)_3^{4-}$ by Monte Carlo simulation of EXAFS spectra

A. Rossberg, S. Tsushima, A. C. Scheinost

The sampling time of an EXAFS photoelectron, typically $\sim 10^{-16}$ s, is much shorter than the atomic vibrational periods of $\sim 10^{-13}$ s. In this short time period, EXAFS probes a unidimensional canonical distribution of instantaneous interatomic distances r for each coordination shell, i.e. a snapshot of the radial pair distribution function (PDF) [1]. The PDF, which shows the probability of finding an atom in the range r to $r + dr$, contains information about the absorber-backscatterer distances, coordination numbers, the atomic disorder and the effective pair potential. All known fitting algorithms assume either Gaussian peak shapes or adapted peak shapes to model the *a priori* unknown PDF. If only single scattering contributes to the EXAFS signal, then up to now inverse algorithms or Monte Carlo (MC) based methods are able to produce the PDF without any *a priori* knowledge of the peak shape. In many environmental relevant systems, however, multiple scattering (MS) contributes to the EXAFS signal. Therefore, we have complemented our MC algorithm [2] by MS. Here we show the results for the aqueous $\text{UO}_2(\text{CO}_3)_3^{4-}$ complex.

EXPERIMENTAL. The EXAFS spectrum of aqueous $\text{UO}_2(\text{CO}_3)_3^{4-}$ was measured at room temperature in transmission mode. The standard data treatment was done with EXAFSPAK. The theoretical scattering phases and amplitudes were calculated with FEFF802 [3] using the XRD data of swartzite [4].

RESULTS. As initial structural MCTFA input, we used 1000 replicates of the $\text{UO}_2(\text{CO}_3)_3^{4-}$ complex structure calculated by density functional theory (DFT) (Fig. 1). The atoms were moved successively relative to the U-atom along a random vector with a random length between 0 – 0.1 Å. For each complex structure, the MS paths were determined and calculated with FEFF802. After each movement of one atom, the theoretical spectrum is compared with the experimental spectrum by using a normalized fit residual. We used the Metropolis algorithm for checking the validity of each atomic movement [5]. The structural parameter determined by MC, DFT and shell fitting are in good agreement (Tab. 1). The MC-derived PDFs show nearly Gaussian peak shapes (Fig. 2). Only the PDF of O_{eq} shows a more pronounced deviation from a Gaussian peak shape at ~ 2.55 Å (Fig. 2, arrow). Moreover, some of the O_{eq} atoms move to distances of about ~ 2.83 Å. Note that this peak in the PDF does not arise from the correlation with the C atoms at 2.89 Å.

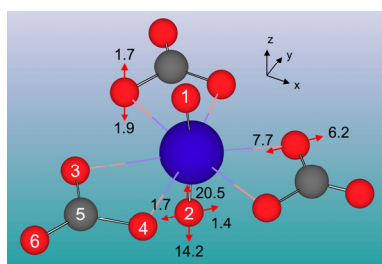


Fig. 1: Structure of $\text{UO}_2(\text{CO}_3)_3^{4-}$ complex and the energy required to move atoms by 0.1 Å (in kJ/mol.) as obtained by DFT.

Tab. 1: Structural parameters of the aqueous $\text{UO}_2(\text{CO}_3)_3^{4-}$ complex determined by DFT (a), MCTFA (b) and by shell fit (c).

| Shell | CN | R [Å] | σ^2 [Å ²] | σ_z [Å ²] |
|--------------------|-------------------|-------------------|------------------------------|------------------------------|
| U–O _{ax} | 2.0 ^a | 1.81 ^a | 0.0019 ^b | |
| | 1.9 ^b | 1.80 ^b | 0.0015 ^c | |
| | 2.0 ^{c*} | 1.80 ^c | | |
| U–O _{eq} | 6.0 ^a | 2.46 ^a | 0.0069 ^b | 0.0300 ^b |
| | 5.7 ^b | 2.46 ^b | 0.0061 ^c | |
| | 6.0 ^{c*} | 2.44 ^c | | |
| U–C | 3.0 ^a | 2.93 ^a | 0.0035 ^b | 0.0140 ^b |
| | 3.0 ^b | 2.89 ^b | 0.0034 ^c | |
| | 3.0 ^{c*} | 2.90 ^c | | |
| U–O _{dis} | 3.0 ^a | 4.19 ^a | 0.0066 ^b | |
| | 2.9 ^b | 4.17 ^b | 0.0022 ^c | |
| | 3.0 ^{c*} | 4.19 ^c | | |

CN: coordination number, R: atomic distance, σ : Debye-Waller factor, σ_z : Debye Waller factor in z-direction, *: constant during fit.

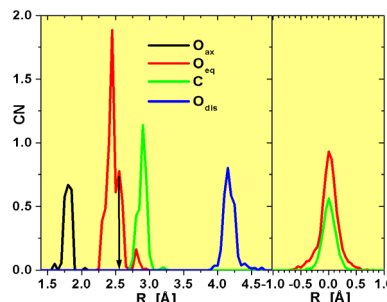


Fig. 2: PDF of the aqueous $\text{UO}_2(\text{CO}_3)_3^{4-}$. Left: radial PDF, right: PDF in z-direction (see Fig. 1). Arrow: see text.

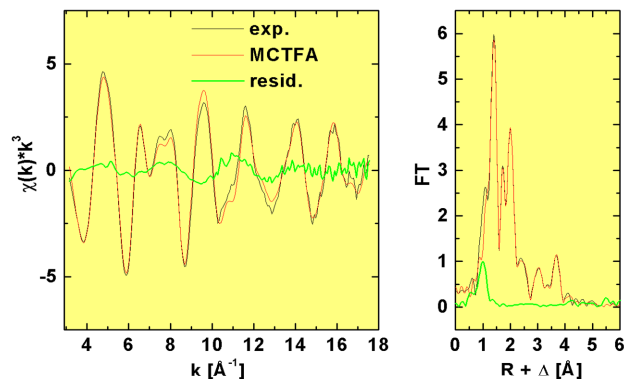


Fig. 3: Comparison of the experimental spectrum with the theoretical spectrum determined by MCTFA.

Due to the inclusion of MS as constraint, the disorder in z-direction can be studied. For O_{eq} the σ_z is ~ 5 times higher than the σ determined from the radial PDF (Tab. 1). This behavior is in line with the DFT-calculated energy (Fig. 1): The energy required to move an O_{eq} atom perpendicular to the equatorial plane (z-direction) is significantly smaller than the energy to move an O_{eq} atom in the equatorial plane along the U– O_{eq} bond.

REFERENCES

- [1] Dalba, G. et al. (1997) *J. Synchrotron Rad.* **4**, 243-255.
- [2] Rossberg, A. et al. (2005) *Anal. Bioanal. Chem.* **383**, 56-66.
- [3] Ankudinov, A.L. et al. (1998) *Phys. Rev. B* **58**, 7565-7576.
- [4] Mereiter, K. (1986) *Neues Jahrb. Mineral.-Mon. hefte* **11**, 481-492.
- [5] Winterer, M. (2000) *J. Appl. Phys.* **88**, 5635-5644.

The coordination of U(IV) sulfate in aqueous solution

C. Hennig, J. Claußner,¹ A. Ikeda, K. Schmeide, V. Brendler, A. C. Scheinost, W. Kraus,² F. Emmerling²

¹Department of Research Technology, FZD, Dresden, Germany; ²Federal Institute for Materials Research and Testing, Berlin, Germany

20 000 t of uranium has been recovered from the uranium mine Königstein in Saxony between 1967 and 1991. Sulfuric acid has been used to perform an *in situ* leaching of uranium ore, the so-called solution mining, where the acid has been injected directly into the ore deposit. A large amount of uranium containing sulfuric acid remained in pores of the concerned sandstone rocks. There is a fundamental requirement for the risk assessment concerning the contamination of drinking water aquifers with uranium and other toxic heavy-metals in this area.

Actually, the speciation and complex formation of U(IV) in sulfuric media is not well understood. The current NEA thermodynamic database reports only two sulfate species, USO_4^{2+} and $\text{U}(\text{SO}_4)_2(\text{aq})$ [1]. This was the motivation to develop a spectro-electrochemical cell (see cover picture) to perform *in situ* EXAFS measurements under anoxic conditions maintaining uranium in reduced oxidation state [2]. Figure 1 shows EXAFS spectra of 50 mM U(IV) in sulfate media with increasing $[\text{SO}_4]^{2-}$ at pH 1 [3].

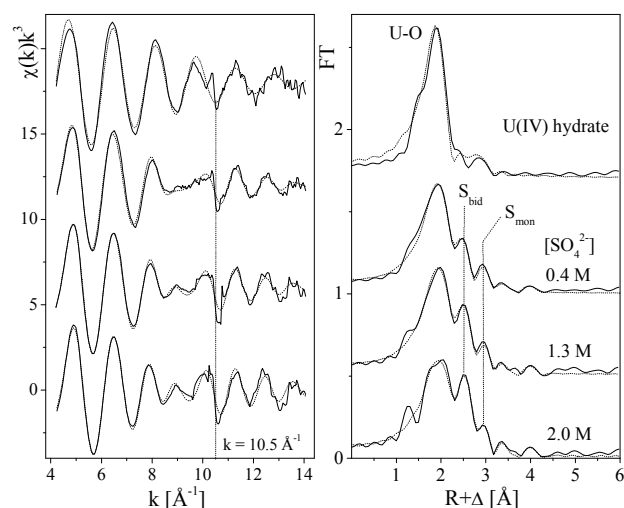


Fig. 1: U L_{3} -edge k^3 -weighted EXAFS data (left), and the corresponding Fourier-transforms (right) of U(IV) hydrate and sulfate species. The dotted line in the EXAFS spectrum indicates the $[2p4f]$ double-electron excitation [4].

The pure U(IV) hydrate is coordinated by nine water molecules with a U–O distance of 2.40 Å. The Fourier-transformed spectrum of U(IV) sulfate comprises two additional peaks at 3.08 Å and 3.67 Å, indicative of bidentate and monodentate sulfate groups, respectively [3,5]. Figure 2 shows the coordination number $N_{S_{bid}}$ and $N_{S_{mon}}$ as a function of the sulfate concentration. The coordination number $N_{S_{bid}}$ increases, whereas $N_{S_{mon}}$ decreases with increasing $[\text{SO}_4]^{2-}$. Hence, with increasing sulfate concentration the bidentate coordination becomes more dominant. In consequence, U(IV) in acidic solutions with high sulfate concentration can be coordinated by 4 and 5 SO_4^{2-} molecules. EXAFS can provide the coordination number and the type of sulfate coordination, but not the spatial arrangement of the ligands.

Therefore, in further experiments, where the pH value has been restricted to 1.5, single crystals have been grown from this solution with the aim to preserve the solution

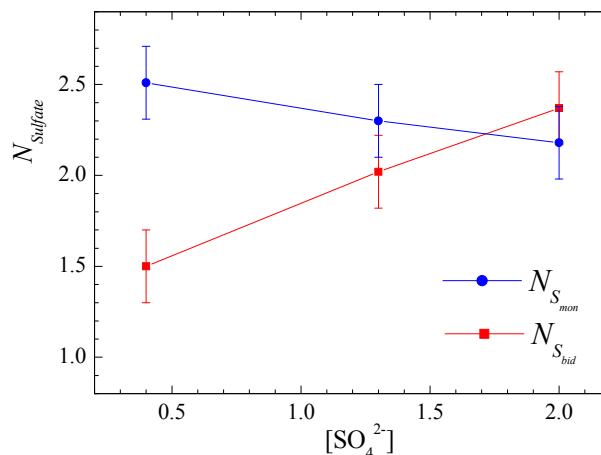


Fig. 2: U(IV) sulfate coordination at pH 1. Number of sulfur neighbors $N_{S_{bid}}$ and $N_{S_{mon}}$ as function of $[\text{SO}_4]^{2-}$.

species in the crystal structure [6]. The obtained compound $\text{Na}_{1.5}(\text{NH}_4)_{4.5}[\text{U}(\text{SO}_4)_5 \cdot \text{H}_2\text{O}] \cdot \text{H}_2\text{O}$, shown in Fig. 3, crystallizes in the triclinic space group P with two $[\text{U}(\text{SO}_4)_5 \cdot \text{H}_2\text{O}]^{6-}$ units in the unit cell. In this structure U(IV) is coordinated by 2 monodentate and 3 bidentate sulfate ions and one water molecule. This coordination may represent the coordination geometry of the solution species. The high coordination numbers of 4 and 5 sulfate groups which have been observed can count for a high solubility and stability of U(IV) sulfate in aqueous solution which may enforce the migration of uranium in a low pH environment.

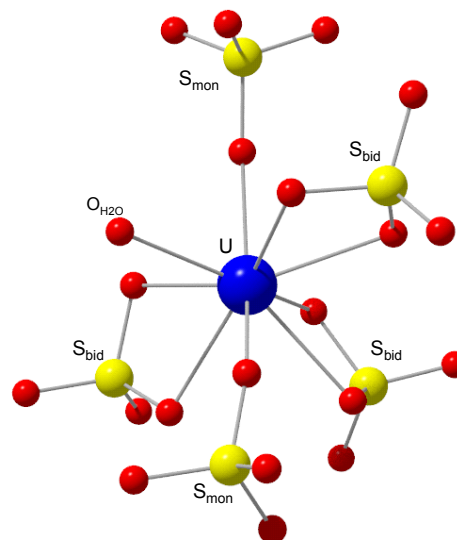


Fig. 3: Coordination of the $[\text{U}(\text{SO}_4)_5 \cdot \text{H}_2\text{O}]^{6-}$ unit.

REFERENCES

- [1] Guillaumont, R. et al. (2003) *Update on the chemical thermodynamics of U, Np, Pu, Am, Tc*, Elsevier, Amsterdam.
- [2] Hennig, C. et al. (2005) *Inorg. Chem.* **44**, 6655-6661.
- [3] Hennig, C. et al. (2007) *Inorg. Chem.* **46**, 5882-5892.
- [4] Hennig, C. et al. (2007) *Phys. Rev. B* **75**, 035120.
- [5] Hennig, C. et al. (2008) *Radiochim. Acta*, submitted.
- [6] Hennig, C. et al. (2008) *Inorg. Chem.*, in press (DOI: 10.1021/ic701880h).

Stoichiometry and structure of uranyl(VI) hydroxo trimeric complex

S. Tsushima, A. Rossberg, A. Ikeda, K. Müller, A. C. Scheinost

The structure and stoichiometry of uranyl (VI) hydroxo trimer complex was studied by both DFT calculations and EXAFS spectroscopy.

In this work, we applied both B3LYP hybrid density functional theory (DFT) calculations and EXAFS spectroscopy to solve the structures of uranyl(VI) hydroxo trimer complex in aqueous solution. One of the main challenges for EXAFS is to prepare solutions in which the target polymeric species are dominant, while in the uranium concentration range suitable for EXAFS measurements, there is always a mixing of several species. Therefore, uranium(VI) concentration and pH was optimized as far as possible based on thermodynamic calculations to reduce the number of coexisting species, while vibrational spectroscopy (FTIR) and UV-vis absorption spectroscopy was used to support the discrimination of coexisting species, in case they could not be avoided experimentally.

DFT STRUCTURES OF URANYL(VI) HYDROXO TRIMER COMPLEXES. Various possible isomers were considered in DFT calculations. All structures were optimized in the aqueous phase at the B3LYP level, and the energy here is the relative Gibbs energy in aqueous phase. In order to make all models stoichiometrically comparable, the Gibbs energy of a water molecule calculated at the same level of theory was added to the Gibbs energy of some of the models.

In Fig. 1, complex C1 was found to have the most stable geometry. This complex has the stoichiometry $(\text{UO}_2)_3(\mu_3\text{-O})(\text{OH})_3(\text{H}_2\text{O})_6^+$ with an oxo bridge in the center. $(\text{UO}_2)_3(\mu_3\text{-O})(\text{OH})_3^+$ and $(\text{UO}_2)_3(\text{OH})_5^+$ are indistinguishable by potentiometric titration because both result in loss of 5 protons. Hence, the thermodynamic data obtained for $(\text{UO}_2)_3(\text{OH})_5^+$ could be that of $(\text{UO}_2)_3(\mu_3\text{-O})(\text{OH})_3^+$. The structure of complex C1 obtained by DFT calculation is similar to that of $[(\text{UO}_2)_3(\text{O})(\text{OH})_3(\text{H}_2\text{O})_6]\text{NO}_3 \cdot 4\text{H}_2\text{O}$ [1,2]. In complex C1 (and in $[(\text{UO}_2)_3(\text{O})(\text{OH})_3(\text{H}_2\text{O})_6]\text{NO}_3 \cdot 4\text{H}_2\text{O}$) the average atomic distances are 3.834 Å (3.81 Å) for U–U, 1.788 Å (1.78 Å) for U–O_{ax}, 2.214 Å (2.21 Å) for U–O_{center}, 2.542 Å (2.45 Å) for U–O_{water}, and 2.391 Å (2.42 Å) for U–O_{OH}, hence all distances except for the U–O_{water} distance show very good agreement between the DFT-derived structure of the aqueous complex and the crystal structure of the solid.

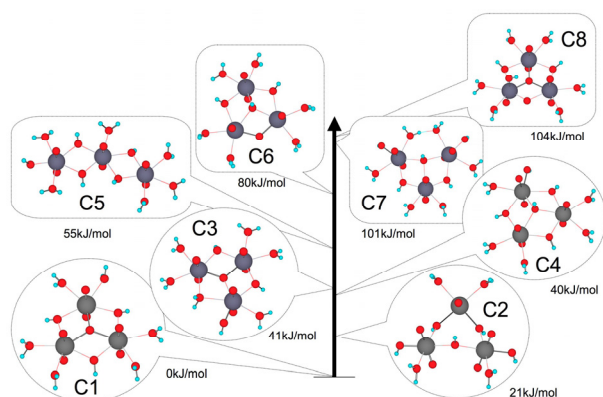


Fig. 1: The structures and relative Gibbs energies of various isomers of $(\text{UO}_2)_3(\text{OH})_5^+$ and its stoichiometric equivalent $(\text{UO}_2)_3(\mu_3\text{-O})(\text{OH})_3^+$ as obtained by B3LYP calculations.

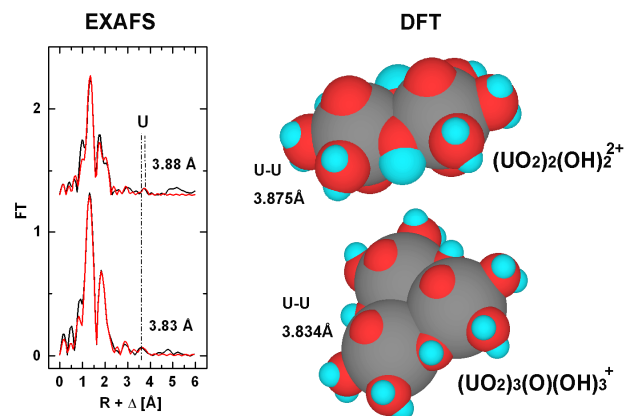


Fig. 2: Both EXAFS and DFT show that the trimer complex $(\text{UO}_2)_3(\text{O})(\text{OH})_3^+$ has the U–U distance which is significantly shorter than that of the dimer complex $(\text{UO}_2)_2(\text{OH})_2^{2+}$ confirming the presence of oxo bridging in the trimer complex.

EXAFS SPECTROSCOPY. The k^3 -weighted EXAFS spectra of the uranyl(VI) dimer and trimer samples and corresponding Fourier-transforms are shown in Fig. 2. According to the FTIR and UV-vis measurements, the samples contain mixtures of UO_2^{2+} , $(\text{UO}_2)_2(\text{OH})_2^{2+}$ and $(\text{UO}_2)_3(\text{OH})_5^+$. The formation of polynuclear complexes is confirmed by EXAFS for both samples which show U–U backscattering. By shell fitting we obtained a U–U radial distance of 3.82 – 3.83 Å, which is in line with the trimer complex $(\text{UO}_2)_3(\text{OH})_5^+$. For dimer sample, a weak FT peak at 3.71 Å could be fitted by 0.5 U atoms at a radial distance of 3.88 Å. The U–U distances found here show good agreement with crystal structure data and the DFT calculations. The averaged U–U distances are 3.875 Å (DFT) versus 3.88 Å (EXAFS) for $(\text{UO}_2)_2(\text{OH})_2^{2+}$, and 3.834 Å (DFT) versus 3.81 – 3.82 Å (EXAFS) for $(\text{UO}_2)_3(\mu_3\text{-O})(\text{OH})_3^+$. A shorter U–U distance of 3.81 – 3.82 Å in the trimeric complex suggests the presence of the central oxo bridging instead of the OH bridging. The U–U coordination number is less than 1 and hence too small for the dimer and the trimer. This is related to the fact that the sample was a mixture of monomeric and polymeric species. In addition, the CN obtained from EXAFS always have an error of 10 ~ 20 %. Clearly, the coordination numbers obtained from EXAFS do not help to identify the polymer structures, while the U–U distances give reliable results.

To summarize, the EXAFS spectra of two uranyl(VI) samples show two distinct U–U distances of 3.88 Å and 3.81 ~ 3.82 Å which correspond to $(\text{UO}_2)_2(\text{OH})_2^{2+}$ and $(\text{UO}_2)_3(\mu_3\text{-O})(\text{OH})_3^+$, respectively. These distances agree well with the results of the DFT calculations. Our combined DFT and EXAFS results confirm that $(\text{UO}_2)_3(\text{OH})_5^+$ in aqueous solution exists as $(\text{UO}_2)_3(\mu_3\text{-O})(\text{OH})_3^+$ with an oxo central bridging.

ACKNOWLEDGEMENTS. The authors acknowledge generous allocation of computation time at the Center for Information Services and High Performance Computing (ZIH), Dresden University of Technology.

REFERENCES

- [1] Åberg, M. (1970) *Acta Chem. Scand.* **24**, 290.
- [2] Åberg, M. (1969) *Acta Chem. Scand.* **23**, 791.

Determination of the fluorescence characteristics of a U(V)-carbonate species, $[\text{U}(\text{V})\text{O}_2(\text{CO}_3)_3]^{5-}$ at low temperature

K. Großmann, T. Arnold, A. Ikeda, R. Steudtner G. Geipel

The fluorescence of the only stable aqueous uranyl(V) carbonate complex $[\text{U}(\text{V})\text{O}_2(\text{CO}_3)_3]^{5-}$ was determined in a frozen solution of 0.5 mM uranium and 1.5 M Na_2CO_3 at pH 11.8 at 153 K (-120°C). The U(V)/U(VI) ratio in the investigated sample was 96/4 (M/M). Two different wavelengths of 255 nm and 408 nm, respectively were used as excitation wavelength to study the fluorescence properties of the U(V)-carbonate species, $[\text{U}(\text{V})\text{O}_2(\text{CO}_3)_3]^{5-}$. The resulting U(V) fluorescence emission bands were detected for both excitation wavelengths between 380 to 440 nm with a maxima at 405 nm (excitation with 255 nm) and 414 nm (excitation with 408 nm), respectively.

EXPERIMENTAL. A starting material of $\text{Na}_4[\text{UO}_2(\text{CO}_3)_3]$ was synthesized from $\text{UO}_2(\text{NO}_3)_2 \cdot 6\text{H}_2\text{O}$ according to the procedure reported previously [1]. This uranyl(VI) carbonate compound was dissolved in 1.5 M Na_2CO_3 solution (pH = 11.8) to give a concentration of 0.5 mM U(VI). Then bulk electrolysis was performed to reduce the prepared U(VI) solution to U(V) by using Pt mesh working- and counter electrodes and a Ag/AgCl reference electrode [2]. UV/Vis absorption measurements were carried out to confirm the oxidation states of U in the sample solution. The spectral change before and after the electrolysis was identical with those observed on the previously-reported U(V) preparation [2,3], suggesting that U(VI) was successfully reduced to U(V). The U(V)/U(VI) ratio in the reduced sample was estimated to be 96/4 (M/M) from the absorbances at 448 nm by assuming that the U(V) species has no absorbance at this wavelength. The U(V) solution was excited from the ground state to the excited state with a 255 nm and a 408 nm pulsed laser beam, obtained from a pulsed (10 Hz) OPO laser. The pulse power was typically 1 mJ per pulse and the pulse width was about 5 ns. The emission spectra were measured using an intensified CCD camera and a spectrograph, respectively.

RESULTS. Figure 1 shows the fluorescence emission spectra of the frozen $[\text{U}(\text{V})\text{O}_2(\text{CO}_3)_3]^{5-}$ species at the excitation wavelengths of 255 nm and 408 nm. It clearly demonstrates, that the $[\text{U}(\text{V})\text{O}_2(\text{CO}_3)_3]^{5-}$ species can be excited with both wavelengths (255 nm and 408 nm). The different excitation wavelength leads to two similar but not identical emission signals. The emission signals show a maxima at 405 nm for the excitation with 255 nm and 414 nm for the excitation with 408 nm, respectively. However the extinction coefficient was much higher and the spectra was better structured for the 255 nm excitation wavelength in comparison with the 408 nm excitation wavelength. Comparing the U(V) fluorescence data in this study with results published by Steudtner et al. [4] for a meta-stable U(V) solution at pH 2.4 revealed that the fluorescence emission peak maxima for the U(V) carbonate solution is shifted to lower wavelengths (see Fig.2). Steudtner et al. found a peak maximum at 440 nm. The peak maximum for the U(V) carbonate solution in our study was detected at 405 nm and 414 nm. This is in agreement with kryogenic laser fluorescence investigations of uranium(V) carbonates [5]. In U(VI) systems the

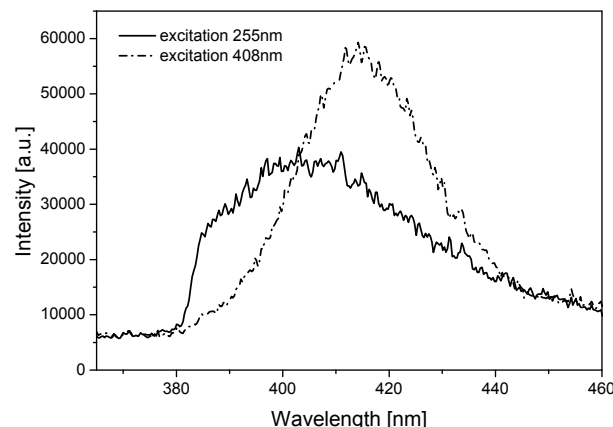


Fig. 1: Fluorescence emission spectra of the $[\text{UO}_2(\text{CO}_3)_3]^{5-}$ species at excitation with 255 nm and 408 nm at 153 K.

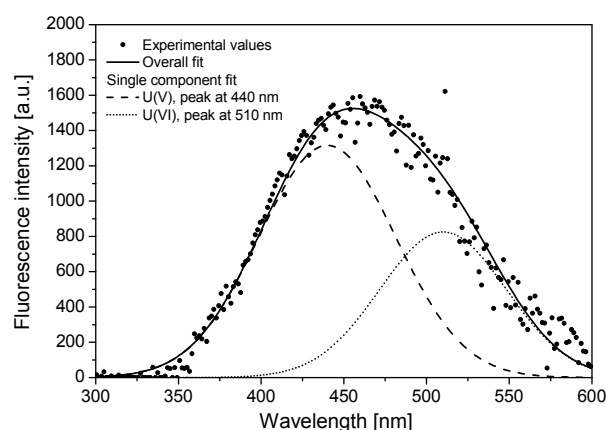


Fig. 2: Deconvoluted fluorescence emission spectrum of U(V) at excitation with 255 nm at 298 K [4].

fluorescence emission bands for U(VI) carbonates are significantly shifted to lower wavelength (by approximately 15 nm) compared to U(VI) hydrolysis species or U(VI) phosphates at room temperature (RT). Fluorescence studies of organic matter under cryogenic conditions show also a blue shift of the emission maxima when compared to fluorescence studies at RT [6].

ACKNOWLEDGMENTS. We thank the German Research Council (DFG) for financial support (project no. AR 584/1-1 and HE 2297/2-1).

REFERENCES

- [1] Chernyaev, I. I. (1986) *Complex Compounds of Uranium*, Israel Program for Scientific Translations, Jerusalem, Israel.
- [2] Ikeda, A. et al. (2007) *Inorg. Chem.* **46**, 4212-4219.
- [3] Mizuoka, K. et al. (2005) *Inorg. Chem.* **44**, 4472-4474.
- [4] Steudtner, R. et al. (2006) *Inorg. Chem. Comm.* **9**, 939-941.
- [5] Wang et al. (2004) *Environ. Sci. Technol.* **38**, 5591-5597
- [6] Zelent, B. et al. (2007) *J. Fluoresc.* **17**, 37-42.

Uranium speciation – From mineral phases to mineral waters

G. Geipel

Uranium speciation studies have been performed in environmental aquatic samples. Since the important carbonate species do not show any luminescence properties at ambient temperatures a cryogenic technique has been used.

Uranium ammunition can generate locally high concentrations of uranium in the environment. Weathering processes of the uranium metal lead in a first step to the formation of uranium minerals [1]. Depending on the composition of the soil, the formation of several types of minerals can be estimated. Especially the content of phosphate from fertilizers and the aluminum from soil components are involved in the mineral formation.

By use of time-resolved laser-induced fluorescence spectroscopy (TRLFS), the mineral type can be determined without any destruction. A large database of luminescence spectra, obtained from uranium minerals of the collection of the Technical University Mining Academy Freiberg, enables us to identify the formed uranium mineral [2]. In the experiment, described in [1], we found that mainly the mineral sabugalite was formed. Other experiments with pure calcium and phosphate containing solution lead to the formation of the mineral meta-autunite [3].

In a second step the formed minerals than undergo further weathering processes, forming dissolved uranium species. In the former uranium mining areas of eastern Germany, we could discover a new dissolved uranium carbonate species [4,5]. However, the uranium concentration of about 2 mg/L in these mining related waters is relatively high. Nevertheless, the carbonate and calcium concentration are high enough to form a very stable dicalcium-uranyl-tricarbonate species. This species is of great importance, as its existence explains the uranium migration at the Hanford site [6].

In addition to the calcium species, it can be stated that also the other alkaline earth elements form this type of alkaline earth uranyl carbonate species [7,8-10].

Following the uranium migration in the soil, we could detect in the experiments that mainly carbonate species are formed. The pure carbonate species do not show any luminescence properties at room temperature. Therefore, the samples have to be frozen to temperatures below 220 K [11], in order to minimize the dynamic quench effect of the carbonate anion. This increases also the luminescence intensity and the luminescence lifetime of all carbonate containing species.

Nevertheless, in one case of the soil experiment also hydroxo species were found. This may be connected to a non-equilibrium with atmospheric CO₂ in this column.

Following the possible transport of uranium under environmental conditions, we may start with the weathering of uranium compounds in the soil or in a mining waste rock pile. The seepage water contains about 2 mg/L uranium, and the speciation is mainly influenced by the formation of the dicalcium-uranyl-tricarbonate species. The input of these seepage water leads to a dilution of the uranium by about three orders of magnitude. Using the cryogenic technique in TRLFS [12], we could also determine the uranium speciation in the river water nearby the former uranium mining area. The uranium concentration was

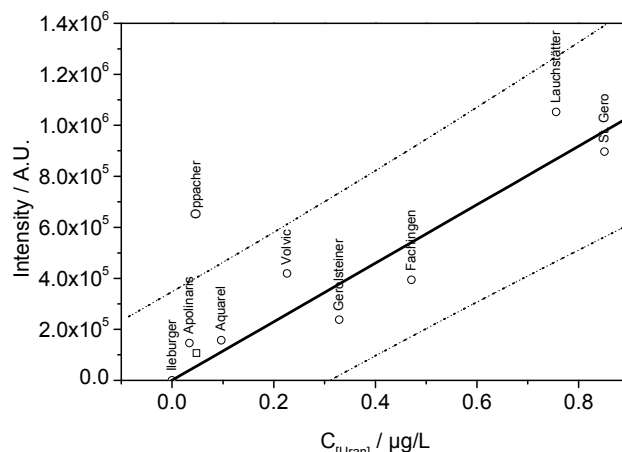


Fig. 1: Dependence of the luminescence intensity of table waters as function of the uranium concentration.

about 2 µg/L uranium and in the river water mainly uranyl-tricarbonate species are formed.

Additionally, uranium can migrate down to the groundwater. In this case, uranium may come back to the food chain by the production of mineral waters. We have studied the uranium speciation in several German mineral waters with uranium concentrations between 50 ng/L and 5 µg/L. In agreement with speciation calculations, the sparkling and the calcium poor waters contain uranium as uranyl-tricarbonate species, whereas the non-sparkling waters – if they are rich in calcium – clearly show the formation of the dicalcium-uranyl-tricarbonate species. Using cryogenic TRLFS, the detection limit for uranium species was estimated to be about 50 ng/L. Figure 1 shows the dependence of the luminescence intensity of uranylcarbonate species of several common table waters as a function of the uranium concentration determined by ICP-MS. Additionally, a Hungarian medicinal water shows a uranium concentration of 150 µg/L. Due to the high mineralization of this water, also the dicalcium-uranyl-tricarbonate species was determined.

In summary, it can be concluded that the most natural waters contain uranium as tri-carbonate species. According to investigations of Carriere [13], these uranium species are less hazardous than phosphate and citrate species.

REFERENCES

- [1] Schimmack, W. et al. (2007) *Radiat. Environ. Biophys.* **46**, 221–227.
- [2] Geipel, G. et al. (2000) *Radiochim. Acta* **88**, 757–759.
- [3] Baumann, N. et al. (2006) *Sci. Total Environ.* **366**, 905–909.
- [4] Bernhard, G. et al. (1998) *J. Alloy. Compd.* **201**, 271–273.
- [5] Bernhard, G. et al. (2001) *Radiochim. Acta* **89**, 511–518.
- [6] Wang, Z. et al. (2004) *Environ. Sci. Technol.* **38**, 5591–5597.
- [7] Geipel, G. (2005) *Effects of Mg, Ca, Sr and Ba on geochemical uranyl speciation*, in: PACIFICHEM 2005, Honolulu.
- [8] Geipel, G. et al. (2006) *Geochim. Cosmochim. Acta* **70**, A196.
- [9] Dong, W.M. et al. (2006) *Environ. Sci. Technol.* **40**, 4689–4695.
- [10] Geipel, G. et al. (2008) *Spectrosc. Acta Pt. A-Molec. Biomolec. Spectr.*, in press.
- [11] Geipel, G. (2006) in: *Handbook of Applied Solid State Spectroscopy*, p. 577–593, Springer, Heidelberg.
- [12] Bernhard, G. et al. (2007) *Vom Wasser* **105**, 7–10.
- [13] Carriere, M. et al., (2004) *Chem. Res. Toxicol.* **17**, 446–452.

The U(VI) complexation with 2,3-dihydroxynaphthalene investigated using fs-TRLFS

H. Moll, M. Glorius, M. Eilzer, G. Geipel, G. Bernhard

The complexation of the uranyl ion (UO_2^{2+}) in the aqueous 2,3-dihydroxynaphthalene system was investigated using time-resolved laser-induced fluorescence spectroscopy with ultrafast pulses (fs-TRLFS) between pH 2 and 12. Two complexes, a 1 : 1 and a 1 : 2, were found with averaged stability constants of $\log \beta_{111} = 20.5 \pm 1.4$ and $\log \beta_{121} = 29.9 \pm 0.5$, respectively.

A special group of natural bioligands with a high potential to bind actinides are siderophores of the pyoverdinin-type [1-3]. Pyoverdins are secreted under iron limited conditions from *Pseudomonas* spp., which are ubiquitous aerobic soil bacteria. The preferred binding places for metals at the pyoverdinin molecule are the hydroxamic acid group at the peptide chain and the catechol functionality of the chromophore. In this study, we simulate the catechol function with a simple model ligand, 2,3-dihydroxynaphthalene [LH_2].

EXPERIMENTAL. Three series of TRLFS experiments were performed. In runs one and two, we varied the U(VI) concentration, 10^{-6} M to $5 \cdot 10^{-3}$ M, at [LH_2] of $5 \cdot 10^{-5}$ M at fixed pH of 2.1 and 4.1; in the third run, [LH_2] and [U(VI)] were kept constant at $1 \cdot 10^{-4}$ and $2 \cdot 10^{-5}$ M, respectively, while varying the pH between 2.0 and 12.0. The spectra were evaluated using the factor analysis program SPECFIT. Details are summarized in [2,3]. Experimental details of the fs-TRLFS setup are given in [4].

RESULTS. The pH sensitivity of the luminescence spectra of 2,3-dihydroxynaphthalene is depicted in Fig. 1.

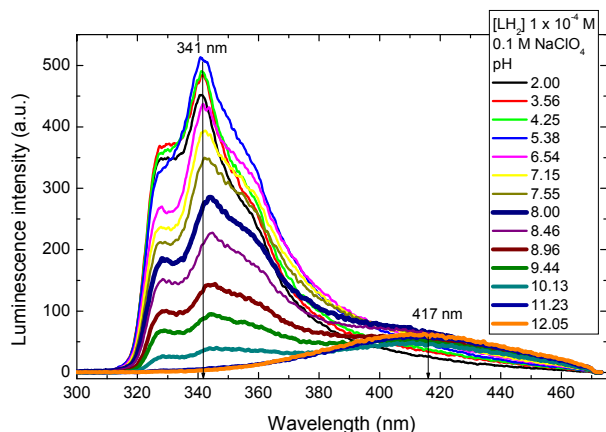


Fig. 1: TRLFS spectra of 2,3-dihydroxynaphthalene as a function of pH.

At $\text{pH} \leq 8$, the sum TRLFS spectra are characterized by an emission maximum at 341 nm with shoulders at 327 and 350 nm. At $\text{pH} \geq 8$, the influence of a second species having an emission maximum at 417 nm dominates the spectra shown in Fig. 1. The luminescence intensity (Fig. 2) slightly increased up to pH 5.4. Then the intensity decreased as a function of pH and is from pH 10 pH-independent. The two ligand species are characterized by luminescence lifetimes of 12.5 ± 2.2 and 1.63 ± 0.4 ns. In the absence of U(VI), completely different luminescence properties were observed compared to those of the natural pyoverdinin-mixture reported in [3].

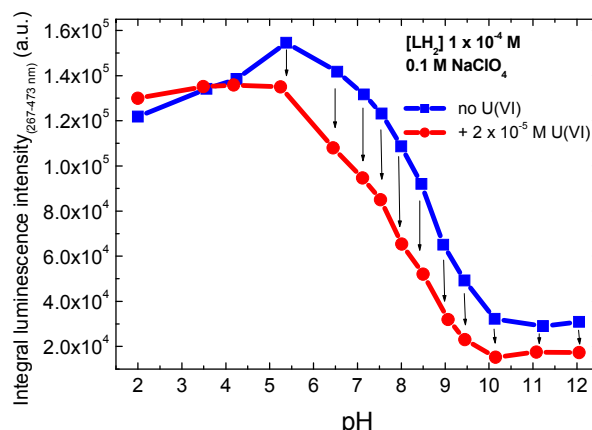


Fig. 2: Luminescence intensity measured in the U(VI)-2,3-dihydroxynaphthalene system as a function of pH.

The evaluation of the pH-dependent TRLFS spectra showed one pK value of 8.37 ± 0.11 . The deprotonation of the second catechol group could be confirmed by UV-vis spectroscopy and results to $\text{pK}_2 = 12.37 \pm 0.20$. Both values are in agreement with the potentiometry based deprotonation constants reported in [5]. In all samples containing UO_2^{2+} at $\text{pH} > 4$, a strong quenching of the 2,3-dihydroxynaphthalene luminescence was observed (Fig. 2). It follows that the UO_2^{2+} -2,3-dihydroxynaphthalene species emit no luminescence light. This is in agreement with our observations in the UO_2^{2+} -*P. fluorescens* (CCUG 32456) pyoverdinin system [3]. The luminescence lifetimes were not influenced within the investigated pH range. This indicates that a static luminescence quench process occurs due to the complex formation reactions. We could describe the U(VI) speciation with the following averaged formation constants: $\log \beta_{111} = 20.5 \pm 1.4$ and $\log \beta_{121} = 29.9 \pm 0.5$. 1 : 1 and 1 : 2 uranyl 2,3-dihydroxynaphthalene complexes based on potentiometric titrations were first reported in [5]. Our spectroscopically based stability constants are smaller as the values in [5]. One explanation could be the nebulous discussion of the stoichiometry of the formed species. This makes a recalculation of the formation constants for a direct comparison difficult. To our knowledge this is the first detailed characterization of aqueous 2,3-dihydroxynaphthalene species and their interaction with UO_2^{2+} using fs-TRLFS.

ACKNOWLEDGEMENTS. This work was funded by the BMWi under contract number: 02E9985.

REFERENCES

- [1] Bouby, M. et al. (1999) *Czech. J. Phys.* **49**, 147-1550.
- [2] Moll, H. et al. (2008) *BioMetals*, in press.
- [3] Moll, H. et al. (2008) *Geomicrobiol. J.*, submitted.
- [4] Geipel, G. et al. (2004) *Spectrochim. Acta* **60**, 417-424.
- [5] Bartusek, M. (1967) *Collection Czechoslov. Chem. Commun.* **32**, 757-773.

Complexation of uranium(IV) by citric acid studied by UV-vis spectroscopy

K. Schmeide, V. Brendler

The complexation of uranium(IV) by citric acid was studied as function of acidity (1 M, 0.5 M, 0.1 M $[H^+]$) by UV-Vis spectroscopy. Stability constants for 1 : 1 and 1 : 2 uranium(IV) citrate complexes of the type $M_pH_qL_r$ were determined with $\log \beta_{101} = 13.5 \pm 0.2$ and $\log \beta_{102} = 25.1 \pm 0.2$.

Data for the U(IV) complexation with inorganic and organic ligands are scarce. In this study, for the U(IV) complexation the model ligand citric acid was chosen which stands for a variety of organic ligands in aqueous systems. According to the NEA Thermodynamic Database [1] the stoichiometry of the U(IV) citrate species formed and thus, the stability constants are still uncertain [1].

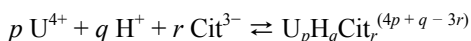
EXPERIMENTAL. Sample solutions were prepared in a glove-box (N_2 atmosphere) using CO_2 -free solutions. The U(IV) concentration was kept constant at $1 \cdot 10^{-3}$ M, the citric acid concentration was varied between 0 and 0.2 M. The concentration of hydrogen ions (1, 0.5, 0.1 M) was adjusted by adding aliquots of 5 M $HClO_4$ simultaneously taking into consideration the $[H^+]$ stemming from the U(IV) stock solution. The amount of U(VI) in the samples was ≤ 1.2 % of the total U as determined by fluorescence spectroscopy.

The UV-vis absorption spectra were recorded with a UV/vis/NIR spectrophotometer (CARY-5G, Varian) in the spectral range from 900 to 300 nm. The spectra were analyzed between 446 and 524 nm and between 570 and 727 nm. The stability constants were calculated with the factor analysis program SPECFIT.

RESULTS. The complexation of U(IV) with citric acid has been investigated in dependence on hydrogen ion concentration. From the pK_a values reported for citric acid in [1] follows that the citric acid is completely protonated in the pH range applied in this work (about pH 0 up to pH 1.0), thus, not contributing to the ionic strength. That means, the ionic strength of the sample solutions is mainly determined by $[H^+]$.

Exemplary, Fig. 1 shows the evolution of the U(IV) spectrum in the two wavelength ranges analyzed for increasing citric acid concentrations (0 to 0.2 M) at an acidity of $[H^+] = 0.5$ M.

The experimental data were analyzed considering the most basic form of the citrate anion Cit^{3-} . The U(IV) citrate complexation reaction can be expressed as:



For the calculation of the stability constants, 8 datasets were analyzed (4 series of experiments ($[H^+] = 1$ M, 0.5 M, 0.1 M (2x)) with 2 wavelength ranges each). Thereby, the formation of 1 : 1 and 1 : 2 complexes was detected in the citrate media. Within the experimental uncertainty, the stability constants determined are independent of the acidity of the sample solutions and thus, of the ionic strength. The mean values of the stability constants were determined with $\log \beta_{101} = 13.5 \pm 0.2$ and $\log \beta_{102} = 25.1 \pm 0.2$. Due to the strong complexation of U(IV) by citric acid, the U(IV) hydrolysis is impeded and furthermore, U(IV) is stabilized against oxidation.

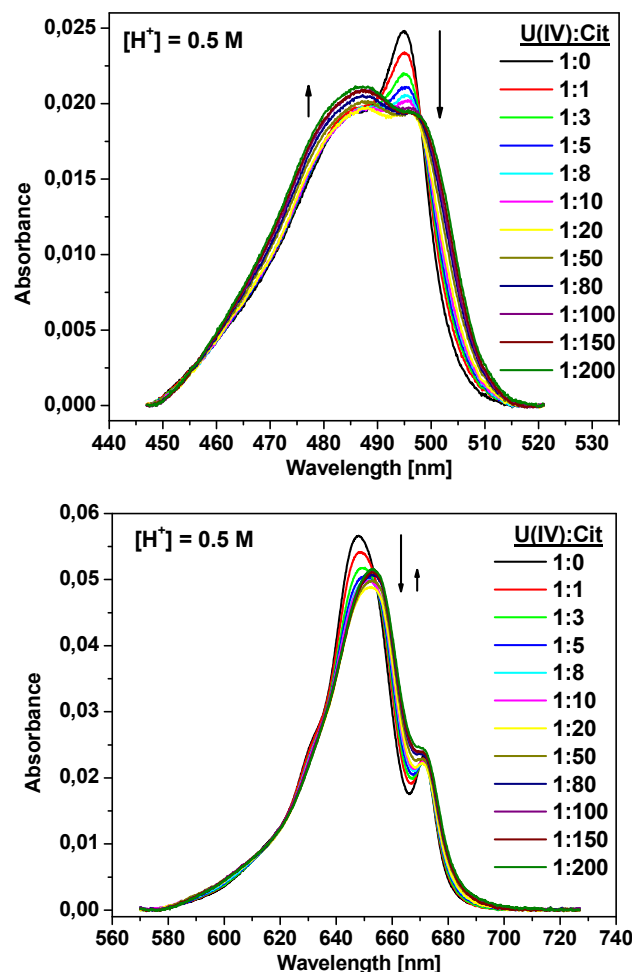


Fig. 1: Two wavelength ranges of the UV-vis spectra for $1 \cdot 10^{-3}$ M U(IV) as a function of the citric acid (Cit) concentration at $[H^+] = 0.5$ M.

The $\log \beta$ values determined for 1 : 1 and 1 : 2 complexes in this work are higher than the values reported by Nebel et al. [2] with 11.5 and 19.5, respectively.

From Tab. 1 follows that the $\log \beta$ obtained fit well in the series of $\log \beta$ determined for the complexation of further tetravalent actinides by citric acid.

Tab. 1: Stability constants for the system An(IV) citrate.

| | Pu(IV) | Np(IV) | U(IV) | Th(IV) |
|--------------------|----------------------|--------------------|----------------------------|--------------------|
| $\log \beta_{101}$ | 15.3 [3] 17.6 [4] | 13.6 ± 0.3 [5] | 13.5 ± 0.2 11.5 [2] | 11.6 [6] 13 [2] |
| $\log \beta_{102}$ | 30.2 [3] 30.0 [4] | 25.3 ± 0.3 [5] | 25.1 ± 0.2 19.5 [2] | 21.1 [6] 21 [2] |

ACKNOWLEDGEMENTS. This work was funded by the BMWi under contract number 02E10156.

REFERENCES

- [1] Hummel, W. et al. (2005) *Chemical Thermodynamics of Compounds and Complexes of U, Np, Pu, Am, Tc, Se, Ni and Zr with Selected Organic Ligands*, Elsevier, Amsterdam.
- [2] Nebel, D. et al. (1966) *Z. Phys. Chem.* **233**, 73-84.
- [3] Nebel, D. (1966) *Z. Phys. Chem.* **232**, 161-175.
- [4] Yule, L. (1991) Thesis, University of Wales, Aberystwyth.
- [5] Bonin, L. et al. (2007) *Radiochim. Acta* **95**, 371-379.
- [6] Raymond, D.P. et al. (1987) *Inorg. Chim. Acta* **140**, 309-313.

TRLFS and UV-Vis studies of the uranium(VI)–citrate system at low pH value

A. Günther, R. Steudtner, K. Schmeide

Citric acid plays an important role in the metabolism of different organisms and can bind different heavy metals. We investigated the interaction of this organic acid with uranium(VI) in aqueous solution spectroscopically using time-resolved laser-induced fluorescence spectroscopy and UV-vis spectroscopy. The formed U(VI)-citrate species show no fluorescence under the given experimental conditions. The absorption properties of the UO_2cit^- and $(\text{UO}_2)_2(\text{cit})_2^{2-}$ complex species are different to those of the free uranyl cation.

EXPERIMENTAL. The luminescence of the uranyl ion was measured after excitation with laser pulses at 266 nm (Nd:YAG laser system, Spectron Laser systems, SL 401-20, Rugby) and an averaged pulse energy of 250 μJ . The experiments were performed at a fixed uranyl perchlorate concentration of $5 \cdot 10^{-5}$ M. The citric acid concentration was varied between 0 and $5 \cdot 10^{-3}$ M. The absorption spectroscopy measurements were performed using a CARY5G UV-vis-NIR Spectrometer (Varian Co.) at room temperature. The spectra were recorded between 300 and 600 nm. The uranium(VI) concentration was here $1 \cdot 10^{-3}$ M and the citric acid concentration in solutions varied between 0 and $1 \cdot 10^{-1}$ M. All complex formation experiments were performed at an ionic strength of 0.5 M and in the pH range from 2 to 4. The pH value was adjusted with HClO_4 or NaOH .

RESULTS. Figure 1 shows the luminescence emission spectra of uranium(VI) as a function of the total citric acid concentration at pH 3 as an example. It was found that the luminescence intensity decreases with increasing ligand concentration. The uranyl signals of the complex solutions do not shift in comparison to the emission bands of the reference solution without citric acid. The time-resolved spectra show a mono-exponential luminescence decay. That means that the formed uranyl-citrate species do not fluoresce and only the luminescence properties of the free uranyl cation are visible in the spectra. The averaged luminescence lifetime of the free uranyl cation is 1723 ± 219 ns. Dynamic quenching due to the citric acid or the complex species cannot be ruled out. The quantitative analysis of the spectra and determination of the complex formation constants using luminescence spectroscopic data is difficult, because approximately 34 % of the U(VI) is reduced to U(IV) in the citrate system after laser excitation (see Fig. 2).

The spectroscopic evidence of the complex formation between U(VI) and citric acid at low pH values was performed with UV-vis measurements. Fig. 3 depicts UV-vis absorption spectra of uranium(VI) as a function of the citric acid concentration at pH 3 as an example. A significant increase of the absorption maxima and a bathochromic shift of the absorption bands compared to the free uranyl ion were detected. The spectra were analyzed with the factor analysis program SPECFIT [1]. The formed complex species are UO_2cit^- and $(\text{UO}_2)_2(\text{cit})_2^{2-}$. The corresponding formation constants were calculated to be $\log \beta_{101} = 7.43 \pm 0.06$ and $\log \beta_{202} = 18.88 \pm 0.05$ and are comparable with literature data [2].

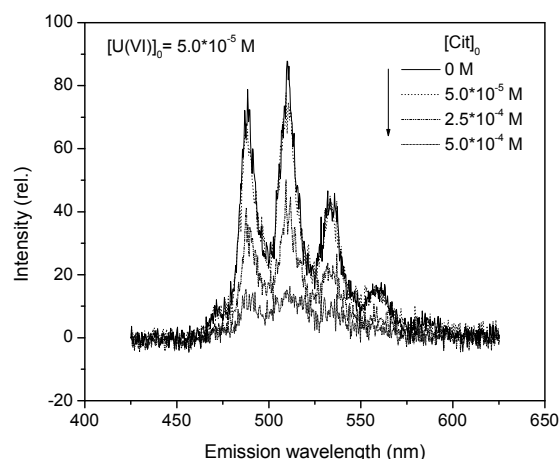


Fig. 1: Luminescence spectra of U(VI) as a function of the citric acid concentration at pH 3, $I = 0.5$ M.

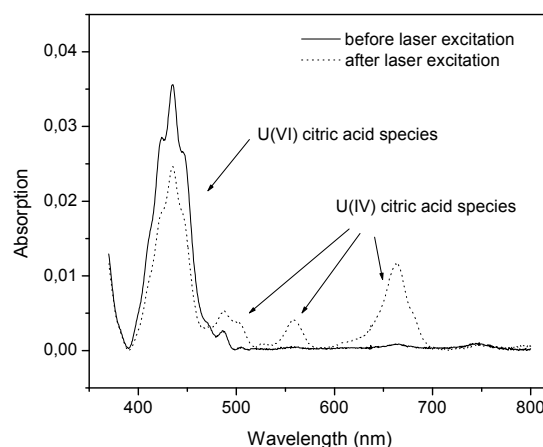


Fig. 2: UV-vis spectra of the uranium – citrate system before and after the excitation with laser energy at 266 nm, $[\text{U(VI)}]_0 = 1 \cdot 10^{-3}$ M, $[\text{Cit}]_0 = 2 \cdot 10^{-3}$ M, pH 3, $I = 0.5$ M.

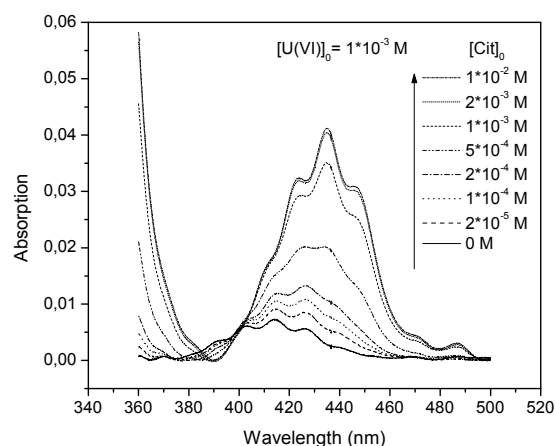


Fig. 3: UV-vis spectra of U(VI) as a function of the citric acid concentration at pH 3, $I = 0.5$ M.

ACKNOWLEDGEMENTS. The BMWi funded this work (02E10156).

REFERENCES

- [1] SPECFIT 32, Spectrum Software – Associates (2003).
- [2] Martell A.E. et al. (1998) *NIST critically selected stability constants of metal complexes database, standard reference database 46, version 5.0*, Texas A & M University, USA.

Comparative EXAFS studies of the complexation of U(VI) with hydroxamic acids in aqueous solution and solids

M. Glorius, H. Moll, A. Rossberg, G. Bernhard

The structure of the solid and aqueous complexes of uranium(VI) with salicylhydroxamic (SHA) and benzohydroxamic acid (BHA) was investigated by U L_{III}-edge EXAFS. For the first time the near-order surrounding of U(VI) was explored in solid complexes with SHA and BHA. The structure of solid and aqueous U(VI)-SHA and -BHA species seems to be different.

We investigated the complex formation of uranium(VI) with the pyoverdin model compounds SHA and BHA with UV-vis spectroscopy and TRLS in previous studies [1,2]. To determine the structure of the U(VI) complexes EXAFS measurements were performed. The EXAFS measurements were done with aqueous solution of the complexes and with solid complexes formed by precipitation. We want to determine the coordination mode of uranium(VI) to hydroxamic acids in aqueous and solid complexes.

EXPERIMENTAL. The test solutions had fixed concentrations of UO₂²⁺ and the ligand of 1·10⁻³ M and 8·10⁻³ M, respectively, within a pH range of 2.5 – 4. The solid complexes were prepared by precipitation. The content of uranium was 50 % in the SHA and 40 % in the BHA complexes. The EXAFS measurements were carried out at the Rossendorf Beamline at the ESRF, Grenoble, France. The U L_{III}-edge spectra of the aqueous complexes were measured in fluorescence mode at room temperature, those of the solid complexes in transmission mode at 15 K using a closed-cycle He-cryostat. The data were processed using WinXAS (ver. 3.1) [3]. Theoretical phases and amplitude functions were calculated with the FEFF8 code [4].

RESULTS. The raw U L_{III}-edge k³-weighted EXAFS spectra and their corresponding Fourier-transforms (FT) of the U(VI)-SHA and U(VI)-BHA system are shown in Fig. 1. The corresponding structural parameters are summarized in Tab. 1.

The differences in the shape (amplitude and frequency) of the EXAFS-oscillations of the ligand containing samples compared to the free uranyl sample U1 in the k-range 6 – 9 point to the presence of uranyl containing complexes

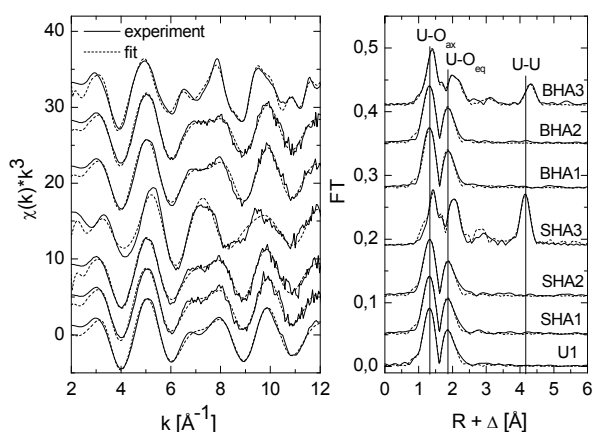


Fig. 1: U L_{III}-edge EXAFS spectra and their corresponding Fourier transformations (FT) of U(VI)-SHA and U(VI)-BHA complexes.

Tab. 1: EXAFS structural parameters for U(VI)-SHA and U(VI)-BHA species.

| Sample | Speciation | Shell | N | R [Å] | σ ² [Å ²] |
|--------|---|--------------------|------|-------------------|----------------------------------|
| U1 | pH 2 | U-O _{ax} | 1.9 | 1.76 ₆ | 0.0016 |
| | 100 % UO ₂ ²⁺ | U-O _{eq} | 5.0 | 2.41 ₈ | 0.0068 |
| SHA1 | pH 2.5 | | | | |
| | 17 % [UO ₂ SHA] ⁺ | U-O _{ax} | 2.2 | 1.76 ₉ | 0.0022 |
| | 32 % UO ₂ (SHA) ₂ | U-O _{eq} | 4.9 | 2.41 ₂ | 0.0065 |
| SHA2 | pH 3 | | | | |
| | 12 % [UO ₂ SHA] ⁺ | U-O _{ax} | 2.2 | 1.77 ₅ | 0.0026 |
| | 76 % UO ₂ (SHA) ₂ | U-O _{eq} | 4.7 | 2.41 ₅ | 0.0063 |
| SHA3 | Precipitate at pH 3.5 | U-O _{ax} | 1.5 | 1.79 ₁ | 0.0008 |
| | | U-O _{eq} | 6.3 | 2.47 ₃ | 0.0042 |
| | | U-U | 1.9 | 4.34 ₉ | 0.0013 |
| BHA1 | pH 3.5 | | | | |
| | 23 % [UO ₂ BHA] ⁺ | U-O _{ax} | 2* | 1.77 ₀ | 0.0014 |
| | 39 % UO ₂ (BHA) ₂ | U-O _{eq} | 4.4 | 2.40 ₉ | 0.0058 |
| BHA2 | pH 4 | | | | |
| | 8 % [UO ₂ BHA] ⁺ | U-O _{ax} | 2.3 | 1.77 ₃ | 0.0027 |
| | 90 % UO ₂ (BHA) ₂ | U-O _{eq} | 4.8 | 2.40 ₂ | 0.0064 |
| BHA3 | Precipitate at pH 4.5 | U-O _{ax} | 1.9 | 1.78 ₉ | 0.0016 |
| | | U-O _{eq1} | 3* | 2.44 ₁ | 0.0033 |
| | | U-O _{eq2} | 2* | 3.54 ₁ | 0.0008 |
| | | U-U | 1.8* | 4.48 ₃ | 0.0027 |

N: coordination number with an uncertainty of 15 %, R: bond lengths with an uncertainty of 0.01 Å (3rd decimal place given as subscripts), σ²: Debye-Waller factor; *: fixed during the fit.

with both hydroxamate ligands. The slightly shorter U-O_{eq} distance of the aqueous complex solutions compared to the free uranyl ion indicates a bidentate coordination of U(VI) via the hydroxamate oxygen atoms [5].

In the SHA- and BHA solids, clearly two uranium atoms with distances of 4.34 Å and 4.48 Å, respectively, were determined. These points to a trinuclear structure where three uranyl units are linked with SHA/BHA molecules. No published data exist to provide a basis for comparison. The comparison of the SHA and BHA parameters in the solid complexes shows differences in all coordination shells which indicates that SHA and BHA forms solid complexes with a different structure.

The near-order surrounding of the linear uranyl unit in both hydroxamate compounds shows differences in solid state and in aqueous solution. In aqueous solution the U-O_{eq} distance is with 2.41 Å (SHA and BHA) significantly shorter compared to 2.47 Å (SHA) and 2.44 Å (BHA) in the solid structures. So we can conclude that the structure of the aqueous U(VI) hydroxamate species is probable different from the structure in the solid complexes. Further experiments (e.g. IR, XRD) are in progress to explore the structure of the solids.

ACKNOWLEDGEMENTS. This work was funded by the BMWi under contract number 02E9985.

REFERENCES

- [1] Glorius, M. et al. (2007) *Radiochimica Acta* **95**, 151-157.
- [2] Glorius, M. et al. (2008) *J. Radioanal. Nucl. Chem.*, in press.
- [3] Ressler, T. (1998) *J. Synchrot. Radiat.* **5**, 118-122.
- [4] Ankudinov, A.L. et al. (1998) *Phys. Rev. B* **58**, 7565-7576.
- [5] Wiebke, J. et al. (2008) *Inorg. Chem.*, in press.

Complexation studies of UO_2^{2+} with benzenesulfonic acid

C. Joseph, K. Schmeide, G. Geipel, G. Bernhard

The complex formation of UO_2^{2+} with benzenesulfonic acid was determined using UV-vis spectroscopy and time-resolved laser-induced fluorescence spectroscopy (TRLFS).

Humic acids (HA) are very large molecules with an immense variety of functional groups. In the literature it was shown that HA contain carboxylate [1] and phenolic hydroxyl groups [2] which are able to complex the uranyl ion. But in addition to these functionalities humic acids comprehend also different sulfur groups. In this work, the complexation ability of a sulfonic acid towards UO_2^{2+} is studied. For this, a simple organic model ligand, benzenesulfonic acid (BSA), is used, that can occur as building block for humic acid.

EXPERIMENTAL. The UV-vis spectroscopy experiments were carried out at a total uranyl concentration of $1 \cdot 10^{-3}$ M as a function of the ligand concentration (0 M to $5 \cdot 10^{-3}$ M) at pH 3.8. The pH adjustments were made with HClO_4 and NaOH. The ionic strength was adjusted to 0.1 M (NaClO_4). The spectra were recorded from 300 to 700 nm using a CARY 5 G UV-vis-NIR spectrometer (Varian Co.) at room temperature. The complex formation constant was determined using the factor analysis program SPECFIT.

The TRLFS experiments were carried out at a total uranyl concentration of $5 \cdot 10^{-5}$ M as a function of the ligand concentration (0 M to $8 \cdot 10^{-4}$ M) at pH 3.8. The pH adjustments were made with HClO_4 and NaOH. The ionic strength was adjusted to 0.1 M (NaClO_4). The spectra were recorded at room temperature using a pulsed Nd:YAG laser system. The excitation wavelength of the uranyl luminescence was 266 nm. The complex formation constant was determined with a slope analysis.

RESULTS. BSA is a very strong acid. In this work, the literature value -6.56 for the acidity constant pK_a [3] is used. Since the UV-vis and TRLFS experiments were done at pH 3.8, the ligand can be regarded as completely deprotonated.

Figure 1 shows the UV-vis spectra of the uranyl ion as a function of the ligand concentration. It is obvious, that the uranyl spectrum at pH 1.0 differs from that at pH 3.8. This can be attributed to different uranyl hydroxy species, which are formed at higher pH and which absorb in the same wavelength range. They have very high molar absorptions, especially $[(\text{UO}_2)_2(\text{OH})_2]^{2+}$ with $101 \text{ L} \cdot \text{mol}^{-1} \cdot \text{cm}^{-1}$ compared to that of the uranyl ion with $9.7 \text{ L} \cdot \text{mol}^{-1} \cdot \text{cm}^{-1}$ [4]. Due to this, the UV-vis spectra in this wavelength range at pH 3.8 show no trend in a distinct direction with increasing ligand concentration. For determining the complex formation constant using SPECFIT the log K of the most dominant hydroxy species, $[(\text{UO}_2)_2(\text{OH})_2]^{2+}$, has to be considered. At an ionic strength of 0.1 M (NaClO_4) it is -5.87 , if the NEA thermodynamic database [5] is used. With the factor analysis program a log K of 4.41 ± 0.39 for a 1 : 1 complex could be determined.

The TRLF spectra of the uranyl ion as a function of ligand concentration show a decrease of the luminescence intensity with increasing BSA concentration (not shown).

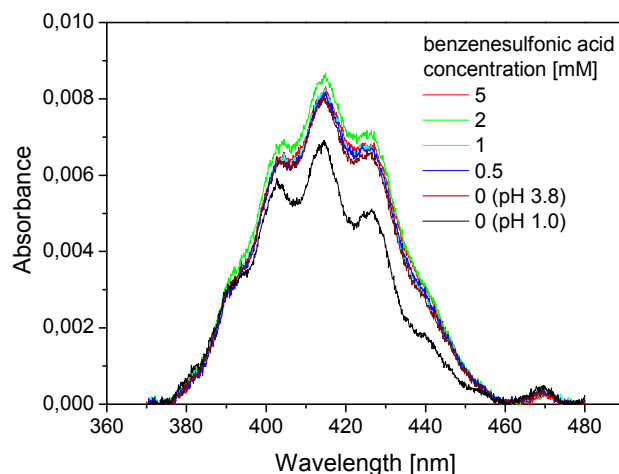


Fig. 1: UV-vis spectra at $1 \cdot 10^{-3}$ M UO_2^{2+} at pH 3.8 as a function of BSA concentration.

This behavior is typical of static luminescence quenching due to the complex formation. The luminescence decay was bi-exponential in all samples, beside the uranyl ion at pH 3.8 also the UO_2OH^+ species shows luminescence. The lifetime of the free uranyl ion decreases with increasing BSA concentration. This indicates an additional dynamic luminescence quenching. With the Stern-Volmer equation the lifetimes (alternatively the revised intensities) can be used to calculate the complex formation constant. The Stern-Volmer plot (Fig. 2) gives a straight line with a slope (K_{SV}), which represents the complex formation constant. The value of $\log K_{SV}$ is 3.52. By using a slope analysis (not shown) a log K value of 3.53 ± 0.04 could be determined.

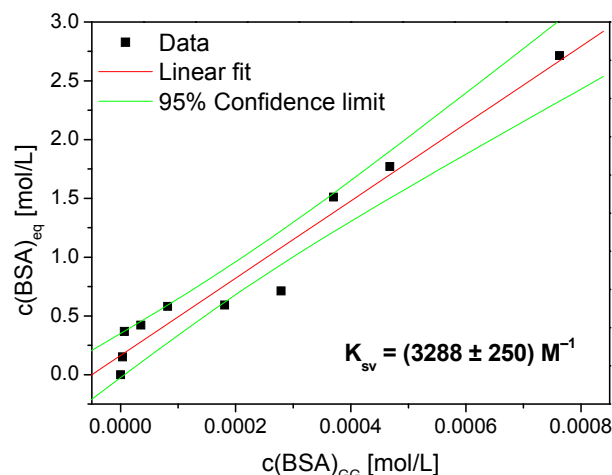


Fig. 2: Stern-Volmer plot (dynamic quenching) of UO_2^{2+} by BSA.

ACKNOWLEDGEMENTS. The Federal Ministry of Economics and Technology funded this work (02E10156).

REFERENCES

- [1] Shanbhag, P.M. et al. (1981) *J. inorg. nucl. Chem.* **43**, 3369-3372.
- [2] Roßberg, A. et al. (1999) *Report FZR-247*, p. 53.
- [3] Cerfontain, H. et al. (1975) *Tetrahedron Lett.* **42**, 3639-3642.
- [4] Meinrath, G. (1997) *J. Radioanal. Nucl. Chem.* **224**, 119-126.
- [5] Guillaumont, R. et al. (2003) *Update on the Chemical Thermodynamics of U, Np, Pu, Am, Tc*, Elsevier, Amsterdam.

Complexation studies of uranium(VI) with 4-hydroxybenzenesulfonic acid

B. Raditzky, G. Geipel, K. Schmeide, G. Bernhard

The complex formation of the uranyl ion (UO_2^{2+}) with 4-hydroxybenzenesulfonic acid (HBSA) was studied by time-resolved laser-induced fluorescence spectroscopy (TRLFS) at pH = 2.5. A 1 : 1 complex was found with the stability constant of $\log K_{101} = 3.90 \pm 0.03$.

Although it is established that humic substances (HA) offer various sulfur containing functional groups [1], the complexation behavior of HA with metal ions by these groups is widely unknown [2]. In this work, the interaction between 4-hydroxybenzene-sulfonic acid (HBSA), used as a model ligand, and U(VI) was studied to determine the complexation behavior of the sulfonic acid group.

EXPERIMENTAL. The TRLFS experiments were carried out at a total uranyl concentration of 0.05 mM as a function of the ligand concentration (0.03 – 0.3 mM) at acidic pH (2 – 3.8), and an ionic strength of 0.1 M (NaClO_4). The spectra were recorded at room temperature using a pulsed Nd:YAG laser system (excitation wavelength 266 nm). The stability constants were determined by a slope analysis and using the factor analysis program SPECFIT. The results were averaged over several independent experiments.

RESULTS. The emission spectra of the solution were measured after excitation. Not only the uranyl ion, also the free HBSA shows a typical luminescence spectrum in the wavelength range between 280 and 360 nm, with a lifetime of about 2 ns. The HBSA also shows excited state energy transfer, observable by the appearance of a second peak between 360 and 480 nm. This second species derogates the measurements, therefore, only the luminescence spectrum of the uranyl ion was considered. Figure 1 shows the luminescence spectra as a function of the ligand concentration at pH = 2.5.

The spectra show a strong decrease of the luminescence intensity of the uranyl ion with increasing ligand concentration at all pH values studied. This is characteristic for static luminescence quenching due to complex formation. In some experiments the lifetime of the free uranyl ion decreases with increasing ligand concentration caused by an additional dynamic quenching process. The determined

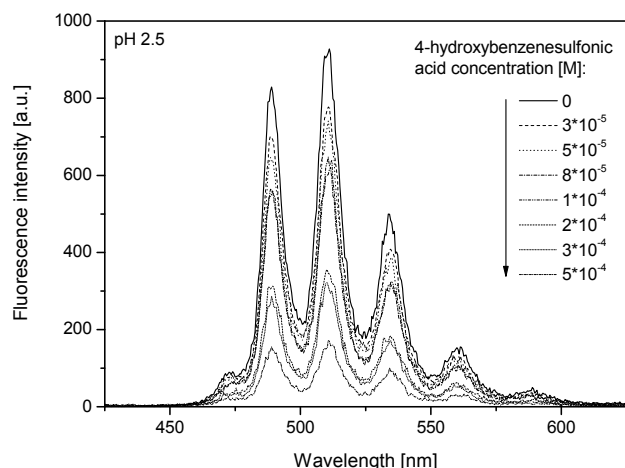


Fig. 1: Luminescence spectra of $5 \cdot 10^{-5}$ M UO_2^{2+} at pH 2.5 as a function of the 4-hydroxybenzenesulfonic acid concentration.

lifetimes could be used to calculate the luminescence intensities if no dynamic quenching occurs. Using a modified logarithmic form of the mass action law the complex stoichiometry and the stability constant were determined graphically via slope analysis. Figure 2 shows the validation plot for the complexation of uranium(VI) with HBSA. In all experiments a slope near 1 was calculated, suggesting a predominant 1 : 1 complex. The intersection conforms to the formation constant $\log K^*$.

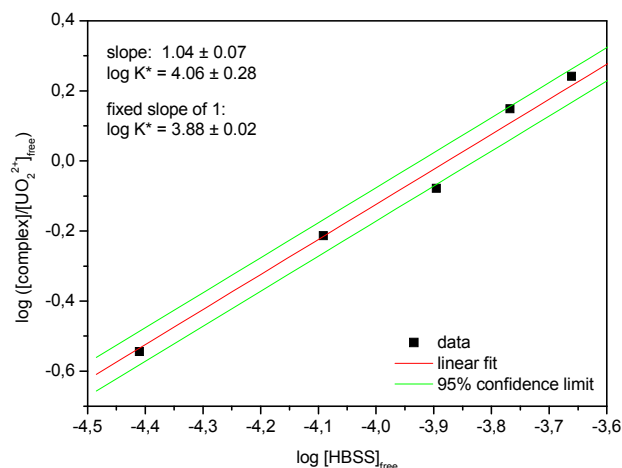
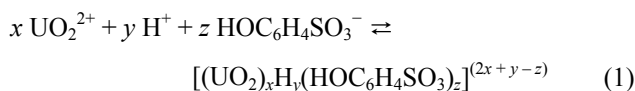


Fig. 2: Validation plot (slope analysis) of uranium(VI) with 4-hydroxybenzenesulfonic acid.

The complex formation of UO_2^{2+} with HBSA can be written as:



The stability constant was determined to be $\log K_{101} = 3.90 \pm 0.03$ using the factor analysis program SPECFIT under consideration of the pH and the protonation constants of HBSA. HBSA offers two protonation constants. In this work, we used a HBSA sodium salt. Thus, the sulfonic acid group can be regarded as completely dissociated. With a $\text{pK}_a = 8.56 \pm 0.05$, determined by potentiometric titration and comparable to those in the literature [3,4], the hydroxylic group should not be deprotonated in the investigated pH range. The SPECFIT calculations show that the phenolic hydroxyl group is not deprotonated in the examined pH range and therefore it is not involved in the complexation.

ACKNOWLEDGEMENT. This study was funded by the Federal Ministry of Economics and Technology (02 E 10156).

REFERENCES

- [1] Xia, K. et al. (1998) *Soil Sci. Soc. Am. J.* **62**, 1240-1246.
- [2] Skyllberg, U. et al. (2006) *Environ. Sci. Technol.* **40**, 4174-4180.
- [3] Zollinger, H. et al. (1953) *Helv. Chim. Acta*, **36**, 1711-1722.
- [4] Bates, R.G. et al. (1943) *J. Res. Bur. Stand.* **31**, 205-223.

Complexation of U(VI) with aromatic acids – A combined computational and experimental study

M. Glorius, A. Moritz,¹ J. Wiebke,¹ H. Moll

¹Institute for Theoretical Chemistry, University of Cologne, Germany

Density functional theory (DFT) and extended X-ray absorption fine structure spectroscopy (EXAFS) are combined to clarify the interaction of uranium(VI) with salicylhydroxamate (SHA), benzohydroxamate (BHA), and benzoate (BA) in aqueous solution. Molecular structures, relative stabilities, and excitation spectra from both theory and experiment give a consistent picture.

The complexation of uranium(VI) with the pyoverdine model compounds SHA, BHA and BA was investigated in previous studies [1,2]. To determine the structure of the 1 : 1 U(VI) complexes, EXAFS measurements were done. In the U(VI)-SHA system there are two possible coordination modes of U(VI), the coordination via the two hydroxamic oxygen atoms ([O,O]-mode) and the coordination via the phenolic oxygen and the nitrogen atom ([N,O']-mode) of the hydroxamate functionality. Because EXAFS is often not sufficient to solve the structure of such U(VI) species, a combination with quantum chemical methods can be useful. So, DFT and EXAFS were used to determine precise molecular structures for the U(VI) complexes. With DFT calculated stabilities and excitation spectra are compared with those from previous experiments [1].

EXPERIMENTAL. EXAFS measurements were performed at fixed SHA, BHA and BA concentrations of $8 \cdot 10^{-3}$ M within a pH range of 2.5 – 4.0 and UO_2^{2+} concentrations of $1 \cdot 10^{-3}$ M and $5 \cdot 10^{-3}$ M at the Rossendorf Beamline (ROBL) BM20 at the ESRF, Grenoble.

The uranium(VI) complexes were completely geometry optimized at the DFT/B3LYP level using the TURBOMOLE v. 5.7 program system. A hybrid-type level 3 solvation model was included. Computational and experimental details are summarized in [3].

RESULTS. The uranyl ion is found to be pentacoordinated by one bidentate ligand and three water molecules. The calculated mean U-O_{ax} and U-O_{eq} bond lengths of $[\text{UO}_2\text{L}(\text{OH}_2)_3]^+$ (L = SHA, BHA) and $[\text{UO}_2(\text{OH}_2)_5]^{2+}$ deviate from experimental EXAFS data by at most -0.017 and $+0.080$ Å, respectively (Tab. 1). The overestimation of the U-O_{eq} distances is due to the known shortcomings of the applied (level 3) solvation model, i.e. the exclusive hydration of the UO_2^{2+} fragment and the neglect of bulk solvation effects.

In case of the relative stabilities the experimental order

Tab. 1: Bond lengths R [Å] for the complexes and the solvated uranyl ion from DFT calculations (th.) including solvation effects compared to experimental (exp.) EXAFS data. For SHA the results for both the [O,O] and [N,O'] mode are given.

| Bond lengths | R_{th} (U-O _{ax}) | R_{exp} (U-O _{ax}) | R_{th} (U-O _{eq}) | R_{exp} (U-O _{eq}) |
|---|---|--|---|--|
| $[\text{UO}_2\text{SHA}(\text{OH}_2)_3]^+$ [O,O]-mode | 1.775 | 1.769 | 2.460 | 2.412 |
| $[\text{UO}_2\text{SHA}(\text{OH}_2)_3]^+$ [N,O']-mode | 1.773 | 1.769 | 2.500 | 2.412 |
| $[\text{UO}_2\text{BHA}(\text{OH}_2)_3]^+$ | 1.774 | 1.770 | 2.461 | 2.409 |
| $[\text{UO}_2(\text{OH}_2)_5]^{2+}$ | 1.749 | 1.766 | 2.496 | 2.416 |

($\log \beta (\text{UO}_2\text{SHA}^+) = 16.3$; $\log \beta (\text{UO}_2\text{BHA}^+) = 7.5$; $\log \beta (\text{UO}_2\text{BA}^+) = 3.0$) is reflected by the calculated gas phase binding energies ($-\Delta E (\text{UO}_2\text{SHA}^+) = 1649$ kJ mol⁻¹; $-\Delta E (\text{UO}_2\text{BHA}^+) = 1615$ kJ mol⁻¹; $-\Delta E (\text{UO}_2\text{BA}^+) = 1509$ kJ mol⁻¹), i.e. the complex stabilities decrease from SHA via BHA to BA. The calculated TD-DFT excitation and measured UV-vis spectra of $[\text{UO}_2\text{L}(\text{OH}_2)_3]^+$ (L = SHA, BHA) are in good agreement, i.e. the differences within the absorption maxima amount at most to 35 nm corresponding to 0.29 eV (Fig. 1). From molecular orbital considerations, the experimentally observed absorption bands are assigned to $\text{UO}_2^{2+} \leftarrow \text{L}^-$ charge transfer transitions. Since in case of $[\text{UO}_2\text{BA}(\text{OH}_2)_3]^+$ no DFT minimum structure could be obtained, for this complex the solvated molecular structure as well as the excitation spectrum are missing.

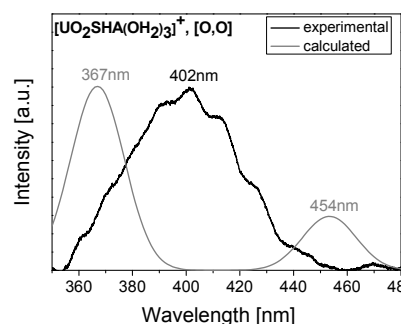


Fig. 1: Calculated B3LYP TD-DFT spectra for the [O,O]-mode of the $[\text{UO}_2\text{SHA}(\text{OH}_2)_3]^+$ complex and experimental UV-vis spectra from aqueous solution.

All considered properties demonstrate that the SHA ligand binds via the two hydroxamic acid oxygen atoms. In case of the [O,O]-mode the agreement between experimental EXAFS and calculated mean U-O_{eq} bond lengths is clearly better (ΔR : 0.048 and 0.088 Å for [O,O]- and [N,O']-mode, respectively), the calculated gas phase binding energy is by 39 kJ mol⁻¹ higher, and the deviation of the calculated from the experimental absorption maximum is about two times smaller ($\Delta\lambda$: 35 and 80 nm for [O,O]- and [N,O']-mode, respectively) than for the [N,O']-mode (Fig. 2).

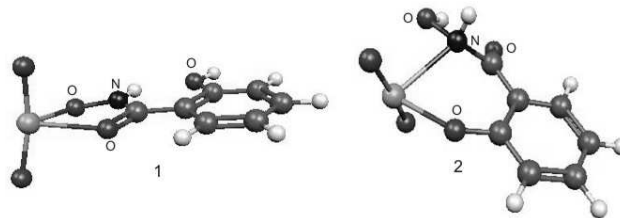


Fig. 2: Gas phase molecular structures of the (1) [O,O]- and (2) [N,O']-mode of the 1 : 1 complex in the U(VI)-SHA system.

ACKNOWLEDGEMENTS. This work was funded by the BMWi under contract number 02E9985 (experimental part) and the DFG (theoretical part).

REFERENCES

- [1] Glorius, M. et al. (2007) *Radiochim. Acta* **95**, 151-157.
- [2] Glorius, M. et al. (2008) *J. Radioanal. Nucl. Chem.*, in press.
- [3] Wiebke, J. et al. (2008) *Inorg. Chem.*, in press.

Reduction of uranium(VI) by glucose

R. Steudtner, I. Gründig,¹ G. Geipel

¹University of Applied Sciences, Dresden, Germany

The chemical speciation and the oxidations state of uranium are of basically importance for the transport of uranium in geo- and biosphere. The aqueous uranium cycle is partitioned in three zones. In the oxic zone near the surface U(VI) complexes were formed by inorganic and organic ligands. Furthermore, it is possible that uranium precipitations, as uranium(VI) colloids or reduced uranium(IV), migrate from the oxic zone through the anoxic zone into the sediment. Potentially electron donors for the anaerobic chemical or anaerobic microbial reduction of U(VI) are dissimilatory metal-reducing bacteria, Fe(II), H₂ or organic carbon such as sugar or carbon acids [1-4].

Glucose is one of the naturally-occurring organic substances, which can be oxidized by microbial, enzymatic, catalytic and chemical routes [5]. In the present study, we investigated the reduction of uranyl(VI) in the presence of glucose and different sugar derivates in the environmental pH range by UV-vis spectroscopy.

EXPERIMENTAL. Solutions containing U(VI) concentrations of $1 \cdot 10^{-4}$ M and of $5 \cdot 10^{-4}$ M, and glucose or sugar derivate concentrations from $1 \cdot 10^{-5}$ M to $1 \cdot 10^{-1}$ M with an ionic strength of 0.1 M NaClO₄ were investigated by reduction experiments in the pH range from 4 to 9. The samples were shaken several times under light emission and the pH values were readjusted. When precipitation was observed the solutions were centrifuged for 25 min. by 3500 rpm. The centrifugate was separated and the precipitate was dissolved in 1 M HClO₄. By the redox studies in a buffer system solutions of uranium(VI) $5 \cdot 10^{-4}$ M and 0.1 M glucose were prepared in a citrate buffer (60,3 % citric acid monohydrate 21.014 g/L + 200 ml 1 M NaOH; 39,3 % 0.1 M NaOH) and were shaken different times under light emission.

RESULTS. Figure 1 shows the reduced U(VI) by glucose at two different start concentrations of U(VI) dependent from the pH value.

A reduction of U(VI) was not observed at pH 4, whereas a reduction to U(IV) was found with increasing the pH values. Maximum reduction was observed at pH 5 and 6.

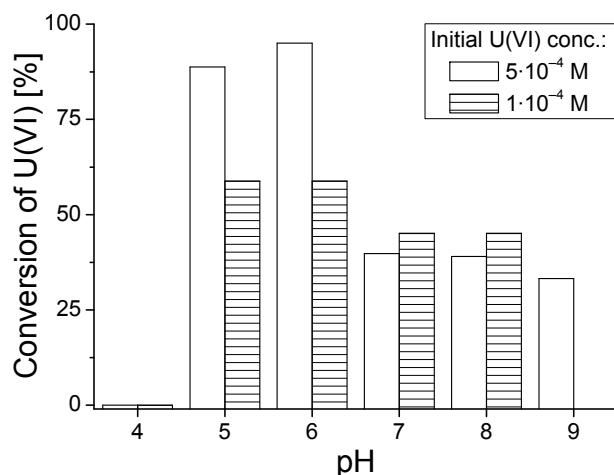


Fig. 1: Reduced uranium(VI) in the pH range from 4 to 9.

Tab. 1: Percentage of uranium(VI) which is reduced by various sugar derivate at pH 6 after 7 days.

| Sugar derivate | Reduced uranium(VI) [%] |
|---------------------|-------------------------|
| Glucose | 93.0 |
| Fructose | 91.8 |
| Xylose | 69.6 |
| Glucosamin | 7.0 |
| N-acetyl-glucosamin | 7.0 |

Starting with higher U(VI) concentrations, the amount of U(IV) was found to be > 90 % whereas at lower concentrations only 60 % of the initial U(VI) was reduced. In the pH range from 7 to 9, an average of ~ 40 % of U(VI) was converted into U(IV). The lower reduction rate in this pH range can be explained by co-precipitation of U(VI) hydroxo species which were dissolved in 1 M HClO₄ and therefore detracted from the redox system.

The results of the reduction by various sugar derivates are shown in Tab. 1.

The redox capacities are influenced by the sort of sugar derivate. The redox capacities can be described by the following order:

C₆ – sugar > C₅ – sugar > substituted sugar.

A water soluble U(IV)-citrat species was found after reduction of U(VI) in the buffer system at pH 6. Figure 2 shows the comparison of the absorption spectra in the buffer system and in 1 M HClO₄.

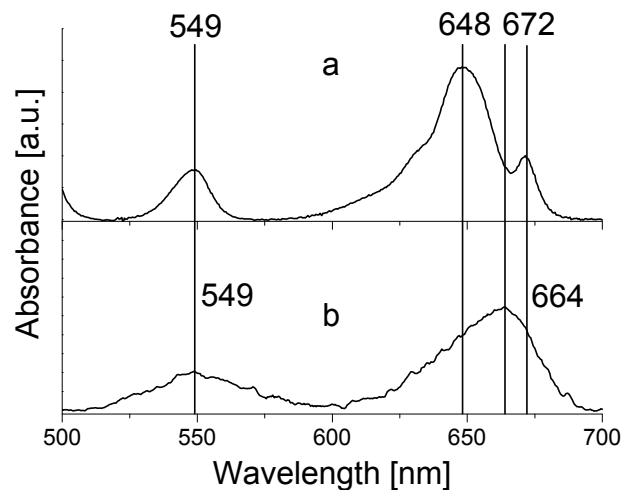


Fig. 2: U(IV) absorption spectra in 1 M HClO₄ (a) and as U(IV)-citrat species at pH 6 (b).

REFERENCES

- [1] Wall, J.D. et al. (2006) *Annu. Rev. Microbiol.* **60**, 149-166.
- [2] Neiss, J. et al. (2007) *Environ. Sci. Technol.* **41**, 7343-7348.
- [3] Neuberger, C. (1908) *Biochem. Zeitschr.* **13**, 305-320.
- [4] Suzuki, Y. et al. (2006) *Radiochim. Acta* **94**, 579-583.
- [5] De Wit, D. (1992) Thesis, Delft University of Technology, Delft.

Fluorescence properties of glucose at low temperatures

T. Arnold, K. Großmann

Time resolved laser-induced fluorescence spectroscopy (TRLFS) measurements of glucose at room temperature (RT) and under cryogenic conditions were carried out using an excitation wavelength of 266 nm. It was found that glucose showed no fluorescence properties at room temperature. At $-73\text{ }^{\circ}\text{C}$ only a very weak fluorescence signal was observed. In contrast to these TRLFS measurements, strong fluorescence signals of glucose were obtained when measured at $-173\text{ }^{\circ}\text{C}$ and in particular at $-263\text{ }^{\circ}\text{C}$. In addition, it was found that with decreasing temperature the peak maxima are shifted to lower wavelengths. For the measurement at $-263\text{ }^{\circ}\text{C}$ three distinct emission maxima were found at 465.9 nm, 479.2 nm and 492.7 nm. The fluorescence lifetime of glucose is also temperature dependent and follows an Arrhenius like behavior, i.e. it becomes longer with decreasing temperature. For the TRLFS measurement at $-263\text{ }^{\circ}\text{C}$ (10 K) a fluorescence lifetime of 866.8 ns was calculated.

EXPERIMENTAL. Glucose was prepared as 1 M standard solution. This solution was subsequently transferred in a cuvette and sealed. Then the samples were put in a freezer at $-20\text{ }^{\circ}\text{C}$ for approximately 15 hours. After that the frozen samples were measured in a refrigerator cryostat (RDK 10-320, Oerlicon Leybold, Dresden, Germany) at the desired measurement temperature. To study the fluorescence properties of glucose, an excitation wavelength of 266 nm was used (Inlite II Laser, Continuum, Santa Clara, U.S.A). The laser energy was checked with a power meter (Labmaster Ultima, Coherent, Inc., Santa Clara, U.S.A) just before it entered the cryostat and readjusted if necessary. The fluorescence emission was coupled into a fiber optic mounted perpendicular to the excitation beam. The fiber optic was connected to a spectrograph (Acton Research, Model:1236 OMA 500 mm, Princeton Instruments, Acton, U.S.A) and an adjacent ICCD-camera (Roper Scientific, Princeton Instruments, Stuttgart, Germany) where the fluorescence light was detected. The frozen glucose sample was measured at temperatures of $-73\text{ }^{\circ}\text{C}$, $-173\text{ }^{\circ}\text{C}$, and $-263\text{ }^{\circ}\text{C}$. Each temperature was represented by one individual sample. In addition, a 1 M glucose solution was measured at RT.

RESULTS. Figure 1 shows that the fluorescence intensity of glucose is strongly dependent on temperature and increases with decreasing temperature. It shows three distinct peak maxima. These peak maxima are dependent on temperature and are slightly shifted to lower wavelengths with decreasing temperature, as shown in Fig. 1. This is in agreement with observations made by Lakowicz and Balter [1]. For the measurement at $-263\text{ }^{\circ}\text{C}$ the emission maxima were found at 465.9 nm, 479.2 nm and 492.7 nm. In contrast to these measurements, no fluorescence of glucose was observed at RT, and only a very weak signal was found at $-73\text{ }^{\circ}\text{C}$. The fluorescence lifetime of glucose can be described by an Arrhenius like behavior and increases with decreasing temperature. No fluorescence lifetimes could be calculated at RT and at $-73\text{ }^{\circ}\text{C}$, since no or only a very weak fluorescence signal of glucose was observed, respectively. To calculate fluorescence lifetimes of glucose the TRLFS measurements with the high

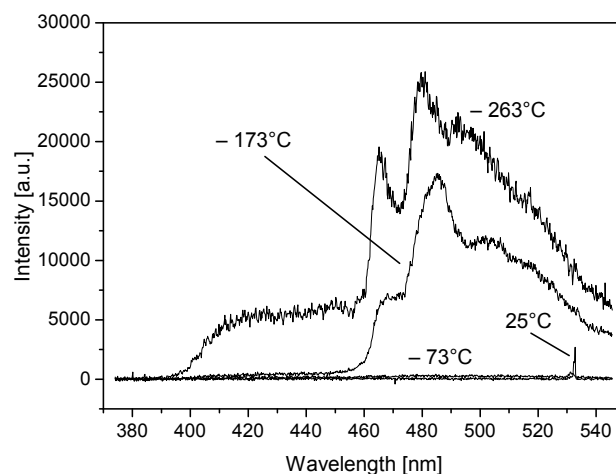


Fig. 1: Fluorescence emission spectra of glucose measured at $25\text{ }^{\circ}\text{C}$, $-73\text{ }^{\circ}\text{C}$, $-173\text{ }^{\circ}\text{C}$ and $-263\text{ }^{\circ}\text{C}$. The figure shows an increasing fluorescence intensity with decreasing temperature.

Tab. 1: Calculated fluorescence lifetimes of glucose at temperatures of $-173\text{ }^{\circ}\text{C}$ and $-263\text{ }^{\circ}\text{C}$ using an excitation wavelength of 266 nm.

| Temp. [$^{\circ}\text{C}$] | RT | -73 | -173 | -263 |
|------------------------------|----|-------|-------------------|-------------------|
| Lifetime [ns] | — | — | 552.95 ± 0.12 | 866.81 ± 0.21 |

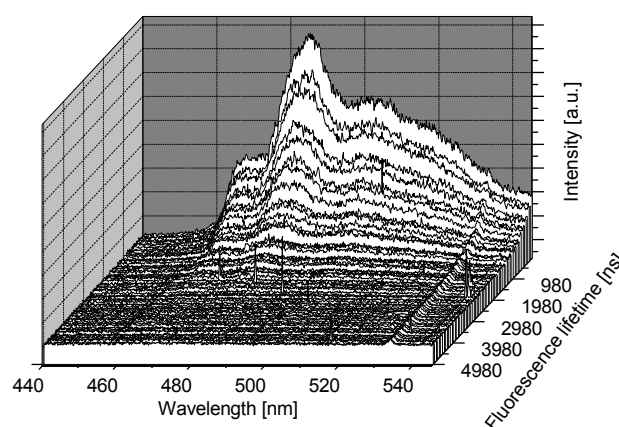


Fig. 2: TRLFS spectra of glucose measured at $-163\text{ }^{\circ}\text{C}$.

fluorescence intensities at $-173\text{ }^{\circ}\text{C}$ and $-263\text{ }^{\circ}\text{C}$ were used. For the TRLFS measurement at $-173\text{ }^{\circ}\text{C}$ a fluorescence lifetime of 553 ns and for the TRLFS measurement at $-263\text{ }^{\circ}\text{C}$ a fluorescence lifetime of 866.8 ns was calculated, as shown in Tab. 1. A TRLFS spectra of the glucose sample measured at $-163\text{ }^{\circ}\text{C}$ is shown in Fig. 2. The TRLFS signal is not related to U(VI) carbonate, since the respective lifetimes are different. The results show that glucose in biological samples can be directly studied by laser fluorescence microscopy and laser fluorescence spectroscopy.

ACKNOWLEDGMENTS. We thank the German Research Council (DFG) for financial support (project no. AR 584/1-1).

REFERENCES

[1] Lakowicz, J.R. et al. (1982) *Photochem. Photobiol.* **36**, 125-132.

The influence of the temperature on the band positions of luminescence spectra

C. Götz, G. Geipel

The influence of the temperature on the luminescence emission band positions in the uranyl phosphate system at pH 5 was investigated.

The influence of the temperature on the intensities of luminescence spectra and on the lifetimes of the luminescent species are known and well investigated [1]. The influence of the temperature on the band positions of the luminescence emission bands are firstly described in 1914 [2] for several uranyl complexes.

EXPERIMENTAL. The luminescence spectra from 10^{-5} M uranyl perchlorate, 0.1 M sodium perchlorate and 10^{-3} M phosphorous acid containing solutions at pH 5 were measured in the temperature range from 123 – 333 K. Time-resolved fluorescence spectra were recorded with an Inlite laser (Continuum; excitation wavelength: 266 nm, energy: ~ 1 mJ) and an intensified CCD camera (Roper-Scientific; delay time: varied, gate time: 100 μ s). At liquid state the quartz cuvette were cooled and heated with a temperature-controlled cuvette holder (Temperature Control Quantum Northwest) connected to a water bath circulator (Lauda RM6). In frozen state the sample was cooled with a liquid nitrogen jet. The cooling jet and the temperature were controlled by a special device (KGW Isotherm Kaltgasanlage Typ 50) and software (KGW Kaltgas Tool).

RESULTS. The luminescence spectra show four emission bands near 503, 524, 546 and 571 nm. This emission bands are assigned to the species UO_2HPO_4 [3]. For this species the temperature dependency of the emission bands in frozen state are shown in Fig. 1. The band positions decrease with increasing temperature. The shift seems to be linear, because the regression factor r^2 of linear fit mostly exceeds 0.8. In the liquid state a temperature dependency could not be found. The band positions seem to be randomly distributed. Because the observations in the different states are not in agreement, the variation of band positions at one TRLFS experiment was investigated. The error increases with the number of frame, because the intensity of the peak decreases. Figure 2 shows an example at -30°C . The relative deviation does not exceed 10 % of the FWHM (full width of half maximum) of the peak. The variation of the band positions are nearly in the same range than over the whole temperature range. So the temperature dependency observed in frozen state is doubtful. The luminescence lifetimes of this system show a similar behavior. The decreasing of the lifetime in the frozen state (Fig. 3) is in agreement with former investigations [4] and with theory, but the randomly distribution in the liquid state is not. Further investigations on the temperature dependency will provide more clarity and can explain some contradictory results.

REFERENCES

- [1] Lakowicz, J.R. (2006) *Principles of Fluorescence Spectroscopy*, Springer, Baltimore.
- [2] Nichols, E.L. et al. (1914) *Phys. Rev.* **3**, 457-463.
- [3] Narasimham, K.V. et al. (1962) *Spectroc. Acta* **18**, 1055-1058.
- [4] Steudtner, R. et al. (2006) *Report FZD-459*, p. 19.

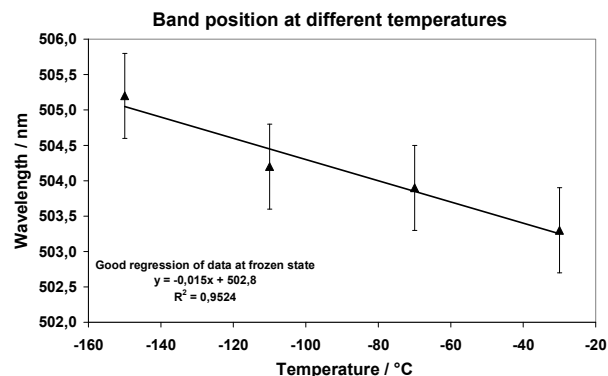


Fig. 1: Temperature dependency of band positions.

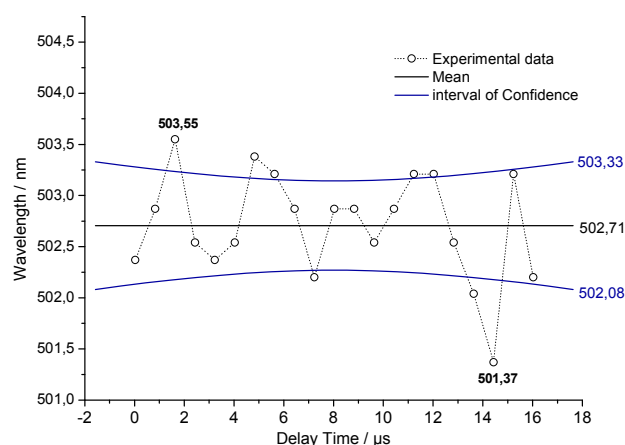


Fig. 2: Variation of band positions at one TRLFS experiment.

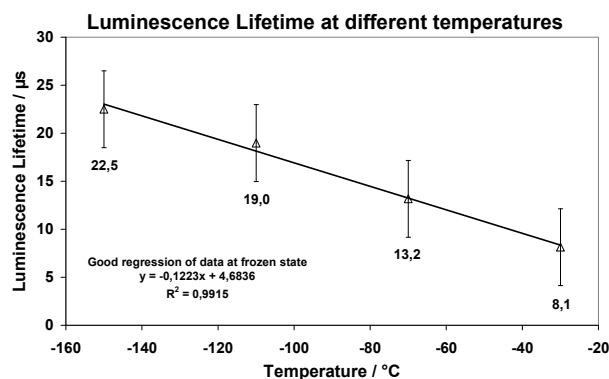


Fig.3: Temperature dependency of the fluorescence lifetime.

Infrared spectroscopic investigation of Np species in aqueous solution

K. Müller, H. Foerstendorf, V. Brendler

The first IR spectra of Np(V/VI) in low concentrated aqueous solutions are presented. We have shown that ATR-FTIR spectroscopy provides reliable data for the verification of thermodynamic speciations. In contrast to the predicted speciation, the spectroscopic results indicate the presence of different Np(VI) species in the pH range 3 – 5.9.

Current knowledge about different neptunyl species is mainly based on thermodynamic calculations relying on data obtained by non-structural experiments [1]. A spectroscopic verification of these speciations is still lacking. Up to now ATR-FTIR spectra have not been measured of neptunium (Np) in aqueous solution.

Thus, the aim of this study is the first IR spectroscopic identification of Np species, in particular in the micromolar concentration range.

EXPERIMENTAL. The diluted Np(V) and Np(VI) solutions were prepared from 0.1 M stock solutions using high purity double-deionized water.

ATR-FTIR spectra of aqueous solutions were measured on a Bruker Vertex 80/v vacuum spectrometer. The used ATR accessory is described elsewhere [2].

Sample preparation and analysis were done at room temperature (25 °C) under normal atmosphere.

RESULTS. The characteristic absorption bands of Np(V) and Np(VI) in very acidic aqueous solutions occur in the IR spectra at 817 and 964 cm^{-1} (Fig. 1). They are assigned to the asymmetric stretching vibrations of the free neptunyl ions NpO_2^+ and NpO_2^{2+} , respectively.

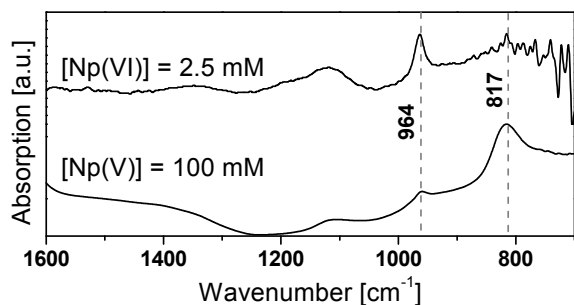


Fig. 1: ATR-FTIR spectra of aqueous Np(V) and Np(VI) solutions at pH 2.

The calculated Np(VI) speciation based on the updated NEA TDB suggests that the free NpO_2^{2+} ion is the most relevant species until pH 4, followed by the dominance of the mixed hydroxo carbonate complex until pH 6 (Fig. 2). Hydroxo complexes in solution are formed only to a very small amount (< 2%).

The Np(VI) absorption bands are observed between 1000 and 900 cm^{-1} (Fig. 3). At pH 3 the band at 964 cm^{-1} is assigned to the free species NpO_2^{2+} . At pH 4 to 4.6 this band is split and shows up at 964 and 927 cm^{-1} . Simultaneously, two bands at 1525 and 1460 cm^{-1} become apparent which are tentatively assigned to coordinated water molecules. A similar behavior was observed for the U(VI) speciation and is assigned to the formation of a trimer hydroxo complex [2]. This is contradictory to the calculated speciation.

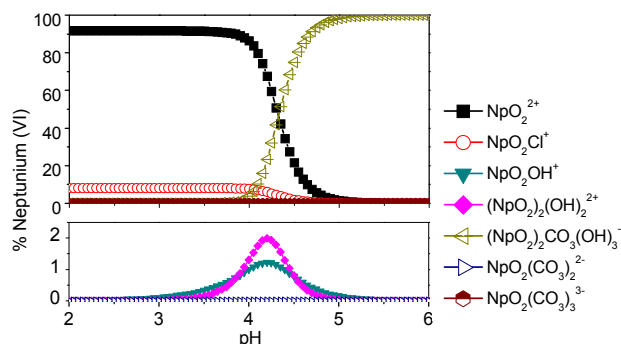


Fig. 2: Np(VI) speciation computed with EQ 3/6 (500 μM Np(VI), 0.1 M NaCl, normal atmosphere).

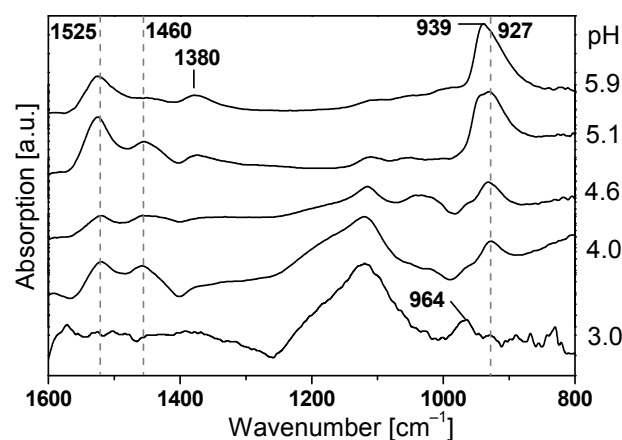


Fig. 3: ATR-FTIR spectra of aqueous Np(VI) solutions at different pH (500 μM Np(VI), 0.1 M NaCl, normal atmosphere).

At pH 5.1 a band at 939 cm^{-1} appears as a shoulder and becomes dominant at pH 5.9. In these spectra a band at 1380 cm^{-1} obviously correlates with the $\nu_{\text{as}}(\text{NpO}_2)$ at 939 cm^{-1} . This spectrum may represent the complexation of Np(VI) with a carbonate ligand as it is predicted by the calculated speciation.

The broad band ranging from 1250 to 1050 cm^{-1} is assigned to residual perchlorate in solution.

ACKNOWLEDGEMENTS. The study is supported by the Deutsche Forschungsgemeinschaft, Grant FO 619/1-1.

REFERENCES

- [1] Guillaumont, R. et al. (2003) *Update on the Chemical Thermodynamics of U, Np, Pu, Am and Tc*, Elsevier, Amsterdam.
- [2] Müller, K. et al. (2007) *Report FZD-459*, p.11-12.

Complexation of Cm(III) with hydroxamic acids investigated by TRLFS

M. Glorius, H. Moll, G. Bernhard

The complex formation of Cm(III) with salicylhydroxamic (SHA) and benzohydroxamic acid (BHA) was studied by time-resolved laser-induced fluorescence spectroscopy (TRLFS). An indirect excitation mechanism for the Cm(III) fluorescence was observed. The stability constants determined either by indirect (360 nm) or direct (395 nm) excitation are consistent.

In continuation of our studies investigating the complexation of pyoverdin model compounds with U(VI) and to address the lack of studies of the complexation of hydroxamic acids with trivalent actinides, this work is focused on the complex formation of two hydroxamic acids with Cm(III) [1]. We want to explore the fluorescence properties and lifetimes of the formed Cm(III) species. Furthermore, we want to determine and compare the stability constants obtained either by indirect (360 nm) or direct (395 nm) excitation of the Cm(III) fluorescence.

EXPERIMENTAL. The fluorescence spectroscopy experiments were carried out at fixed Cm(III) concentration of $3 \cdot 10^{-7}$ M as a function of the ligand concentration (10^{-5} M to 10^{-3} M) between pH 2 and 9. The ionic strength was adjusted to 0.1 M (NaClO₄). The experiments were performed under N₂ atmosphere at 25 °C. The TRLFS spectra were recorded using a flash lamp pumped Nd:YAG-OPO laser system (Continuum). Details on the experimental set-up are summarized in [1].

RESULTS. The fluorescence emission spectra of $3 \cdot 10^{-7}$ M Cm(III) with $1.5 \cdot 10^{-4}$ M BHA as a function of

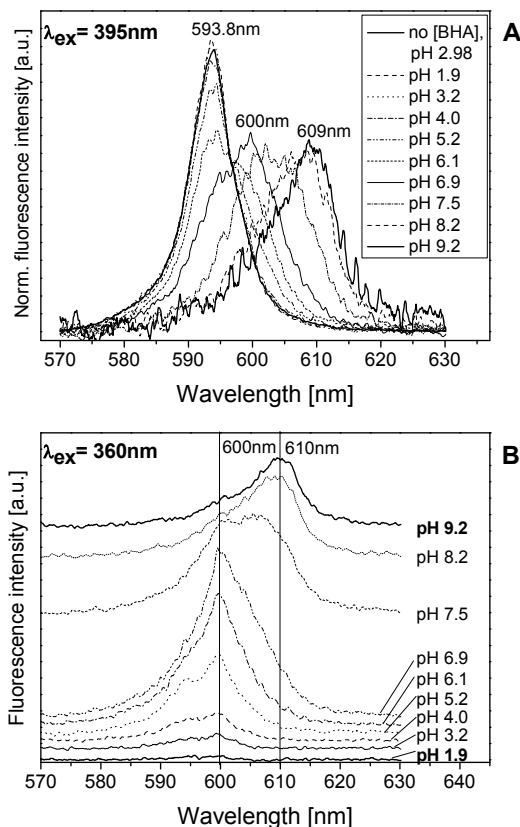


Fig. 1: Fluorescence emission spectra of $3 \cdot 10^{-7}$ M Cm³⁺ and $1.5 \cdot 10^{-4}$ M BHA as a function of pH at an excitation wavelength of 395 nm (A) and 360 nm (B).

pH at an excitation wavelength of 395 and 360 nm are shown in Fig. 1A and B, respectively.

In both hydroxamic acid-Cm(III) systems we observed at an excitation wavelength of 395 nm a pronounced red shift of the emission maxima with increasing pH from the characteristic emission maximum of the Cm³⁺ aqua ion at 593.8 nm via 600 nm to an emission maximum at 608 nm. This indicates the complex formation between Cm(III) and both ligands. At an excitation wavelength of 360 nm (Fig. 1B) we identified an increasing fluorescence intensity and red shift of the emission maxima with increasing pH. From this we can conclude that the concentration of the Cm(III)-hydroxamate species increased with increasing pH. So, the fluorescence properties of Cm(III)-hydroxamate complexes can be also determined by an excitation at 360 nm via an energy transfer from the hydroxamate molecule to the Cm(III). The complexation is accompanied by an increase of the fluorescence emission lifetime. The determined emission maxima, lifetimes and stability constants are summarized in Tab. 1.

Tab. 1: Summary of emission maxima, lifetimes, complex stability constants log β and log k of the identified Cm(III) complexes (L = C₆H₄CONHO).

| Ligand | Cm ³⁺ | SHA | | BHA | |
|--|------------------|-----------------------|--------------|-------------------|-------------------------------|
| Complex M _p L _q H _r | | Cm[LOH] ²⁺ | Cm[LOH,LO] | CmL ²⁺ | CmL ₂ ⁺ |
| p q r | 100 | 111 | 121 | 110 | 120 |
| Emission [nm] | 593.8 | 600 | 608 | 600 | 609 |
| Lifetime [μs] | 68 (1) | 80 (5) | 200 (28) | 85 (8) | 150 (23) |
| log β | | 16.52 (0.14) | 24.09 (0.62) | 6.52 (0.19) | 11.60 (0.50) |
| log K | | 6.47 | 14.04 | 6.52 | 11.60 |

The stability constants determined either by indirect (360 nm) or direct (395 nm) excitation of the Cm(III) fluorescence are consistent and show the applicability of the indirect excitation to determine complex formation equilibria. The log K values of the 1 : 1 complexes of SHA and BHA show, that the two hydroxamic acids form 1 : 1 complexes with curium(III) with similar stability. In case of the 1 : 2 complexes BHA has a lower stability constant than SHA, which indicates a stronger complex formation of Cm(III) with SHA. The larger stability constant of SHA are probably caused by the influence of the additional phenolic OH group.

The complex formation constants of the Cm(III)-pyoverdin species identified by Moll et al. [2] are larger than the constants of the hydroxamic acids. This might be due to the different structure of the pyoverdins and the larger number of functional groups in these molecules in comparison to the hydroxamic acids. The results contribute to a better understanding of the speciation and mobilization of trivalent actinides by hydroxamate compounds by exploring their fluorescence properties.

ACKNOWLEDGEMENTS. This work was funded by the BMWi under contract number 02E9985.

REFERENCES

- [1] Glorius, M. et al. (2008) *Polyhedron*, submitted.
- [2] Moll, H. et al. (2008) *BioMetals*, in press.

Curium(III) complexation with pyoverdins secreted by a groundwater strain of *Pseudomonas fluorescens*

H. Moll, A. Johnsson,¹ K. Pedersen,¹ G. Bernhard

¹Department of Cell and Molecular Biology, Göteborg University, Göteborg, Sweden

The interaction between Cm(III) and pyoverdins was studied using time-resolved laser-induced fluorescence spectroscopy (TRLFS). Three Cm^{3+} -*P. fluorescens* (CCUG 32456) pyoverdin species, CmH_2L^+ , CmHL , and CmL^- , with large formation constants of $\log \beta_{121} = 32.50 \pm 0.06$, $\log \beta_{111} = 27.40 \pm 0.11$, and $\log \beta_{101} = 19.30 \pm 0.17$ could be identified.

Pyoverdins (LH_4) bacterial siderophores produced by ubiquitous fluorescent *Pseudomonas* species, have great potential to bind and thus transport actinides in the environment. Therefore, the influence of pyoverdins secreted by microbes on the migration processes of actinides must be taken into account in strategies for the risk assessment of potential nuclear waste disposal sites. The unknown interaction between Cm(III) and the pyoverdins released by *P. fluorescens* (CCUG 32456) isolated from the granitic rock aquifers at the Äspö Hard Rock Laboratory (Äspö HRL), Sweden, is the subject of this study.

EXPERIMENTAL. The TRLFS experiments were performed under N_2 atmosphere at 25 °C. The $[\text{Cm(III)}]$ was fixed to $3 \cdot 10^{-7}$ M. TRLFS spectra were recorded using a pulsed flash lamp pumped Nd:YAG-OPO laser system. Details on the experimental set-up and the sample preparation are summarized in [1].

RESULTS. An overview of the emission spectra of $3 \cdot 10^{-7}$ M Cm(III) in 0.1 M NaClO_4 measured in the *P. fluorescens* (CCUG 32456) pyoverdin system is presented in Fig. 1.

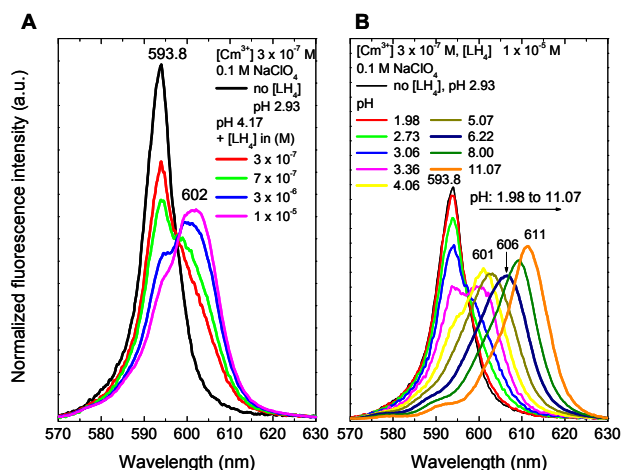


Fig. 1 Fluorescence emission spectra of $3 \cdot 10^{-7}$ M Cm(III) in 0.1 M NaClO_4 measured as a function of the pyoverdin concentration, LH_4 , at pH 4.17 (A); and at a fixed pyoverdin concentration of $[\text{LH}_4] 1 \cdot 10^{-5}$ M as a function of pH (B).

The complexation of curium(III) with these bioligands had started even at pH 4.2 and low pyoverdin concentrations of $3 \cdot 10^{-7}$ M. This is depicted in Fig. 1A by the decreased emission band of Cm^{3+} (aq) at 593.8 nm and the formation of a shoulder at 602 nm. A pyoverdin concentration of $3 \cdot 10^{-7}$ M lies in the range of hydroxamate siderophores identified in a variety of different soils [2]. Figure 1B presents the changes observed in the emission

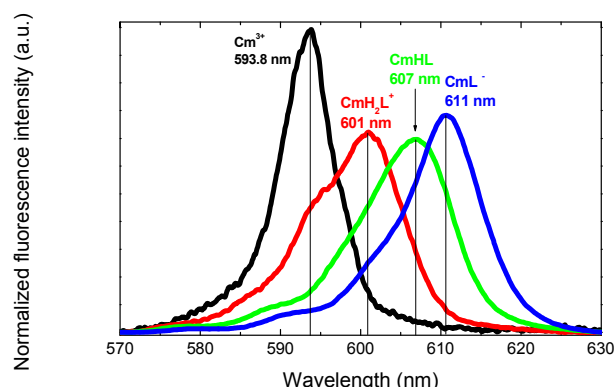


Fig. 2: Fluorescence emission spectra of the single components in the Cm^{3+} -*P. fluorescens* (CCUG 32456) pyoverdin – system, as derived by peak deconvolution using SPECFIT. The spectra are scaled to the same peak area.

spectra at fixed concentrations of Cm(III) and pyoverdin of $3 \cdot 10^{-7}$ M and $1 \cdot 10^{-5}$ M, respectively, as a function of pH. Three different complex species can be differentiated on the basis of their individual emission bands at 601, 606, and 611 nm.

The spectral changes detected were used in the SPECFIT factor analysis program to describe the complex formation reactions occurring in the Cm^{3+} -*P. fluorescens* (CCUG 32456) pyoverdin (LH_4) system. In light of relevant complexation studies of pyoverdin-type bioligands with metals [3,4], and taking into consideration the deprotonation of the pyoverdin molecule, possible Cm(III)-pyoverdin species of the $\text{M}_p\text{H}_q\text{L}_r$ type were introduced into the data analysis procedure. As a result, the variations observed in the emission data (see Fig. 1) could be described by the following equilibria:



Formation constants for reactions (1) - (3) were calculated to be $\log \beta_{121} = 32.50 \pm 0.06$, $\log \beta_{111} = 27.40 \pm 0.11$, and $\log \beta_{101} = 19.30 \pm 0.17$, respectively. The corresponding single-component spectra of the individual species are summarized in Fig. 2.

Strong Cm^{3+} pyoverdin species are formed, indicating the great potential of these unique siderophores to mobilize Cm(III) in the biologically relevant pH range.

ACKNOWLEDGEMENTS. This work was funded by BMWi under contract number 02E9985.

REFERENCES

- [1] Moll, H. et al. (2008) *BioMetals*, in press.
- [2] Powell, P.E. et al. (1980) *Nature* **287**, 833-834.
- [3] Albrecht-Gary, A.M. et al. (1994) *Inorg. Chem.* **33**, 6391-6402.
- [4] Bouby, M. et al. (1999) *Czech. J. Phys.* **49**, 147-150.

Complexation of Eu(III) with urea investigated by TRLFS

A. Heller, A. Barkleit, G. Bernhard

The interaction of urea with europium (Eu^{3+}) in aqueous solution was studied by time-resolved laser-induced fluorescence spectroscopy at various urea concentrations between 0.1 and 5.0 M over a pH range from 2 to 8. It was found that complexation enhances Eu^{3+} fluorescence and that a complex with a lifetime longer than the Eu^{3+} -aquo-ion is formed.

In case of accidental release of trivalent actinides, little is known about their metabolism in the human organism. Therefore, the speciation and complexation in body fluids and particular components needs to be investigated. Europium is a trivalent lanthanide with very good fluorescence properties. It resembles radioactive actinides like curium and actinium due to its analog electronic configuration and similar chemical properties. Urea is the most abundant organic component of mammal urine and the final product of amino acid/protein metabolism and plays a crucial role in ammonia detoxication.

EXPERIMENTAL. The TRLFS measurements were performed under inert gas (N_2) at room temperature and a constant ionic strength of 0.1 (NaClO_4). The total europium concentration was fixed at $3 \cdot 10^{-5}$ M, the urea concentration was varied between 0.1 and 5 M and the pH ranged between 2 and 8. Spectra were analyzed using SPECFIT and ORIGIN to determine the stability constant and the lifetimes, respectively.

RESULTS. The spectra of sole europium in aqueous solution show no differences up to pH 7 with peaks at 591.3 ± 0.1 and 616.7 ± 0.1 nm (literature: 593 and 617 nm [1]). Due to hydroxide formation, the fluorescence intensity and shapes of the peaks change starting at pH 8 (see Fig. 1). The lifetime and number of water molecules in the first coordination sphere (using the equation given by [2]) were determined to be 110.8 ± 4 μs and 9.1, respectively (literature: 110 ± 10 μs and 9 [1]). Addition of urea causes no changes in the Eu^{3+} spectrum when the concentration is below 0.5 M, but adding more ligand results in an increase in fluorescence and the development of a third peak at 612.2 ± 0.1 nm (see Fig. 2) while the positions of the other two peaks remain unef-

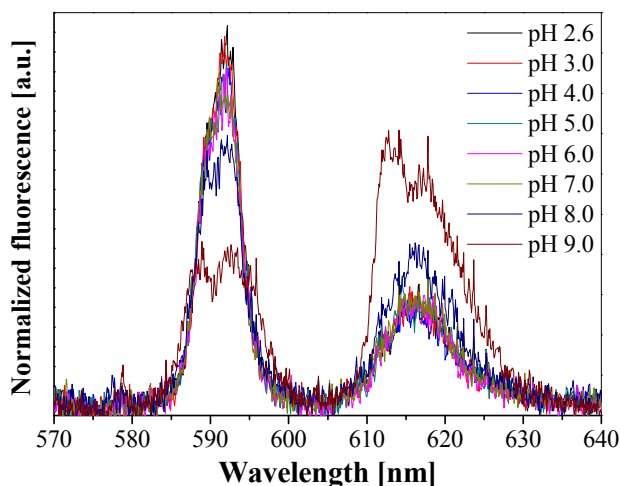


Fig. 1: Fluorescence spectra of the Eu^{3+} -aquo-ion at a fixed europium concentration of $3 \cdot 10^{-5}$ M in dependence of pH.

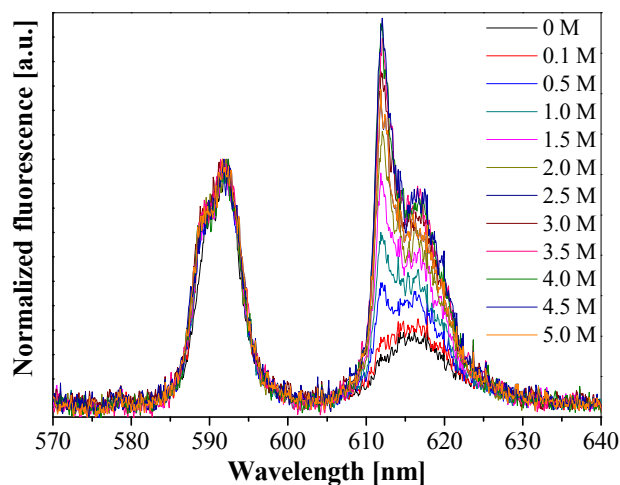


Fig. 2: Fluorescence spectra with urea at a fixed europium concentration of $3 \cdot 10^{-5}$ M and a fixed pH of 4.0 in dependence of the ligand concentration.

ected. At a concentration of 2.5 M urea the complex formation is completed and further ligand addition shows no spectral effects. With more than 120 μs the complex exhibits a longer lifetime than the Eu^{3+} -aquo-ion. In case an 1 : 1 complex is formed, what is most likely, the stability constant was calculated to be $\log \beta = -0.08$, but the number of urea molecules bound to the Eu^{3+} in this complex could not be clarified and is still under investigation. The spectra with 1.0 M urea at various pH show that the complex is stable over a wide range (see Fig. 3). Formation of Eu-hydroxides is observed at $\text{pH} \geq 7$ resulting in an increased fluorescence intensity and the appearance of an additional peak at 578.3 nm (literature: 580 nm [1]).

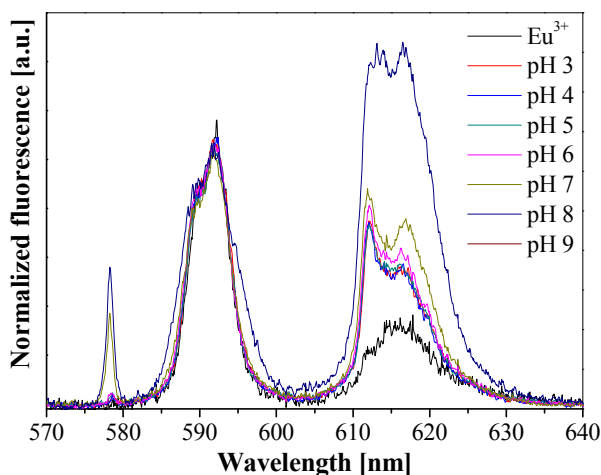


Fig. 3: Fluorescence spectra with urea at a fixed europium concentration of $3 \cdot 10^{-5}$ M and a fixed ligand concentration of 1.0 M in dependence of pH.

ACKNOWLEDGEMENTS. This work was funded by the Deutsche Forschungsgemeinschaft (BE 2234/10-1).

REFERENCES

- [1] Planque, G. et al. (2003) *Anal. Chim. Acta* **478**, 11.
- [2] Kimura, T. et al. (1996) *Radiochim. Acta* **72**, 61-64.

New tripodal polyamines as potential extracting agents for lanthanides and actinides

H. B. Tanh Jeazet, M. Wenzel, Ke. Gloe,¹ G. Geipel, G. Bernhard, K. Gloe¹

¹Department of Chemistry and Food Chemistry, Dresden University of Technology, Dresden, Germany

Liquid-liquid extraction studies of Eu^{3+} and UO_2^{2+} have been carried out using new synthesized tripodal polyamine ligands as complexing agents. A combination of the ligands with octanoic acid as co-ligand leads to an increase of the extraction performance for both metal ions.

The increasing amount of radioactive waste materials caused by nuclear energy production has created a strong interest to study the partition of minor trivalent actinides, An (americium and curium), from trivalent lanthanides, Ln. A promising topic is to search for extractants suited to separate selectively actinides from lanthanides, and then to allow the subsequent transmutation of actinides into short-lived elements. Some sulfur and nitrogen donor containing ligands give high separation factors for An(III) over Ln(III) [1-3]. Tripodal pyridine ligands are promising ligand systems for effective separation of An(III) from Ln(III) [4]. In order to increase the selectivity of actinides over lanthanides, we have designed new tripodal ligands containing more flexible spacer units. We report herein the liquid-liquid extraction of Eu^{3+} and UO_2^{2+} using the synthesized ligands 1-4 (Fig. 1).

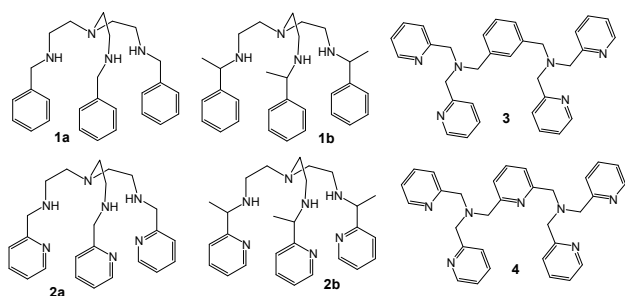


Fig. 1: Examples of tripodal polyamine ligands studied.

EXPERIMENTAL. The ligands were synthesized as previously reported [5-7].

The liquid-liquid extraction experiments were performed at 23 ± 1 °C in microcentrifuge tubes (2 mL) by means of mechanical shaking. The phase ratio $V_{(\text{org})} : V_{(\text{aq})}$ was 1 : 1 (0.5 mL each). The shaking time chosen was 30 minutes for Eu^{3+} and 3 hours for UO_2^{2+} . The extraction equilibrium was reached in all cases during this period. After extraction, all samples were centrifuged and the phases separated. The determination of the metal concentrations in both phases was carried out radiometrically by γ -radiation of ^{152}Eu with a NaI(Tl)-scintillation counter (Cobra II/Canberra-Packard) while that of UO_2^{2+} in the aqueous phase was made by means of ICP-MS method.

RESULTS AND DISCUSSION. The extraction behavior of the synthesized ligands towards Eu^{3+} and UO_2^{2+} was studied using the extraction system $\text{Eu}(\text{NO}_3)_3$ or $\text{UO}_2(\text{NO}_3)_2$ -buffer- H_2O /ligand (co-ligand)- CHCl_3 . This system allows a high selectivity for UO_2^{2+} over Eu^{3+} . Figure 2 shows an overview of the extraction strength for all the ligands studied in presence or in absence of the co-ligand. In each case, the distribution ratio of UO_2^{2+} was higher than that of Eu^{3+} . This tendency reflects the fact that these tripodal ligands favour UO_2^{2+} over Eu^{3+} bind-

ing. The influence of pH on the extraction of Eu^{3+} by the ligands was investigated. The results for **2a** and **3** are shown in Fig. 2. With increasing pH, the extractabilities significantly increase. The maximum extraction is reached between pH 6.5 and 7. This trend is in agreement with the changing protonation state of the ligands. At lower pH values the ligands will be highly protonated, and thus more hydrophilic, leading to a decrease in the extraction behaviour.

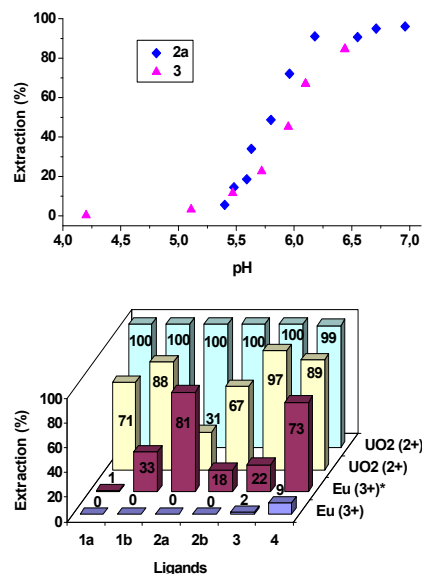


Fig. 2: Extraction of Eu^{3+} and UO_2^{2+} with tripodal polyamine ligands (bottom) and extraction of Eu^{3+} as a function of pH in presence of RCOOH (top). [L] = 0.01 M, $[\text{RCOOH}] = 0.01$ M in CHCl_3 ; $[\text{Eu}^{3+}] = [\text{UO}_2^{2+}] = 10^{-4}$ M, $[\text{NaNO}_3] = 5 \cdot 10^{-3}$ M, pH 5,4 (MES/NaOH buffer); RCOOH = octanoic acid

Further Eu^{3+} extraction studies were done in dependence on the extractant (ligand + co-ligand) concentration. From these studies the preferred composition of the extracted complexes can be deduced using $\text{Log}D_{\text{Eu}}\text{-Log}[L]$ and $\text{Log}D_{\text{Eu}}\text{-Log}[\text{RCOOH}]$ diagrams (Fig. 3). The following compositions for $\text{Eu}:\text{L}:\text{RCOO}$ has been obtained: 1 : 3 : 2 for **2a**, 1 : 2 : 2 for **2b** and 1 : 1 : 3 for **1b**.

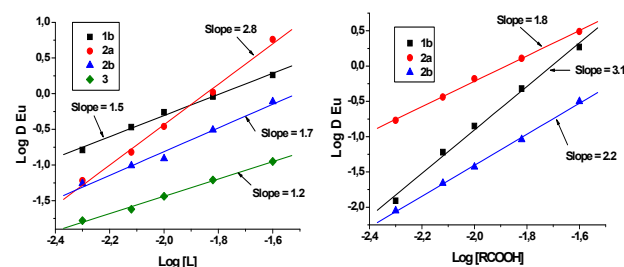


Fig. 3: Extraction of Eu^{3+} as a function of ligand (left) or co-ligand (right) concentration. $[\text{Eu}^{3+}] = 10^{-4}$ M, $[\text{NaNO}_3] = 5 \cdot 10^{-3}$ M, pH 5.4 (MES/NaOH buffer); [Ligand] or [RCOOH] = $5 \cdot 10^{-3}$ M... $2.5 \cdot 10^{-2}$ M in CHCl_3 ; RCOOH = octanoic acid.

REFERENCES

- [1] Zhu, Y. et al. (1995) *Radiochim. Acta*, **68**, 95-98.
- [2] Modolo, G. et al. (1999) *Solv. Extr. Ion Exch.* **17**, 33-53.
- [3] Karmazin, L. et al. (2002) *Chem. Commun.* **23**, 2892-2893.
- [4] Ishimori, K. et al. (2005) *Chem. Lett.* **34**, 1112-1113.
- [5] Naiini, A. A. et al. (1991) *Inorg. chem.* **30**, 5009-5012.
- [6] Deroche, A. et al. (1996) *J. Am. Chem. Soc.* **118**, 4567-4573.
- [7] Antonioli, B. (2007) Thesis, p. 117-136, Dresden University of Technology, Dresden.

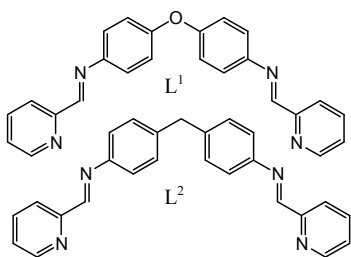
Novel expanded circular helicates formed by copper(II) sulfate and bis-pyridylimine ligands

H. B. Tanh Jeazet, A. Jäger,¹ O. Kataeva,^{2,3} Ke. Gloe,¹ G. Geipel, G. Bernhard, B. Büchner,³ K. Gloe¹

¹Department of Chemistry and Food Chemistry, Dresden University of Technology, Dresden, Germany; ²A.E. Arbusov Institute of Organic and Physical Chemistry, Kazan, Russia; ³Leibniz Institute for Solid State and Materials Research, Dresden, Germany

Novel hexanuclear circular helicate structures resulting from coordination of copper(II) by sulfate and bis-pyridylimine ligands that contain a bis(4-aminophenyl)ether or a bis(4-aminophenyl)methane spacer group have been synthesized and characterized.

The supramolecular synthetic approach permits the design of arrays with complex molecular architectures whose dimensions are greater than those found in traditional covalent-based chemistry [1]. Double-helical molecular architectures have been included in the development of supramolecular chemistry by providing a forum for establishing construction principles [2]. Dimeric M_2L_2 systems (helicates and boxes) [3] and tetrameric M_4L_4 systems (squares and tetrahedra) [4] are well established supramolecular architectures whereas the assembly of hexagonal M_6L_6 arrays are rare. The hexagone represents an important architectural element because of the many polyhedra that are based on this unit. The hexamer also represents the lowest possible nuclearity of circular helicates. Herein we describe a novel and general strategy for the construction of hexanuclear circular helicates (**I** and **II**) with copper(II) using bis-bidentate Schiff base ligands, bis[4-(2-pyridylmethyleneamino)phenyl]ether (**L**¹), and bis[4-(2-pyridylmethyleneamino)phenyl]methane (**L**²). Some trinuclear circular helicates were previously reported with structure analogous ligands [5].



EXPERIMENTAL. Ligands **L**¹ and **L**² were prepared via the previously reported method [6].

Synthesis of $[Cu(L^1)SO_4]_6$ (**I**)

Copper sulfate hexahydrate (6.6 mg, 0.03 mmol) in water/acetonitrile (1.5 mL) was added to **L**¹ (15.0 mg, 0.04 mmol) in a mixture methanol/acetonitrile (1 : 1; 1 mL). Dark green needles of the title compound were obtained by slow diffusion of diethylether into the resulting solution after 2 months. The crystals were collected, washed with ether, and dried under vacuum. Found: C, 48.22 %; H, 4.28 %; N, 9.04 %; S, 5.57 %. Cal. for $[Cu(L^1)SO_4]_6 \cdot 18H_2O$; C, 48.69 %; H, 4.09 %; N, 9.46 %; S, 5.42 %.

Synthesis of $[Cu(L^2)SO_4]_6$ (**II**)

The same procedure was used as for the preparation of (**I**). The complex (green block crystals) was obtained after 3 days. Found: C, 49.63 %; H, 3.61 %; N, 9.19 %; S, 5.20 %. Cal. for $[Cu(L^2)SO_4]_6 \cdot 24H_2O$; C, 49.38 %; H, 4.64 %; N, 9.21 %; S, 5.27 %.

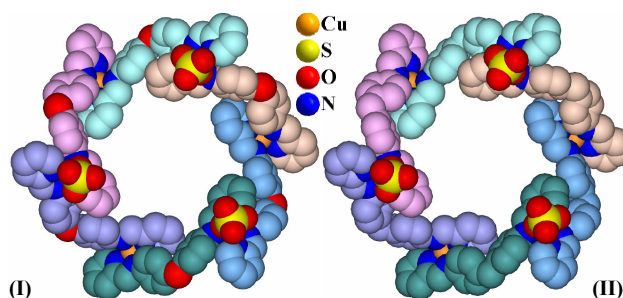


Fig. 1: Space-filling representation of the hexanuclear circular helicates $[Cu(L^1)SO_4]_6$ (**I**) and $[Cu(L^2)SO_4]_6$ (**II**). For clarity, hydrogens are omitted.

RESULTS AND DISCUSSION. The self-assembly of **L**¹ and **L**² with $CuSO_4$ led to the formation of two hexanuclear circular helicates (**I**) and (**II**). These complexes crystallize both in the space group $R\bar{3}$ as determined uniquely by the pattern of systematic absences in the intensity data. The asymmetric unit contains six Cu(II) ions, six ligand molecules and six SO_4^{2-} anions. The structures of these complexes are shown in Fig. 1.

In these complexes, each Cu(II) ion is coordinated by two ligands via pyridyl and imine nitrogen atoms and one chelating sulfate anion. Thus, a distorted octahedral configuration is observed around the metal centers in the complexes. The Cu-N_{pyridyl} bond lengths are in the range 2.014(3)–2.031(3) Å, while the Cu-N_{imine} bond distances lie in the range 2.051(4)–2.271(3) Å. The bite angles of N_{pyridyl}–Cu–N_{imine} are in the range 78.09(11)°–80.12(15)°. The Cu–OSO₃ bond lengths are in the range 1.961(5)–2.796(3) Å. The radii of the hexagonal cavities formed (half distance between two opposite copper ions) are approximately 10.70 Å for (**I**) and 10.78 Å for (**II**). The distance between two neighboring copper ions are respectively 12.48 and 12.52 Å for (**I**) and (**II**) with Cu···O···Cu and Cu···CH₂···Cu angles of 123.21° and 119.46°. The cavities contain disordered water molecules. These architectures are organised readily utilizing weak face-to-face and edge-to-face π -interactions.

REFERENCES

- [1] Lehn, J. M. (1995) *Supramolecular Chemistry – Concepts and Perspectives*, Wiley-VCH, Weinheim.
- [2] Hannon, J. M. et al. (2004) *Supramol. Chem.* **1**, 7–22.
- [3] Bilyk, A. et al. (1994) *J. Chem. Soc. Dalton Trans.* **19**, 2783–2790.
- [4] Parac, T. N. et al. (1998) *J. Am. Chem. Soc.* **120**, 8003–8004.
- [5] Hannon, M. J. et al. (2007) *Chem. Eur. J.* **13**, 9286–9296.
- [6] Cheng, H. et al. (2000) *J. Chem. Soc. Dalton Trans.* **14**, 2419–2424.

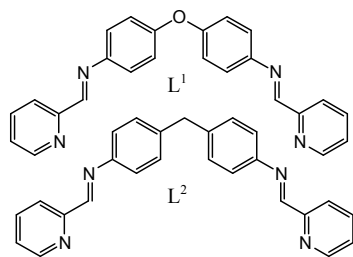
The architecture of self-assembled silver(I) complexes with bis-pyridylimine ligands: From coordination polymers to molecular boxes

H. B. Tanh Jeazet, A. Jäger,¹ A. Heine,¹ M. Wenzel, Ke. Gloe,¹ G. Geipel, G. Bernhard, K. Gloe¹

¹Department of Chemistry and Food Chemistry, Dresden University of Technology, Dresden, Germany

The self-assembly and structural characterization of the new silver(I) coordination polymers $\{[Ag(L^1)]ClO_4 \cdot CH_2Cl_2\}_n$ (I), $\{[Ag(L^2)](ClO_4) \cdot CH_3CN\}_n$ (III) and the molecular box $[Ag_2(L^1)_2](ClO_4)_2$ (II) have been achieved. These complexes are derived from the bis-bidentate Schiff base ligands bis[4-(2-pyridylmethyleneamino)phenyl]ether (L^1) and bis[4-(2-pyridylmethyleneamino)phenyl]methane (L^2).

There is a considerable current interest in the self-assembly approach and its application to control the molecular architecture [1]. The Ag(I) ion is regarded as a soft acid that favours the coordination of soft bases, such as ligands that contain sulfur, pyridine or imine nitrogen [2]. Many topologically promising Ag(I) containing architectures have been synthesized using bidentate building blocks containing different nitrogen donors [3]. One important tool of self-organisation has been the design of ligands which induces cooperative behaviour of coordination bonds and weak non-covalent interactions. From this point of view, a new type of bis-bidentate ligands has been developed [4-8]. Bis[4-(2-pyridylmethyleneamino)phenyl] ether, (L^1) and bis[4-(2-pyridylmethyleneamino)phenyl]methane (L^2), are such compound designed as multidentate ligands for coordination of heavy metal ions. As part of our ongoing studies on the design and preparation of functional materials, we report herein on the self-assembly of the Ag(I) coordination polymers I and III and of the discrete molecular box II with the Schiff base ligands L^1 and L^2 . Similar structures with these ligands were reported previously [7,8].



EXPERIMENTAL. Ligands L^1 and L^2 were prepared via the previously reported method [7,8].

Synthesis of $\{[Ag(L^1)]ClO_4 \cdot CH_2Cl_2\}_n$ (I)

Silver perchlorate (11.0 mg, 0.05 mmol) in acetonitrile (1 mL) was added to L^1 (20.0 mg, 0.05 mmol) in dichloromethane (1 mL). Pale yellow needles of the title compound were obtained by slow diffusion of diethylether vapour into the resulting solution in the dark after 3 days. The crystals were collected, washed with ether, and dried under vacuum. Yield, 27 mg (87.21 %). Found: C, 48.68 %; H, 2.53 %; N, 9.38 %. Cal. for $[Ag(C_{24}H_{18}N_4O)]ClO_4$; C, 49.21 %; H, 3.10 %; N, 9.57 %. MS (ESI) m/z : 863, $[AgL_2]^+$ and 485, $[Ag_2L_2]^{2+}$.

Synthesis of $[Ag_2(L^1)_2](ClO_4)_2$ (II)

Same preparation as for (I), but L^1 was dissolved in the mixture methanol/acetonitrile 1 : 1 (1 mL). Yield, 19 mg (61.37 %). Found: C, 48.89 %; H, 2.80 %; N, 9.51 %. Cal. for $[Ag_2(C_{24}H_{18}N_4O)_2](ClO_4)_2$; C, 49.21 %; H, 3.10 %; N, 9.57 %. MS (ESI) m/z : 911, $[Ag_2L(ClO_4)]^+$

$H_2O + HClO_4]^+$; 610, $[AgLOAC + 2MeOH + H]^+$; and 485, $[Ag_2L_2]^{2+}$.

Synthesis of $\{[Ag(L^2)](ClO_4) \cdot CH_3CN\}_n$ (III)

Same preparation as for (I). Yield, 17 mg (54.80 %). Found: C, 50.98 %; H, 3.35 %; N, 9.39 %. Cal. for $[Ag(C_{25}H_{20}N_4)]ClO_4$; C, 51.44 %; H, 3.45 %; N, 9.60 %.

RESULTS AND DISCUSSION. The self-assembly of L^1 and L^2 with $AgClO_4$ led to the formation of coordination polymers (I), (III) with a 1D zigzag structure and the molecular box (II). The asymmetric unit of (I) and (II) contains one Ag atom, one independent ligand, one dichloromethane [in (I)] or acetonitrile [in (III)] molecule and a ClO_4^- anion while that of (II) consists of a dimeric Ag(I) complex cation, and two perchlorate anions. The structures of these complexes are shown in Fig. 1.

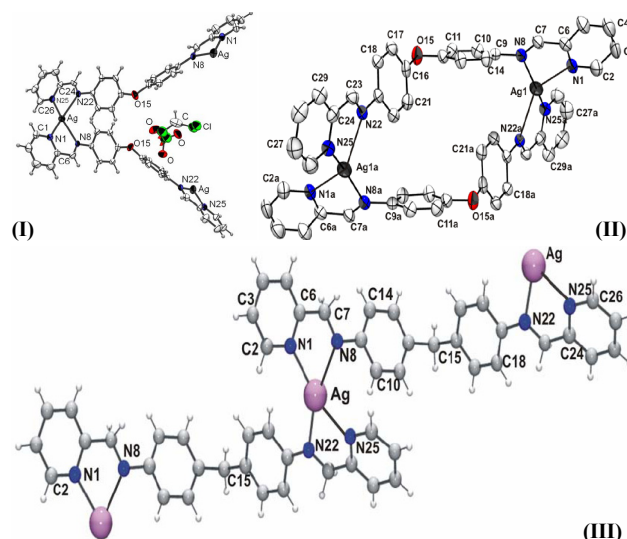


Fig. 1: Local coordination environment of Ag(I) in (I), (II) and (III). Atoms are represented as 50 % thermal ellipsoids.

In these complexes, the Ag(I) ions are coordinated by two Schiff base ligands via pyridyl and imine nitrogen atoms. In contrast to this the cationic molecular box (II) consists in two Ag(I) and two Schiff base ligands L^1 . A four-coordinated distorted tetrahedral configuration is observed around the metal center in all complexes. The $Ag-N_{pyridyl}$ bond lengths are in the range 2.252(3)-2.429(3) Å, while the $Ag-N_{imine}$ bond distances lie in the range 2.307(4)-2.462(3) Å. The bite angles of $N_{pyridyl}-Ag-N_{imine}$ are in the range 71.01(14)°- 72.86(18)°. Also, weak hydrogen bonds, edge-to-face and face-to-face π -interactions play an important role in the self-assembly process.

REFERENCES

- [1] Philp, D. et al. (1996) *Angew. Chem., Int. Ed. Engl.* **35**, 1154-1196.
- [2] Huang-Chun, W. et al. (2006) *Inorg. Chem.* **45**, 295-303.
- [3] Muthu, S. et al. (2002) *J. Chem. Soc. Dalton Trans.* **24**, 4561-4568.
- [4] Enemark, E. J. et al. (1995) *Angew. Chem., Int. Ed. Engl.* **34**, 996-998.
- [5] Albrecht, M. et al. (1996) *Chem. Eur. J.* **2**, 1264-1268.
- [6] Albrecht, M. et al. (1996) *Chem. Commun.* **20**, 2309-2310.
- [7] Cheng, H. et al. (2000) *J. Chem. Soc., Dalton Trans.* **14**, 2419-2424.
- [8] Tesouro Vallina, A. et al. (1999) *Chimia* **53**, 342-343.

Actinides in bio-systems

Uranyl complexation with lipopolysaccharide investigated by TRLFS

A. Barkleit, H. Moll, G. Bernhard

We investigated the interaction of the uranyl cation (UO_2^{2+}) with lipopolysaccharide (LPS) from *Pseudomonas aeruginosa* S10 by using time-resolved laser-induced fluorescence spectroscopy (TRLFS) over a wide pH range (2.5 – 8.0) and at an environmentally relevant low uranium concentration (10^{-5} M). As a result, we determined two UO_2^{2+} -LPS complexes. The uranyl ion is exclusively coordinated to the phosphoryl groups of the LPS molecule.

Microorganisms are very important for the bioremediation of the environment because they are able to adsorb radionuclides and other heavy metals. Lipopolysaccharides form the main part of the outer membrane of Gram-negative bacteria. Generally, LPS consists of a high density of different functional groups for metal binding like carboxyl or phosphoryl groups.

EXPERIMENTAL. LPS from *Pseudomonas aeruginosa* S10 was purchased from Sigma. TRLFS spectra were measured with a fixed uranyl concentration of 10^{-5} M as a function of the LPS concentration, 0.075 – 1.0 g/L. The pH values were varied between 2.5 and 8.0. The spectra were recorded at 22 ± 1 °C using a pulsed Nd:YAG laser system, the excitation wavelength of the uranyl fluorescence was 266 nm with pulse energy of 0.2 – 0.5 mJ.

RESULTS. Figures 1 and 2 summarize the measured static fluorescence spectra of the UO_2^{2+} -LPS system, as a function of the LPS concentration and the pH. For comparison, the uranyl spectra at pH 2.5 (100 % $\text{UO}_2^{2+}(\text{aq})$) and pH 6.0 (main species: $(\text{UO}_2)_3(\text{OH})_5^+$) are included.

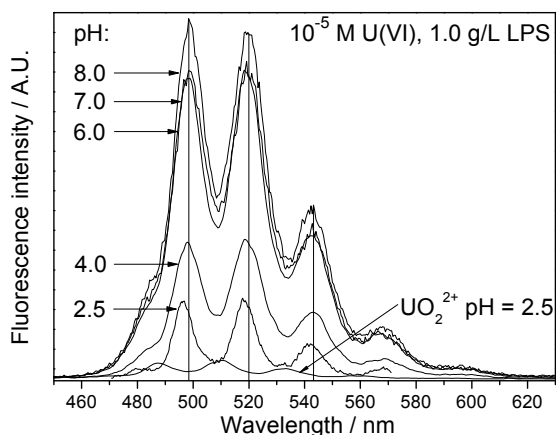


Fig. 1: Fluorescence spectra at fixed uranyl and LPS concentration in dependence of the pH.

Generally a strong increase of the fluorescence intensity, connected with a red shift of the peak maxima of about 10 nm, compared to the free uranyl ion $\text{UO}_2^{2+}(\text{aq})$, was observed. This red shift is characteristic for organic uranyl phosphoryl compounds [1]. The peak maxima and shapes of the spectra remain constant over a wide pH (up to pH = 8.0) and LPS concentration range, no formation of uranyl hydroxide species was detected. This is an indicator of the high stability of UO_2^{2+} -LPS complex species. The time-resolved fluorescence measurements show a bi-exponential decay according to at least two different fluorescent UO_2^{2+} -LPS species over the whole investigated

LPS concentration range and at all pH values. The average lifetimes of $t_1 = 1.1 \pm 0.3$ μs and $t_2 = 12.0 \pm 1.5$ μs appear with different intensities. The shorter lifetime dominates at lower pH and LPS concentration ranges. The intensity of the longer lifetime increases with increasing pH value and increasing LPS concentration. Both lifetimes are clearly different from the lifetime of the free uranyl ion (~ 1.8 μs). Therefore, we can dedicate both determined lifetimes to different UO_2^{2+} -LPS complex species.

The quantitative investigation of the fluorescence spectra was carried out with SPECFIT [2], a computer program which is suitable for factor analysis, stoichiometry analysis, and stability constant calculation. As dissociation constants for the functional groups we used pK_a values after the model of a universal adsorption edge of metals onto bacterial surfaces from Yee and Fein [3] of 5.06 for carboxyl (*Pseudomonas aeruginosa*) and 7.2 for phosphoryl (averaged over 5 different bacteria strains). The mass of phosphorous was detected with ICP-MS to be 0.5 mmol/g LPS. With the simplified postulation, that all phosphorous is bound in phosphoryl groups we took this concentration value for the phosphoryl groups. From the structural model of LPS from *Pseudomonas aeruginosa* [4,5] the concentration of the carboxyl groups is calculated to be 0.2 mmol/g LPS. With these data we calculated possible complex stoichiometries. As a result, two complexes with only deprotonated phosphoryl groups and without any involvement of the carboxyl groups were obtained. The two complexes have a metal-to-ligand ratio of 1 : 1 and 1 : 2, respectively. The complex stability constants were calculated to be $\log \beta_{110} = 8.0 \pm 0.9$ and $\log \beta_{120} = 13.6 \pm 1.0$ ($I = 0.1$ M each). The peak maxima of the spectra were calculated to be 496, 517, 541, 565 nm (1 : 1) and 498, 519, 543, and 567 nm (1 : 2 species).

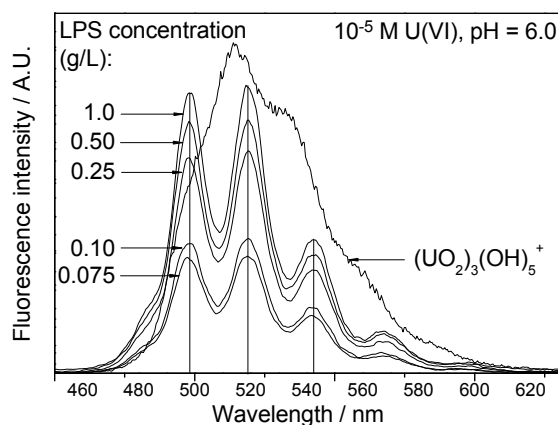


Fig. 2: Fluorescence spectra at fixed uranyl concentration and fixed pH in dependence of the LPS concentration.

ACKNOWLEDGEMENTS. This work was funded by the BMWi under contract number 02E9985.

REFERENCES

- [1] Koban, A. et al. (2007) *J. Inorg. Biochem.* **101**, 750-757.
- [2] Binstead, R.A. et al. (2005) SPECFIT Global Analysis System, Version 3.0.37.
- [3] Yee, N. et al. (2001) *Geochim. Cosmochim. Acta* **65**, 2037-2042.
- [4] Knirel, Y.A. (1990) *Crit. Rev. Microbiol.* **17**, 273-304.
- [5] Knirel, Y.A. (2006) *J. Endotoxin Res.* **12**, 324-336.

ATR-FTIR investigation of the complexation between U(VI) and phosvitin

B. Li, J. Raff, H. Foerstendorf

Phosvitin and its complex with U(VI) were studied in aqueous solution at pH 4, 6, and 8 by attenuated total reflection Fourier-transform infrared (ATR-FTIR) spectroscopy. Different protonated states of phosphate groups on the protein have been clearly shown by the spectra of phosvitin in solution at pH 4, 6, and 8. The determination of the interaction between phosphate groups of phosvitin and UO_2^{2+} ion is demonstrated by the phosphate and uranyl absorption peaks.

Phosvitin is a highly water soluble 25 kDa protein containing 10 % w/w phosphate groups [1]. It serves as an ideal model for the investigation of the interaction of U(VI) with phosphorylated protein side chains by ATR-FTIR spectroscopy.

EXPERIMENTAL. Phosvitin (Sigma) solutions were prepared by resolving the protein in the 0.1 M NaCl (blank solution) to reach a concentration of 5 mg/mL. The solutions were adjusted to pH 4, 6, and 8 with NaOH and HCl. For thermal denaturation, 5 mg phosvitin was incubated in a water bath at 80 °C for 1 h. For the batch experiments, 5 mg phosvitin was incubated with UO_2Cl_2 , BaCl_2 , or PbCl_2 to a total metal concentration of $1 \cdot 10^{-4}$ M in 0.1 M NaCl at pH 4 and 6. In addition, blank experiments without U, Ba and Pb were carried out. The contact time was two days and all experiments were conducted at room temperature. The denatured complex was separated, washed in blank solution at the respective pH, centrifuged, and resuspended in 1 mL blank solution.

The infrared spectra were measured on a Bruker Vertex 80/v FTIR instrument equipped with a flow cell ATR accessory. The protein solution or resuspension was directly injected into the flow cell. Spectral resolution was 4 cm^{-1} , and spectra were averaged from 256 scans. Background correction was achieved by subtracting a spectrum of the blank solution.

RESULTS. Figure 1 shows a comparison of FTIR spectra of phosvitin solution at pH 4, 6, and 8. From the spectra of inorganic phosphate solutions [2], it is obvious that at pH 4 the phosphate groups appear as dihydrogen phosphate, and at pH 8 as monohydrogen phosphate. The phosvitin solution at pH 6 shows a transition phase, but mainly contains monohydrogen phosphate.

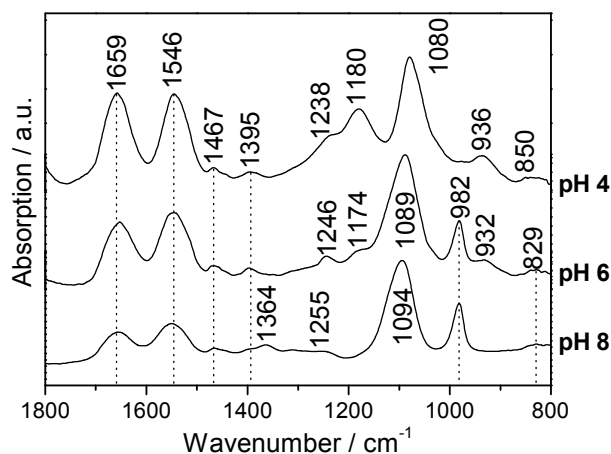


Fig. 1: ATR-FTIR spectra of phosvitin solution at pH 4, 6, and 8.

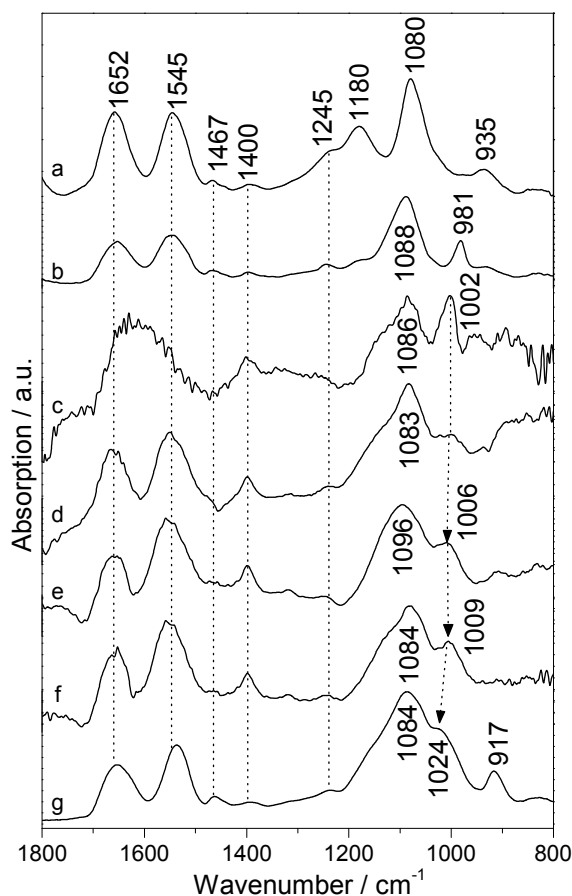


Fig. 2: ATR-FTIR spectra of phosvitin solution at pH 4 (a) and pH 6 (b) and of the resuspensions of the denatured protein recorded at pH 4 (c-g). Denaturation was achieved without any extra substance (c), by thermal denaturation (d), by BaCl_2 (e), by PbCl_2 (f), by 10^{-4} M UO_2^{2+} (g).

In Fig. 2, all FTIR spectra of the denatured proteins at pH 4 (c-g) look similar in comparison to the spectra of the phosvitin solution at pH 6. This indicates that deprotonation occurs during the protein denaturation. It also means that deprotonation cannot be the only piece of evidence to conclude that the metal indeed binds onto the proteins.

By comparing the spectrum of the U(VI) phosvitin complex (g) with the spectra of Ba^{2+} (e), Pb^{2+} (f) protein denaturation, a distinguishable peak is observed at 917 cm^{-1} . This peak is attributed to the ν_{as} mode of UO_2^{2+} indicating a coordination between uranium and the phosphate groups of phosvitin, as in complexations between uranium and organic carboxyl groups the absorption band $\nu_{\text{as}}(\text{UO}_2^{2+})$ typically show up at 923 cm^{-1} [3].

REFERENCES

- [1] Renugopalakrishnan, V. et al. (1985) *J. Biol. Chem.* **260**, 11406-11413.
- [2] Elzinga, E. J. et al. (2007) *J. Colloid Interface Sci.* **308**, 53-70.
- [3] Kakihana, M. et al. (1987) *J. Phys. Chem.* **91**, 6128-6136.

The adsorption of uranium(VI) by milk proteins

H. Zänker, S. Weiß, K. Schreppel, K. Gloe,¹ T. Henle,¹ G. Bernhard

¹Institute of Chemistry and Food Chemistry, Dresden University of Technology, Dresden, Germany

Screening experiments demonstrated that milk proteins (casein, whey proteins) show a high tendency to bind hexavalent uranium. Therefore, the adsorption isotherm of the system uranyl/milk protein at pH 4.6 was determined in order to quantify this tendency.

Two pieces of information are of particular interest: sorption affinity and sorption capacity. They can be derived from the adsorption isotherm.

EXPERIMENTAL. Skim milk was produced by centrifugation of commercial (pasteurised and homogenized) fresh milk for 0.5 h at 5000 g and removing the fat fraction. It was acidified to pH 4.6 (where the casein precipitates). Uranium concentrations of 10^{-7} , 10^{-6} , and 10^{-5} M were adjusted in aliquots of this skim milk. According to thermodynamic calculations the solubility limit of U(VI) is not exceeded for uranium concentrations of $\leq 10^{-5}$ M at pH 4.6.

After a reaction time of 20 h, the skim milk was separated into 3 fractions by ultracentrifugation for 1 h at 285000 g and ultrafiltration of an aliquot of the supernatant through a 10-kD filter. The fractions are:

- the centrifugation pellet (mostly casein),
- the centrifugation supernatant (whey), and
- the 10-kD ultrafiltrate (non-protein constituents such as lactose).

The uranium concentrations in these fractions were analyzed by ICP-MS.

After this screening experiment the adsorption isotherm of U(VI) onto the collective casein / whey protein fraction at pH 4.6 was determined by adjusting similar U concentrations as above in strongly diluted skim milk samples (dilution in order to cover also the area of uranium saturation on the milk proteins). The samples were allowed to equilibrate for 3 d. The differentiation between U adsorbed to the milk proteins and free U was done by 10-kD ultrafiltration and ICP-MS analysis for uranium in the ultrafiltrate. The U concentration in the ultrafiltrate is regarded as the equilibrium concentration of free uranium, c_{eq} , at a given point of the adsorption isotherm. The UO_2^{2+} adsorbed to the milk proteins at this point, Q , is calculated from the U concentrations measured before and after the ultrafiltration and the adjusted protein concentrations.

RESULTS. Table 1 gives the distribution of the uranium in the three fractions of the screening experiment with the undiluted milk. The adsorption isotherm of U(VI) onto the collective casein/whey protein fraction at pH 4.6 is shown in Fig. 1.

DISCUSSION. The screening experiment qualitatively illustrates the high sorption affinity of milk proteins, in particular of casein, for uranium(VI). More than 99.9 % of the uranium is removed by the milk proteins (Tab. 1); U is not even detectable in the 10-kD ultrafiltrate, i.e. the removal of the U is almost complete.

The starting point of a quantitative assessment of sorption data needs to be a physical model of sorption. Important milk proteins (the caseins) form micelles of tens to hundreds of nm in size and even the constituents of such mi-

celles, the macromolecules, have molecular weights of many thousands of daltons, i.e. the milk protein particles are much bigger than the uranyl ions or uranyl complexes in the water. It is this difference which justifies our classification of the reaction between uranyl and the milk proteins as an adsorption reaction.

We regard our system as a two-phase system with the crucial interaction occurring at the protein-water interface. A reasonable approach of describing such a system would be the application of a surface complexation model since it is most plausible that the adsorption reaction proceeds at specific sites, i.e. functional groups, of the proteins. These should be sites of only one type or, at the most, very few groups of different uniform types. However, for one specific (constant) pH value, as in our case, there is no difference between a surface complex formation constant and a Langmuir adsorption constant, K_L [1]. Therefore, we fit our experimental data to a Langmuir isotherm (Fig. 1). The fit provides a reasonable result for uranium equilibrium concentrations of up to 0.3 mg/L ($1.3 \cdot 10^{-6}$ M); experiments with higher equilibrium concentrations are underway. Both, the high sorption affinity (K_L is a measure of the sorption affinity) and sorption capacity, Q_{max} , of the milk proteins for U(VI) are reflected in the fit.

In another article on adsorption of U(VI) onto milk proteins we give a differentiation between the individual sorption properties of casein and whey proteins for uranium(VI) [2].

Tab. 1: Distribution of uranium in undiluted milk at pH 4.6 (screening experiment).

| Adjusted U concentration [M] | Casein [%] | Whey [%] | 10 kD-filtrate of whey [%] |
|------------------------------|------------|----------|----------------------------|
| 10^{-5} | 99.9 | 0.1 | < 0.1 |
| 10^{-6} | 99.7 | 0.3 | < 0.1 |
| 10^{-7} | 86.1 | 13.9 | < 0.1 |

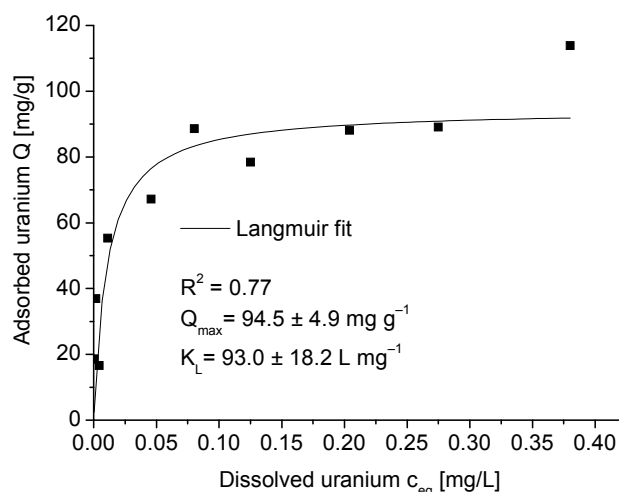


Fig. 1: Adsorption isotherm of U(VI) on the collective casein/whey protein fraction at pH 4.6.

REFERENCES

- [1] Stumm, W. (1992) *Chemistry of the Solid-Water Interface*, Wiley, New York, p. 91.
- [2] Schreppel, K. et al. (2008) this report, p.38.

Comparison of the binding of the uranyl ion to sodium caseinate and whey proteins

K. Schreppel, S. Weiß, H. Zänker, K. Gloe,¹ T. Henle,¹ G. Bernhard

¹Institute of Chemistry and Food Chemistry, Dresden University of Technology, Dresden, Germany

The binding of the uranyl cation by sodium caseinate and whey proteins at pH 4.6 was studied by adsorption and kinetic measurements using ICP-MS. A maximum adsorption of ≥ 87 mg UO_2^{2+} /g caseinate and ≥ 124 mg UO_2^{2+} /g whey protein was observed. Adsorption was completed after 8 hours.

The binding of radionuclides to biological relevant proteins is of interest in nutrition and biochemistry, but the mechanisms of molecular interactions between actinides and lanthanides and possible binding sites as well as consequences resulting therefrom are mostly unknown. Starting with the naturally occurring uranium, we investigated whether milk proteins may be efficient complexing agents due to their high amount of phosphoserine, glutamic acid and aspartic acid functions, which all are potential uranyl binding groups.

EXPERIMENTAL. Aqueous solutions of $\text{UO}_2(\text{NO}_3)_2 \cdot 6\text{H}_2\text{O}$ were prepared in a concentration range from $1 \cdot 10^{-7}$ M to $1 \cdot 10^{-5}$ M and the pH value was adjusted to 4.6, which is the isoelectric point of acid caseinate, so it precipitates at that pH value. The uranium contents of the solutions were analyzed by ICP-MS. By adding a suspension of sodium caseinate (27 g/L) or lyophilized whey protein (6 g/L) in SMUF solution (SMUF = simulated milk ultrafiltrate) contents of 1.42 to 14.20 mg/L caseinate and 0.32 to 3.20 mg/L whey protein were adjusted, respectively [1]. This corresponds to the contents of milk. The pH value was checked and corrected if required. After three days of equilibration samples were taken and unbound UO_2^{2+} was separated by ultrafiltration (Centriprep YM-10, 10 kDa NMGG; Millipore). The UO_2^{2+} concentrations of the obtained filtrates were determined by ICP-MS.

The adsorption isotherms (see Fig. 1) were calculated as described before by Zänker et al. [2].

Kinetic measurements of the complete adsorption of uranyl cations were undertaken by discontinuous determination of the unbound U(VI). Therefore 50 μL of the above solutions of sodium caseinate and whey protein were added to 100 mL of a U(VI) solution of $3 \cdot 10^{-6}$ M each, from which a sample of 5 mL was taken to get the real uranyl concentration. At $t = 0$ min and then every 30 min a sample of 5 mL was taken and the unbound U(VI) was examined as mentioned above.

RESULTS. The data treatment was performed on the basis of FREUNDLICH and LANGMUIR isotherms. Figure 1 and Tab. 1 show that whey proteins reach a higher adsorption of UO_2^{2+} than sodium caseinate. The obtained R^2 values indicate a good fit with both models.

Due to the complex structure of milk proteins, the data obtained by the kinetic measurements could not be used to determine the velocity constant of the adsorption of UO_2^{2+} onto milk proteins. A more precise interpretation was not possible because the number of potential binding groups and the binding mechanism is unknown. But it could be deduced that the adsorption is finished after 8 hours (see Fig. 2).

Tab. 1: Parameters for UO_2^{2+} adsorption by sodium caseinate (Na cas) and whey proteins (whey prot.) based on the FREUNDLICH and LANGMUIR isotherms.

| | FREUNDLICH isotherms | | |
|------------|---|-------------|----------------|
| | K_F [(mg/g)(L/mg) ^{1/n}] | 1/n | R ² |
| Na cas | 108.59 (7.20) | 0.23 (0.03) | 0.91 |
| whey prot. | 124.24 (6.08) | 0.66 (0.06) | 0.98 |

| | LANGMUIR isotherms | | |
|------------|----------------------|-----------------|----------------|
| | q_{\max} [mg/g] | K_L [L/mg] | R ² |
| Na cas | 87.28 (3.57) | 105.17 (23.51) | 0.95 |
| whey prot. | 435.61 (166.90) | 0.42 (0.23) | 0.96 |

K_F , 1/n: FREUNDLICH constants related to the adsorption capacity and sorption intensity of the sorbent; q_{\max} , K_L : LANGMUIR constants related to the maximum adsorption of UO_2^{2+} onto milk proteins and the equilibrium adsorption constant.

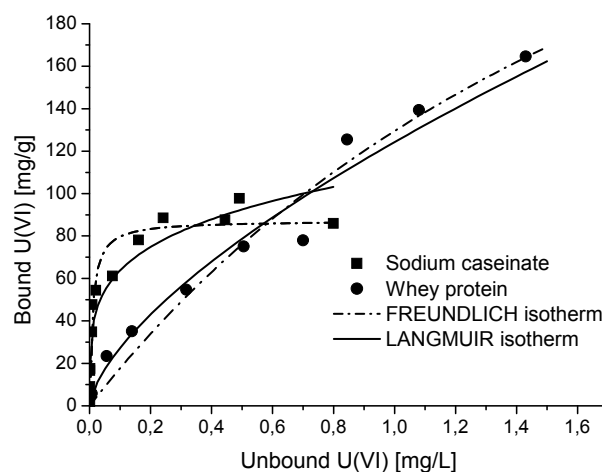


Fig. 1: LANGMUIR and FREUNDLICH isotherms for the adsorption of UO_2^{2+} by sodium caseinate and whey proteins.

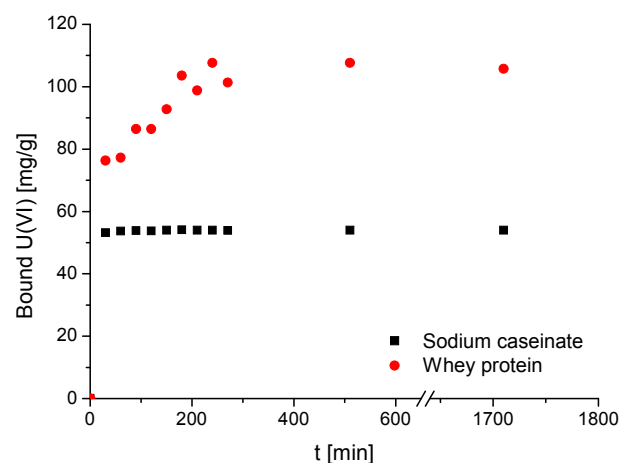


Fig. 2: Adsorption of UO_2^{2+} by sodium caseinate and whey protein vs. time.

REFERENCES

- [1] Jenness, R. et al. (1962) *Neth. Milk & Dairy J.* **85**, 153-164.
- [2] Zänker, H. et al. (2008) this report, p. 37

Characterization of the S-layer protein of *Bacillus spec. B12*

K. Pollmann, U. Weinert, K. Flemming, F. Lederer, T. Raff, J. Raff

Structure, posttranslational modifications and primary structure of the uranium binding S-layer protein of *Bacillus spec. B12* were investigated.

Surface layer proteins (S-layers) of bacteria isolated from uranium mining waste piles exhibit high uranium binding capacities. Previous analyses demonstrated that especially the S-layer protein of the bacterial strain *Bacillus spec. B12* exhibit a high uranium binding potential of up to 561.1 mg U/g protein at pH 6 (unpublished data), making it attractive for bioremediation purposes. In the present study the primary structure and posttranslational modifications of the S-layer protein were studied.

MICROSCOPIC ANALYSES. Atomic Force Microscopy (AFM) was performed using a JPK NanoWizard II (JPK Instruments) and a Nanoscope IIIa (Digital Instruments). Fourier analyses show a p2 symmetry of the purified and recrystallized S-layer with lattice constants of 8.6 nm and 9.6 nm. The symmetry angle of the S-layer unit cell can be determined to be 83° whereas the characteristic angle between the lattice and the tube axis is 40°. The influence of S-layer symmetries on U binding capacity is still unknown and has to be elucidated in future.

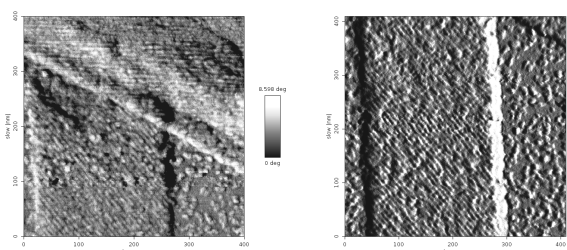


Fig. 1: AFM images (left: amplitude image; right: phase image) of purified and recrystallized S-layer of *Bacillus spec. B12* on mica. Mode: Intermittent contact mode in air; cantilever: Silicon non-contact cantilever, resonance frequency: 320 kHz.

POSTTRANSLATIONAL MODIFICATIONS. Post-translational modifications of S-layers such as glycosylation or phosphorylation play a crucial role for the (bio-) chemical properties of the protein and influence its metal binding capacities [1]. The glycosylation of the S-layer proteins of *B. spec. B12* was investigated by a colorimetric method [2]. Absorption spectra (Fig. 2) demonstrate that the proteins are modified by sugar residues, potentially rhamnose. The amount was determined as 4.74 mol sugar/mol protein. However, the spectral differences between different kinds of sugar residues are too small for a reliable identification, and further analysis is required.

SEQUENCE ANALYSES. Structural and biochemical properties of a protein are affected by its primary structure. Therefore the primary structure of the S-layer protein of *B. spec. B12* was investigated. N-terminal and internal sequences of the S-layer protein were determined after digestion of the purified protein by the endoproteinase Glu-C, electrophoretic separation and subsequent transfer on a PVDF blotting membrane. N-terminal amino acid sequences of 9 fragments were determined using an ABI 494A Procise HT sequencer.

For DNA sequencing primers were constructed based on the protein sequence information. For gene amplification

vectorette libraries were constructed according to the manufacturer's instructions. PCR amplifications were performed as described previously [3]. Obtained PCR products were purified and sequenced from each strand using a Perkin-Elmer Applied Biosystems 377 instrument.

The entire sequence of the S-layer protein gene of *B. spec. B12* indicates one ORF of 2586 bp encoding a protein of 862 aa. The ORF starts with ATG and is preceded by a typical ribosome-binding site (ggagg) with a distance of 14 bp between the middle A of this sequence and the start codon. The S-layer protein has a signal peptide of 29 aa that is responsible for the protein secretion to the cell surface. The theoretical mass of the mature protein is 88.8 kDa, which is in accordance with the mass determined by SDS gel electrophoresis. The calculated pI value of the mature protein is 5.79.

The primary structure of the S-layer protein shows typical S-layer features such as a high content of lysine (10.6 %) and valine (11.9 %) and the absence of cysteine. The N-terminal region contains three S-layer homologous (SLH) domains. Sequence comparisons show a high identity (91 % – 96 %) with the S-layer protein EA1 of *B. anthracis* str. Ames, *B. thuringiensis* str. Al Hakam, *B. cereus* E33L, and *B. cereus* G9241, although sequence information revealed that B12 does not belong to the *B. cereus* group.

Interestingly, another S-layer protein gene was found to be encoded by *B. B12*. Using the vectorette method, the sequence of this silent gene was determined. The gene shows all features of an intact S-layer gene and the putative protein has a high identity of 82 % with the S-layer protein Sap of *B. anthracis* str. Ames. However, internal protein sequence data could not prove the expression of this gene.

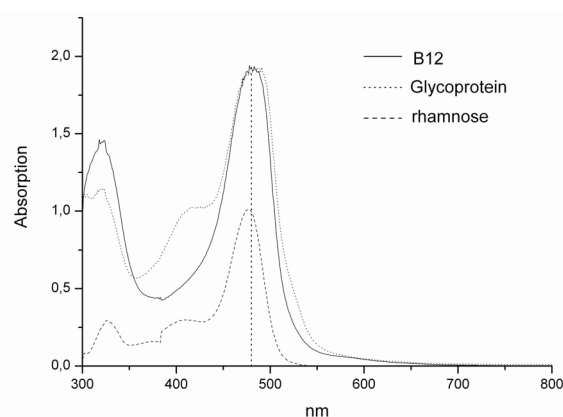


Fig. 2: UV-vis spectra of rhamnose, glycoprotein, and S-layer protein of *B. spec. B12* after treatment with sulphuric acid and phenol.

ACKNOWLEDGEMENTS. We thank R. Getzlaff and I. Plumeier (HZI, Braunschweig) for protein sequencing and J. Barner (JPK Instruments, Berlin) and S. Matys (TU Dresden) for providing AFM images.

REFERENCES

- [1] Raff, J. et al. (2004) *Report FZR-400*, p. 24.
- [2] Dubois, M. et al. (1956) *Anal. Chem.* **28**, 350-356.
- [3] Pollmann, K. et al. (2005) *Microbiology* **151**, 2961-2973.

Comparison of three different methods for the detection of glycosylated S-layer proteins

U. Weinert, M. Vogel,¹ J. Raff

¹University of Applied Science, Dresden, Germany

Former studies indicate that the S-layer proteins from several *Lysinibacillus* and *Bacillus* isolates are not glycosylated. However, many papers point out that the majority of S-layer proteins from bacteria are glycoproteins [1]. For this reason we tested and compared different methods for their detection. Since standard staining methods did not provide reliable results we developed a modified colorimetric method which allows the reproducible and accurate determination of glycoproteins.

Within the radioecological research on the interaction of bacteria with actinides, several *Lysinibacillus* and *Bacillus* strains were isolated from the uranium mining waste pile "Haberland" near Johannegeorgenstadt in Saxony, Germany. Some of them are carrying surface layer (S-layer) proteins with highly interesting properties promising for biotechnological and nanotechnological applications. In this regard, the metal binding, the chemical stability and possible modification sites are of particular interest. These properties depend not only on the primary structure of the protein itself, but also on posttranslational modifications, such as glycosylation and phosphorylation. Whereas the latter can be easily determined, the degree of glycosylation of investigated S-layer proteins was still doubtful.

EXPERIMENTAL. The different isolates were grown at room temperature and overnight in Nutrient Broth (8 g/L, Mast Group Ltd., Merseyside, UK) medium. The S-layers were extracted according to the protocol in reference [2]. For the detection of glycoproteins, the following methods were compared: Schiff's staining was performed on a 10 % SDS gel referring to a protocol in reference [3]. Antibody staining was performed on a PVDF membrane with DIG Glycan detection kit (Roche, Diagnostic GmbH, Mannheim). For both methods 15 µg of each S-layer protein was used and α-glycoprotein was chosen as positive reference. The colorimetric method was performed according to the protocol of Dubois [4] with 1 mg of each S-layer protein and rhamnose as standard sugar molecule.

RESULTS. The staining with Schiff's reagent shows a negative result for glycosylation on all S-layers (data not shown). In contrast, the DIG Glycan staining demonstrated that the S layer proteins from JG-B7, JG-B62 and JG-B5T are glycol proteins, whereas the JG-A12 S-layer protein is not glycosylated (Fig. 1). The results for the JG-B12 and JG-B58 S-layer proteins are inconclusive. In

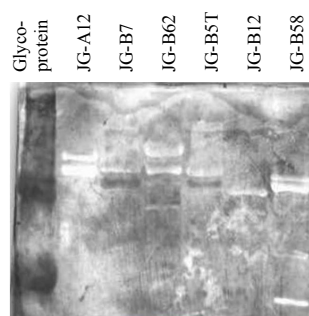


Fig. 1: Membrane after staining with DIG glycan detection kit. Dark bands are glycosylated proteins and shiny bands are non glycosylated proteins.

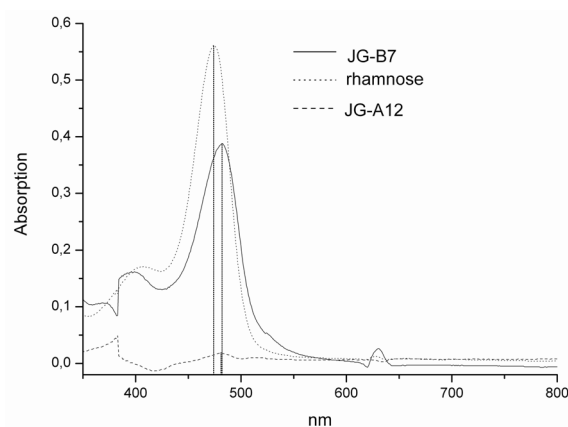


Fig. 2: UV-vis spectra of JG-B7, JG-A12 and rhamnose after treating with sulfuric acid and phenol.

case of the colorimetric method according to Dubois, clear results were obtained for all investigated S-layer proteins. Figure 2 shows representative spectra of the S-layer proteins from JG-A12 and JG-B7 as well as from rhamnose after treating with sulfuric acid and phenol. It can be seen that the JG-A12 S-layer protein is not glycosylated as its spectrum shows no maxima in the range between 470 and 490 nm.

In this region, all sugars have their maxima when they are detected with this method. Furthermore, the detection showed that JG-B12 and JG-B58 are clearly glycosylated in contrast to the antibody staining to the detection with DIG Glycan detection kit. Additionally, Dubois' method allows the quantification of the sugar residues. Table 1 shows the degree of glycosylation of different S-layer proteins and their absorption maxima found after treating with sulfuric acid and phenol. As shown in Fig. 2, it can be seen that they are only slightly glycosylated. This may be the reason for the failure of the Schiff's staining. The different maxima indicate that these S-layer proteins are glycosylated with different sugar residues. However, the difference between the maxima of all tested sugars is too small to clearly identify the sugar residues on the S-layer proteins.

Tab. 1: Absorption maxima of different S-layer proteins after treating with sulfuric acid and phenol. Glycosid content in mol/mol (S-Layer). Rhamnose was used as a reference substance for quantification.

| S-layer | Absorption maxima (nm) | Sugar residues (mol/mol) |
|---------|------------------------|--------------------------|
| JG-A12 | – | 0.03 |
| JG-B5T | 477 | 2.46 |
| JG-B7 | 482 | 1.93 |
| JG-B12 | 482 | 4.74 |
| JG-B58 | 477 | 2.33 |
| JG-B62 | 482 – 485 | 3.79 |

REFERENCES

- [1] Sleytr, U. B. (1997) *FEMS Microbiol. Rev.* **20**, 5-12.
- [2] Raff, J. (2002) Thesis, University of Leipzig, Leipzig.
- [3] Zacharius, R. M. et al. (1969) *Anal. Biochem.* **30**, 148-152.
- [4] Dubois, M. et al. (1956) *Anal. Chem.* **28**, 350-356.

Spectroscopic and microscopic studies on the interactions of *Paenibacillus* sp. JG-TB8 with U(VI)

T. Reitz, M. Merroun, S. Selenska-Pobell

In this study it is demonstrated that cells of the bacterial strain *Paenibacillus* sp. JG-TB8 are involved in the immobilization of U(VI) under acidic aerobic conditions by bioaccumulation and biomineralization processes. The cells accumulated up to 85 mg uranium per g dry biomass. Uranium was precipitated as a meta-autunite like mineral phase on the cell surface as well as in the cells. The activity of an acidic phosphatase was demonstrated in the uranium treated cell samples and may liberate the inorganic phosphate groups, which seem to be responsible for the uranium precipitation.

Microbial cells are known to interact in multiple ways with toxic metals and radionuclides and thus alter the mobility of these elements in the environment [1]. To investigate the influence of the bacterial isolate *Paenibacillus* sp. JG-TB8 on uranium mobility under acidic aerobic conditions a combination of wet chemistry, spectroscopy and microscopic techniques was used.

EXPERIMENTAL. The strain JG-TB8 was isolated from an anaerobic microbial consortium, consisting of *Firmicutes* and mesophilic 1.1b-*Crenarchaeota*, recovered from a uranium mining waste pile near the town of Johanngeorgenstadt, Germany. The strain was cultivated in LB-medium. Cells were harvested after reaching the mid-logarithmic growth phase and incubated for different periods of time with 0.5 mM uranyl nitrate in 0.1 M perchloric acid at a pH of 4.5 under aerobic conditions. The sample preparations for X-ray absorption spectroscopy and transmission electron microscopy were performed after an incubation time of 48 h [2]. Acidic phosphatase activity was determined via the enzymatic hydrolysis of 4-methylumbelliferyl phosphate to 4-methylumbelliferon at pH 5.5.

RESULTS. U(VI) sorption studies showed that the cells of JG-TB8 accumulated 65 mg U/g dry biomass from a solution with an uranium concentration of 120 mg U/L within the first 20 minutes of incubation. After 48 h the amount of bound uranium was raised up to 85 mg per g of dry biomass (data not shown).

X-ray absorption spectroscopy was used to characterize the local coordination of uranium associated with cells of the studied bacterium at molecular scale. XANES analyses showed that the oxidation state of uranium bound to the cells was unchanged. The EXAFS spectrum of the U(VI) complexes formed by the cells of *Paenibacillus* sp. JG-TB8 showed a high similarity to that of meta-autunite, indicating that the radionuclide was precipitated by the cells as a meta-autunite-like phase.

TEM analyses demonstrated that these uranium precipitates were located at the cell surface as well as intracellular as needle-like fibrils or in polyphosphate granules (Fig. 2). Future work will be focused on the interactions of JG-TB8 with U(VI) under anaerobic conditions, which correspond to the natural environment of the strain, and the results will be compared to those reported in this study.

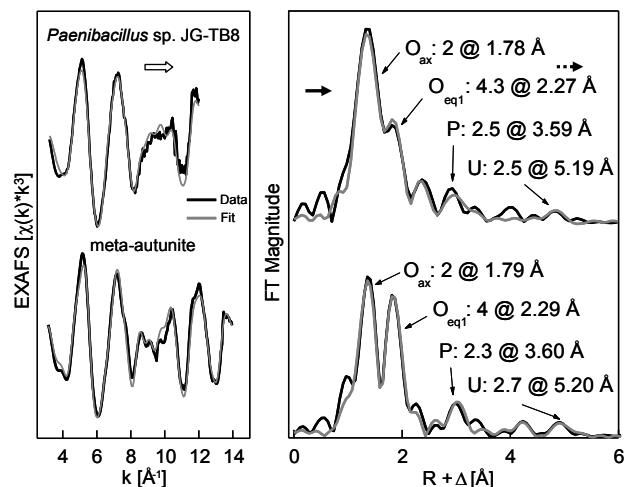


Fig. 1: EXAFS spectra of the U(VI) complexes formed by the cells of *Paenibacillus* sp. JG-TB8 and of meta-autunite.

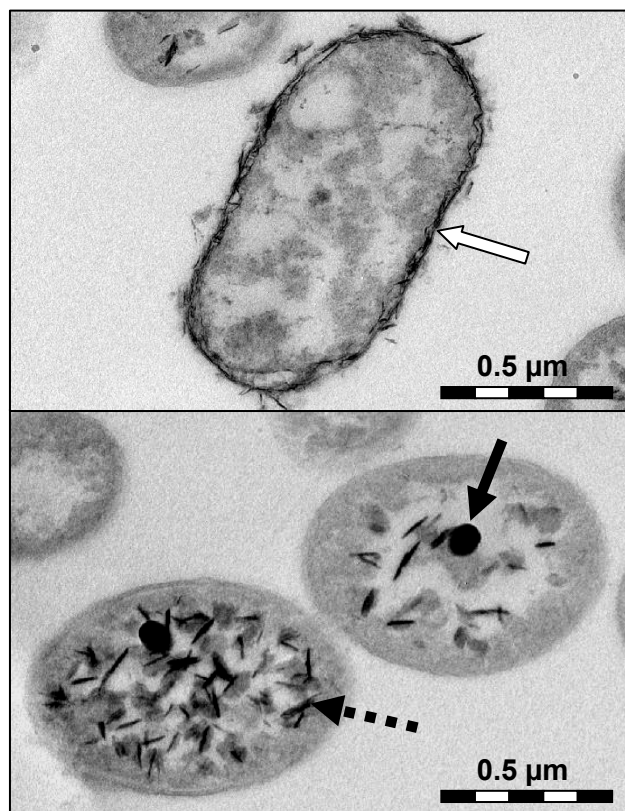


Fig. 2: Transmission electron micrographs of the U accumulates deposited by the cells of JG-TB8. Arrows indicate U(VI) on the cell surface (white arrow), as intracellularly needle-like accumulates (dotted arrow) and in polyphosphate granules (black arrow).

ACKNOWLEDGEMENTS. We acknowledge the assistance of the Electron Microscopy Services, University of Granada, Spain and of the ROBL group at the ESRF, Grenoble, France.

REFERENCES

- [1] Pedersen, K. et al. (2005) *J. Nucl. Radiochem. Sci.* 6, 11-15.
- [2] Merroun, M.L. et al. (2005) *Appl. Environ. Microbiol.* 71, 5532-5543.

Comparison of the U (VI) complexation of different S-layers by means of ATR-FTIR spectroscopy

B. Li, U. Weinert, H. Foerstendorf, J. Raff

The interactions between U(VI) and the different surface layer proteins (S-layer), which were purified from different bacteria isolates from the uranium mining waste pile in Johanngeorgestadt, were investigated by attenuated total reflection Fourier-transform infrared (ATR-FTIR) spectroscopy. The U(VI) carboxyl group complexation was verified by spectra recorded after one hour and after two days of U(VI) incubation. The complexation of U(VI) with phosphate, however, could not undoubtedly be identified on the basis of the ATR-FTIR spectra.

As the outermost subcellular structure of many bacteria and archaea, S-layers play an important role for selective binding of heavy metals, for example the UO_2^{2+} [1]. The main aim of this study is to explore which functional groups on the S-layer interact with the UO_2^{2+} and why different S-layers bound different quantities of UO_2^{2+} .

EXPERIMENTAL. Glycosylation and phosphorylation of all the investigated S-layers were determined by colorimetric methods.

A solution of 5 mg S-layer of the isolate JG-A12 in 1 mL MilliQ water was adjusted to pH 4. 0.25 mg S-layer in 50 μL was then immobilized using a 50 kDa dialysis membrane on the ATR crystal. U(VI) solutions were prepared by diluting UO_2Cl_2 stock solution in 0.1 M NaCl to a U concentration of $1 \cdot 10^{-4}$ M at pH 4. After one hour of UO_2^{2+} influx through the flow system coupled with a microdialysis compartment, the flow was changed to the blank solution (0.1 M NaCl, pH 4) for one hour to remove the remaining dissolved UO_2^{2+} in the system.

5 mg S-layer was incubated with $1 \cdot 10^{-4}$ M UO_2Cl_2 in 0.1 M NaCl at pH 4, 6, and 8 for two days at room temperature. The pellet was separated, washed with the blank solution at the respective pH values, and directly positioned on the ATR crystal. The difference spectra were calculated against the blank solution.

RESULTS. Out of all the investigated S-layers, only JG-B62 and JG-B58 are slightly phosphorylated, and four of seven are slightly glycosylated (Tab.1).

Figure 1 shows that during the first hour of incubation, UO_2^{2+} has interacted with the S-layer protein with hardly any post-translational modification. The peak at 922 cm^{-1} is a typical ν_{as} mode of UO_2^{2+} when it interacts with or-

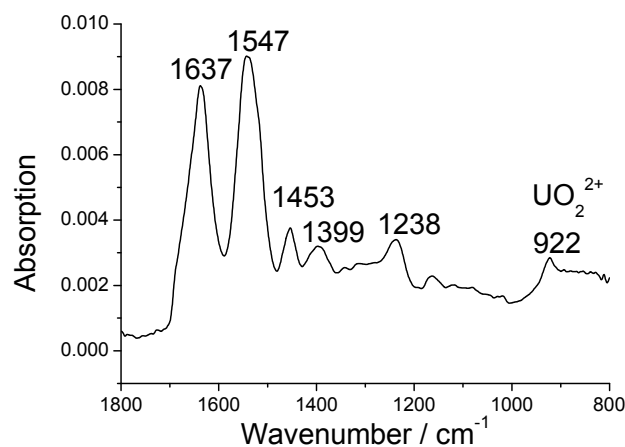


Fig. 1: ATR-FTIR spectrum of JG-A12 UO_2^{2+} interaction at pH 4 with the flow system coupled with a microdialysis compartment.

ganic carboxyl groups [2]. Together with the peak at 1399 cm^{-1} , which demonstrates the ν_{s} of carbonate, we conclude that carboxyl groups on the protein (from Glu and Asp) are involved in the UO_2^{2+} S-layer interaction.

Figure 2 shows a comparison of FTIR spectra of all the S-layer U(VI) complexes from the batch experiments at pH 4. In spite of the different content of the phosphate groups and sugar groups the spectra look much alike. The only minor difference is that the spectra of JG-B62 and JG-B58 show an additional weak peak at 1078 cm^{-1} , which may indicate phosphate groups [3].

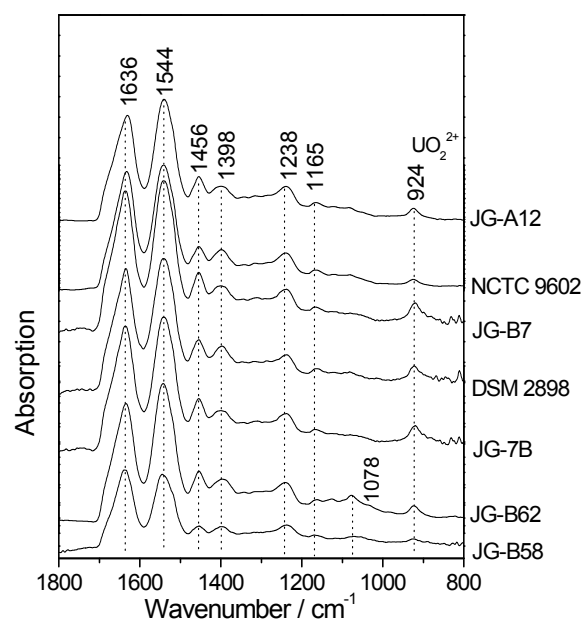


Fig. 2: ATR-FTIR spectra of uranyl(VI) complexes of different S-layers recorded at pH 4.

Tab. 1: Post translational modification of all investigated S-layers.

| S-layer from isolates or reference strains (R) | Phosphate content [mol/mol S-layer] | Sugar content [mol/mol S-layer] |
|--|-------------------------------------|---------------------------------|
| JG-A12 | 0.19 | 0.03 |
| NCTC 9602 (R) | 0.21 | 0.22 |
| JG-87 | 0.02 | 1.93 |
| DSM 2898 (R) | 0.12 | 1.50 |
| JG-7B | 0.04 | 0.07 |
| JG-B62 | 2.30 | 3.79 |
| JG-B58 | 1.01 | 2.33 |

REFERENCES

- [1] Merroun, M. L. et al. (1992) *Appl. Environ. Microbiol.* **174**, 7971-7981.
- [2] Kakihana, M. et al. (1987) *J. Phys. Chem.* **91**, 6128-6136.
- [3] Li, B. et al. (2008) this report, p. 36.

Spectroscopic characterization of Pt complexation and nanocluster formation on *Bacillus sphaericus* JG-A12 S-layer

U. Jankowski, K. Fahmy,¹ C. Hennig, S. Selenska-Pobell, M. Merroun

¹Institute of Radiation Physics, FZD, Dresden, Germany

A combination of X-ray absorption spectroscopy (XAS) and Fourier-transform infrared (FT-IR) spectroscopy was used to investigate the coordination of sorbed Pt(II) to the S-layer sheets of *B. sphaericus* JG-A12 at molecular scale and to characterize the formation of Pt nanocluster using this protein layer as a template.

EXPERIMENTALS. *B. sphaericus* JG-A12 was routinely grown in NB medium. The preparation of the S-layer protein was performed as described in [1]. For sorption of Pt(II) on S-layers of *B. sphaericus* JG-A12, 10 mg of dialyzed protein were incubated in 100 mL of a solution of 3 mM K_2PtCl_4 for 72 h at room temperature in the dark. Pt(II) was reduced by the addition of a few drops of 100 mM p-dimethylaminobenzaldehyde (DMAB) to produce Pt(0)-nanoparticles. The metalized protein samples were centrifuged (20 min, 10000 x g) and dried in an oven (12 h, 70 °C).

RESULTS. pH-induced infrared absorption changes indicate a structural stabilization when the Pt(II) is bound to the studied S-layer protein. The COO^- -stretching absorptions reveal a predominant Pt(II) coordination by carboxylate groups of the S-layer sheets.

These results are in agreement with the previously published coordination of Pd(II) by the carboxylic groups of Asp and Glu acids of the studied S-layer [2]. Additionally, a significant alteration of the secondary structure of the protein was observed during the reduction of the samples (Fig. 1).

Pt L_{III} -edge EXAFS spectra of the Pt/S-layers of *B. sphaericus* JG-A12 in presence and in absence of DMAB are shown together with Pt foil in Fig. 2. In the sorption sample three main peaks are found at bond distances of 2.01, 2.48 and 2.82 Å corresponding to Pt-O₁/N, Pt-O₂ and Pt-C bonds, respectively. These distances were identified using Pt-O, Pt-N and Pt-C backscattering phase and amplitude functions obtained from atomic coordinates of $Pt_2O_{10}N_6C_2H_{16}$ [3] using FEFF8 program. These results indicate that Pt is mainly bound to carboxyl and/or amine residues of the S-layer protein. In the S-layer Pt-reduced sample, the Pt is present in two different phases, one metallic (Pt-Pt) and one complexed to the functional groups of the S-layer template. For the sorbed phase, the distances found are comparable to those found in the Pt-bound S-layer sample (above). For the metallic phase, the interatomic distances found are very close to the ones of the metallic foil (2.76, 3.91, 4.80 and 5.46 ± 0.02 Å). The coordination numbers (N) and Debye-Waller factors (σ^2) are substantially smaller than the bulk ones showing the presence of small metal particles.

REFERENCES

- [1] Raff, J. (2002) *Report FZR-358*.
- [2] Fahmy, K. et al. (2006) *Biophys. J.* **91**, 996-1007.
- [3] Sakai, K. et al. (1998) *J. Am. Chem. Soc.* **120**, 11353-11363.

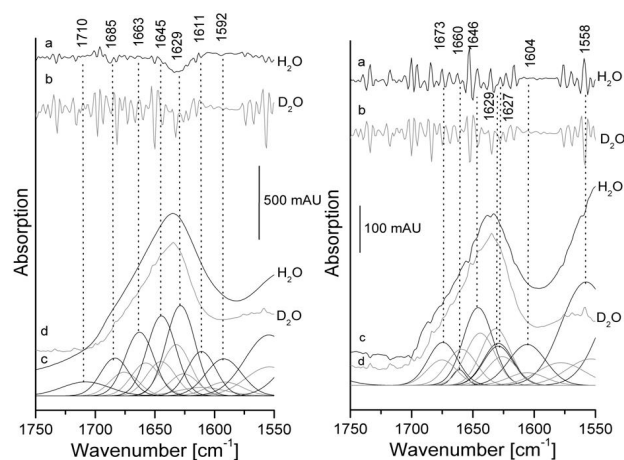


Fig. 1: IR spectra of Pt bound on S-layer (left) in H₂O (c) and in D₂O (d) and of Pt-nanoparticles formed on this protein layer (right). Spectra are produced with the 2nd derivation (a,b) of raw data.

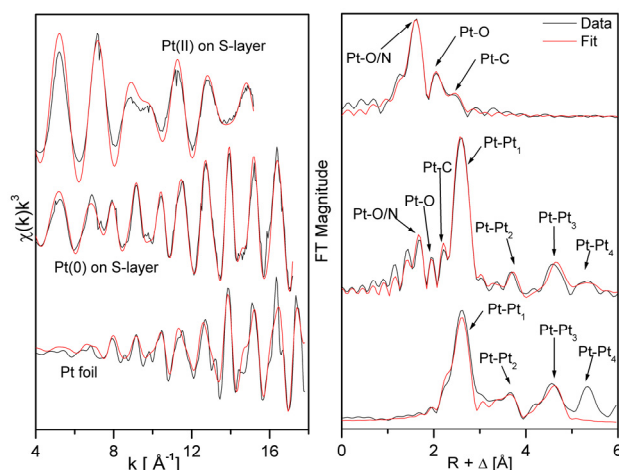


Fig. 2: Pt L_{III} -edge EXAFS spectra (left) and their corresponding FT (right) of the sorbed and reduced platinum on S-layer of *B. sphaericus* JG-A12 and Pt foil.

Influence of uranium on oxygen consumption in multispecies biofilms assessed with microsensors

E. Krawczyk-Bärsch, T. Arnold, K. Großmann, A. Wobus,¹ S. Hofmann¹

¹Institute of Microbiology, Dresden University of Technology, Dresden, Germany

Oxygen consumption rates were calculated from the steady-state O₂ microprofiles measured in the upper layers (< 70 μm) of multispecies biofilms, which were fed with uranium in ecologically relevant concentrations (1 · 10⁻⁵ M). Compared to the oxygen consumption rates of 6.34 nmol cm⁻³ s⁻¹ in biofilms without the addition of uranium, the high consumption rates of up to 68 nmol cm⁻³ s⁻¹ in the top layer of the biofilm fed with uranium indicate that the addition of uranium (VI) results in an increase of the microbial metabolic activities in the upper biofilm layers. This response is a prompt reaction of the microbes which is already clearly detectable only two hours after the addition of uranium.

EXPERIMENTAL. Multispecies biofilms were cultured on glass slides in biofilm reactors in a standard culture medium (Sifin; TN 1171) with a pH of approximately 7.2 and in air atmosphere condition at room temperature (20 °C) for two months. One reactor was fed with UO₂(ClO₄)₂ to adjust the total uranium concentration in the culture medium to 1 · 10⁻⁵ M. After three weeks, oxygen microsensor studies were carried out with biofilms exposed to uranium and in biofilms free of uranium. Concentration profiles of oxygen versus biofilm depths were measured in each biofilm in flow cells by electrochemical microsensors from Unisense with a tip diameter of 10 μm. The measured concentration profiles were biogeochemically interpreted by a numerical procedure [1] to calculate the oxygen consumption rates with a precise prediction of the location of the oxygen consumption zones. The procedure is based on a series of least square fits to the measured steady-state concentration profiles, followed by comparisons of these fits through statistical *F*-testing.

RESULTS. In Fig. 1 are shown the measured values of the oxygen concentration versus biofilm depth for the biofilm exposed to a uranium concentration of 1 · 10⁻⁵ M together with the calculated oxygen profile. This profile fits the measured data points perfectly. The oxygen pro-

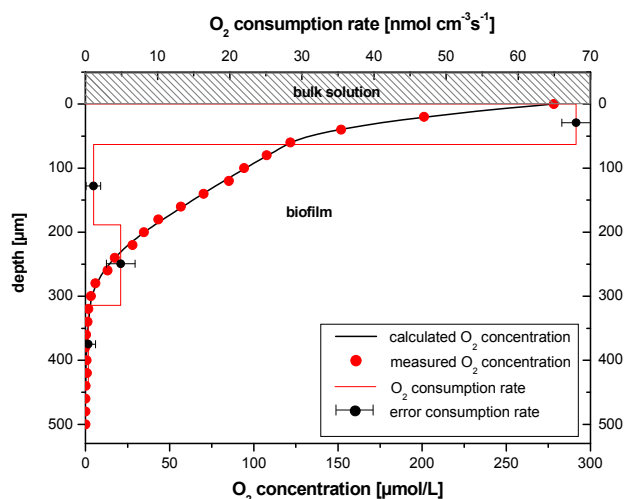


Fig. 1: Measured O₂ concentrations in the biofilm exposed to a uranium concentration of 1 · 10⁻⁵ M (points), and the calculated best-fitting O₂ concentration profile (line).

file exhibits significant O₂ consumptions at almost all depths. Four consumption zones were identified as calculated with the numerical procedure PROFILE. In the upper layer of the biofilm, between the surface and a depth of 63 μm, the highest oxygen consumption rate of 68 nmol cm⁻³ s⁻¹ was obtained.

In contrast, the calculated oxygen consumption rate of the upper layer in the biofilm grown in a reactor free of uranium is significantly lower (Fig. 2). Here, the first zone showed a consumption rate of 6.34 nmol cm⁻³ s⁻¹. The zone ranged from the biofilm surface up to a depth of 74 μm. Then a second zone followed, which reached up to the bottom of the biofilm, with an oxygen consumption rate of 1.23 nmol cm⁻³ s⁻¹.

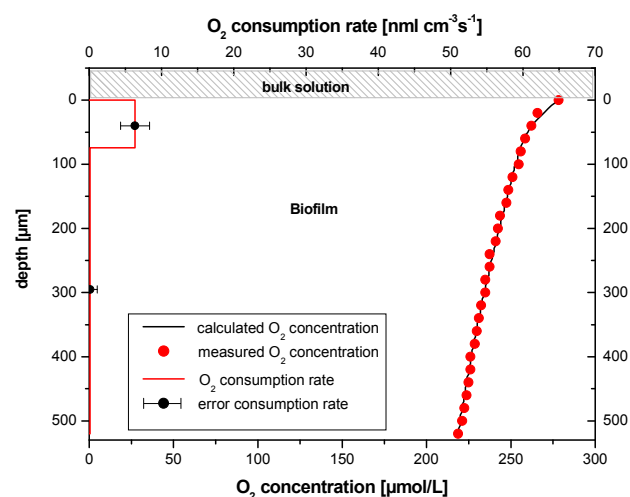


Fig. 2: Measured O₂ concentrations in the biofilm free of uranium (points), and the calculated best-fitting O₂ concentration profile (line), and connected O₂ consumption (line).

The results reveal that the addition of uranium in ecologically relevant concentrations (1 · 10⁻⁵ M) to stable multispecies biofilms has a strong effect on the oxygen concentration and consumption rates in biofilms due to a stimulation of the metabolism of the microbes and, consequently, on their respiratory activity and oxygen consumption.

ACKNOWLEDGEMENTS. The authors thank Peter Berg for valuable discussions concerning the numerical model PROFILE, the EU for financial support within the European research project FUNMIG, and the German Research Council (DFG) for funding the project under the contract no. AR 584/1-1.

REFERENCES

[1] Berg, P. et al. (1998) *Limnol. Oceanogr.* **43**, 1500-1510.

New experimental setup for the determination of the differences between the chemical and radiological toxicity of actinides in algae

Ma. Vogel, A. Günther, J. Raff

First experiments for the determination of the chemical toxicity of actinides were performed with *Chlorella vulgaris* in the presence of the environmental relevant uranium concentration of $1 \cdot 10^{-5}$ M. No significant effect of uranium on algal growth could be detected in comparison to cells cultivated without uranium. The uranium concentration in the medium decreased during cultivation.

The aim of the commenced study is to differentiate between the radiological and chemical toxicity of actinides in dependence on the oxidation state, bioavailability and speciation (pH). Because of the ubiquitous occurrence of algae and their relevance as part of the natural food chain, different algae are included in our investigations starting with *C. vulgaris* and continuing with *Volvox*. The influence of actinide species on algal survival and growth will be investigated by measuring growth curves and respiration quotients in the presence of different aqueous and immobilized actinide species. A combination of Warburg manometry with radiochemical analysis as well as microscopic and spectroscopic techniques will be used. The starting point of the study is the determination of the conditions under which *C. vulgaris* could be cultivated without and in presence of uranium. Experiments with resuspended *C. vulgaris* cells showed already that the cells bind uranium and remove it nearly completely from the solution at pH 5 and 6 [1].

EXPERIMENTAL. *Chlorella vulgaris* was grown in liquid glucose-glycine-medium under air supply and light until the culture reaches the steady state growth phase. The pH of the culture medium was adjusted with HCl and NaOH. The purity of the algae culture was verified by light microscopy. Growth of the culture was followed by absorption measurements and calculation of the corresponding cell numbers. Uranium was added as uranyl nitrate to obtain a total concentration of $1 \cdot 10^{-5}$ M in the culture media. The uranium concentration in the culture medium after biomass separation was determined by ICP-MS analysis.

RESULTS. The green algae *C. vulgaris* was grown at pH values between 3.6 and 8 in a glucose-glycine-medium. The growth curves in the pH range from 6–8 (Fig. 1) show the typical phases of algae growth. A cultivation of algal cells at pH values lower than 6 was not possible. Although the algal cells were exposed to $1 \cdot 10^{-5}$ M uranium, no significant differences in growth behavior occurred in comparison to those cells which were cultivated without uranium (Fig. 1,2).

The uranium speciation in the medium was calculated with the computer program EQ3/6, however, not considering the possible influence of glucose on the uranium speciation. At pH 6 and 7, the uranyl species $\text{UO}_2\text{HPO}_4(\text{aq})$ and UO_2PO_4^- are the main species in the medium. At pH 8, additionally $\text{UO}_2(\text{CO}_3)_3^{4-}$, $\text{UO}_2(\text{CO}_3)_2^{2-}$ and $(\text{UO}_2)_2\text{CO}_3(\text{OH})_3^-$ are formed. The amount of uranium in the media decreased during cultivation compared to the initial solution (Fig. 2). Precipitation as uranyl phosphates as well as immobilization on and in algal cells

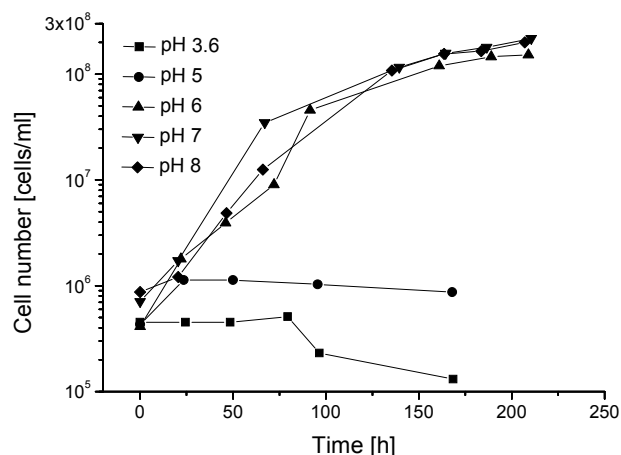


Fig. 1: Growth curves of *C. vulgaris* at different pH values.

could be a possible explanation for the uranium removal in the given pH range. To clarify this issue, detailed spectroscopic analyses of the aqueous medium, possible precipitates in the medium and the algal cells are intended. Radiological and chemical toxicity could not be detected under the given conditions because of the low uranium concentration and decreased bioavailability caused by uranium immobilization. It is known that the used uranium concentration is sufficient to cause inhibition of algal growth [2]. But the content and nature of the organic and phosphate compounds present in the medium may also play an important role and may prevent adverse effects on algal growth.

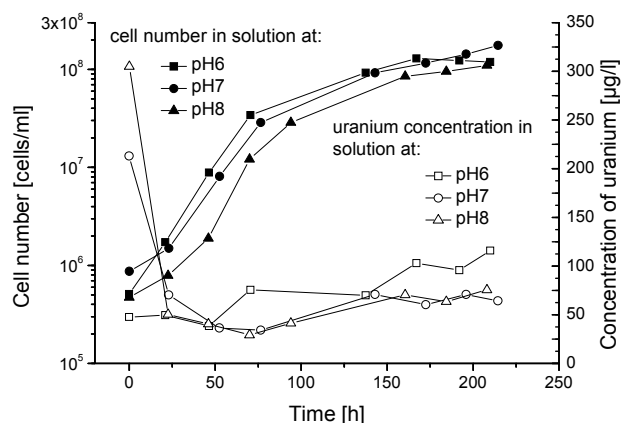


Fig. 2: Growth curves of *C. vulgaris* exposed to uranium at different pH values. At the beginning of the experiment the total uranium concentration was $1 \cdot 10^{-5}$ M.

Further experiments will investigate the effect of higher uranium concentrations and modified bioavailability of complexed uranium on the growth of *C. vulgaris*. Additionally, the measurement of respiratory rates should offer a useful instrument to determine the differences between chemical and radiological toxicity of actinides in algal cells.

REFERENCES

- [1] Günther, A. et al. (2008) *Biometals*, in press.
- [2] Hogan, A. C. et al. (2005) *Aquat. Toxicol.* **75**, 343-353.

Intracellular uranium accumulation in cell suspensions of rape

K. Viehweger, G. Geipel

Uranium is a widespread radioactive toxic heavy metal inducing a basic tolerance similar as shown for other heavy metals in plants [1]. Here we describe initial experiments to investigate some of the main components of U homeostasis: uptake and cellular sequestration revealed by confocal microscopy and cell fractionation after U exposure. Time-resolved laser-induced fluorescence spectroscopy (TRLFS) enabled a deeper insight in possible cellular ligands of U.

EXPERIMENTAL. Suspension-cultured cells of rape (*Brassica napus*) were grown in a medium according to Linsmaier and Skoog [2] in a 9-day growth cycle. Cell fractions were obtained by two-phase-partition [3] with slight modifications. Time-resolved laser-induced fluorescence spectroscopy (TRLFS) was performed using a pulsed Nd:YAG laser pumping a MOPO module equipped with an ICCD detection system.

RESULTS. Addition of U to rape cell suspensions caused a rapid decrease of the heavy metal concentration in the culture medium. To test the hypothesis that the cell wall can act as a cation exchanger and thus binds the UO_2^{2+} , confocal microscopy was performed. Figure 1 shows that U has been taken up rapidly into the cell without any affinity to the cell wall. It is probably accumulated in vesicles closed to the tonoplast. The cells obviously have an active U homeostasis indicated by their viability which is shown by the cytoplasmic accumulation of the pH-dependent dye SNARF-4F. Cell viability was proven up to 100 μ M U for 48 hours (probed by MTT assay or fluorescein ester + propidium iodide labeling, data not shown). To gain an insight in possible molecular interactions between different cell compounds and U, cells were incubated 24 hours with 10 μ M U. Subsequent fractionation was performed by two-phase-partition. Fraction purity and vesicle sidedness were demonstrated by the example

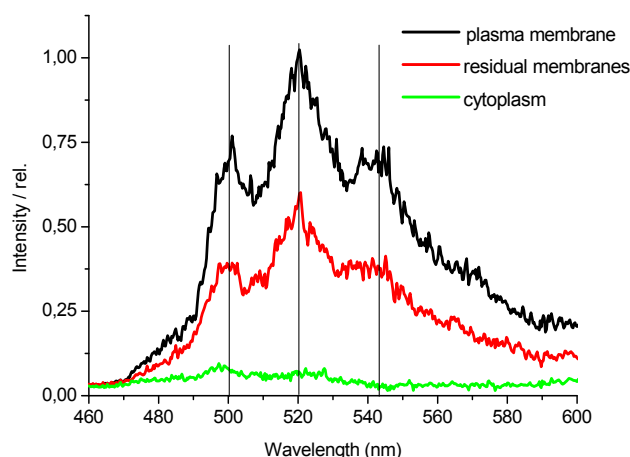


Fig. 2: Luminescence spectra of cell fractions, which were incubated with 10 μ M U, spectra were recorded at Ex 410 nm.

of a marker enzyme of the plasmamembrane (ATPase activity, data not shown).

Luminescence spectra of different cell fractions (Fig. 2) were recorded by TRLFS. These spectra indicate very similar species of U complexes in the plasma membrane and residual membranes. In contrast there is a really different spectrum of the cytoplasm, suggesting another U speciation.

The luminescence lifetimes (Tab. 1) reveal different molecular environments of U in the individual cell fractions. The data presume a high affinity of U for its ligands in the membranes. This is confirmed by initial binding experiments with plasmamembrane vesicles (data not shown).

Tab. 1: Calculated luminescence lifetimes measured luminescence decay behaviour.

| Luminescence lifetimes | |
|--------------------------------|-----------------------|
| τ (U – plasma membrane) | $1.02 \pm 0.02 \mu$ s |
| τ (U – residual membrane) | $0.72 \pm 0.02 \mu$ s |
| τ (U – cytoplasm) | $0.67 \pm 0.02 \mu$ s |

Further investigations should identify the transport-mechanism of a possible U-complex at the plasmamembrane and clarify the U speciation in the cytoplasm. For this purpose it is crucial to understand some of the cellular reactions of heavy metal homeostasis.

ACKNOWLEDGEMENTS. We thank S. Gürtler for committed technical assistance.

REFERENCES

- [1] Clemens, S. (2001) *Planta* **212**, 475-486.
- [2] Linsmaier, E.M. et al. (1965) *Physiol. Plant.* **18**, 100-127.
- [3] Larsson, C. et al. (1994) *Methods Enzymol.* **228**, 451-469.

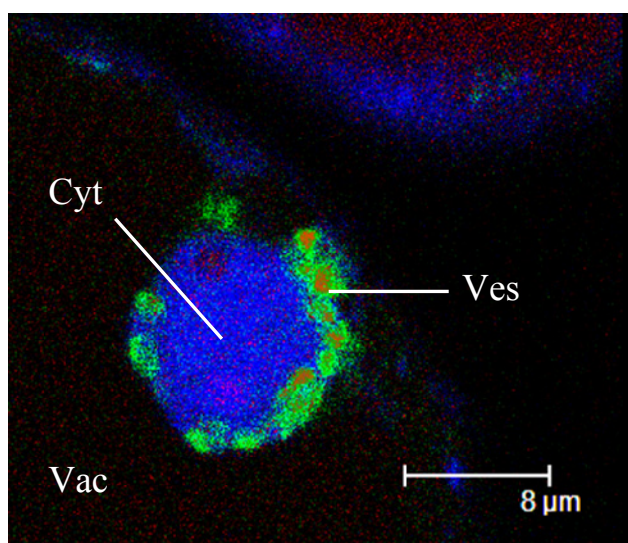


Fig. 1: Intracellular U sequestration 15 min. after exposure of 25 μ M U shown by confocal microscopy, overlay image results from Ex 405 nm/Em 460-530 nm (green coloured) and Ex 543 nm/Em 630-660 nm (blue coloured), cells are counterstained with 2 μ M SNARF-4F AM.

Interaction of actinides with solid phases

ISDA – Integrated sorption database for interactions of chemotoxic and radioactive contaminants with mineral systems in geologic formations

A. Richter, V. Brendler, T. Brasser,¹ C. Scherschel,² M. Veerhoff,² C. Klinger³

¹Gesellschaft für Anlagen- und Reaktorsicherheit mbH, Braunschweig, Germany; ²erd_sicht Dr. Veerhoff & Scherschel GbR, Alfter, Germany; ³Deutsche Montan Technologie GmbH – DMT, Essen, Germany

A cooperative project aims at the provision of necessary conditions for reliable predictions of the spatial and temporal migration of chemotoxic contaminants and radionuclides. The focus of the project is the integration and advancement of the existing sorption databases RES³T (FZD) [1] and SODA (GRS) [2] to one web-availably databank tool with a harmonized user interface. This database comprises comprehensive geochemical information on the characterization of contamination retention of rocks in a subsurface waste disposal.

The database RES³T – Rossendorf Expert System for Surface and Sorption Thermodynamics – is the first mineral specific digital database and is based on the concept of surface complexation (Surface Complexation Modeling – SCM). The elements covered comprises the actinides and fission products as well as the heavy metals and As, but also major constituents of the background media. The database has been maintained beyond the end of the project in 2004.

The sorption database SODA comprises information and distribution coefficients (K_D) with regard to the retardation behavior of non-radioactive pollutants contained in chemotoxic wastes which are to be disposed of in deep geological formations.

The new integrated databank tool ISDA allows the access to the already acquired knowledge in terms of several aspects of a possible contaminant cycle at underground waste disposal more easily and to utilize it in practice. Thus, a base for risk analyses will be provided in consideration of several potential scenarios.

The work is done jointly by the Institute of Radiochemistry, the Gesellschaft für Anlagen- und Reaktorsicherheit Braunschweig (GRS), the Deutsche Montan Technologie GmbH Essen (DMT), and erd_sicht Dr. Veerhoff & Scherschel.

In addition to the mere datasets, also a multitude of references is filed with partially detailed assessments of data collection, experimental setup, etc. The aim is to enable the user to make a qualified data search and a critical data evaluation via a comfortable query of the database content without a specific knowledge of the database structure (knowledge based system).

The following possibilities are offered:

- Directed search of data currently available for contaminants and rocks to get reliable input data for site evaluations.
- Appraisal of the spreading of sorption data (statistical analyses).
- Verification and comparison of SCM model predictions with the conventional sorption data filed in the database.
- Deduction of SCM parameters from conventional sorption data filed in the database and computation of K_D values vice versa by geochemical speciation calculations with involvement of SCM.
- Access to the data inventory via internet.

Figure 1 shows the structure of the K_D query.

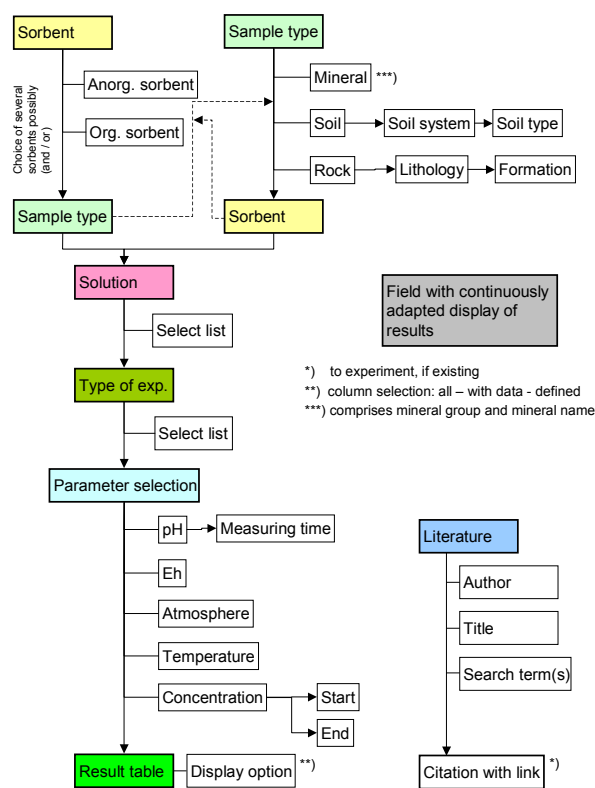


Fig. 1: Structure of the K_D query in ISDA.

The Institute of Radiochemistry contributes to the following work packages:

- Integration of the sorption databases SODA and RES³T (convergence of table structure and internal relations of SODA and RES³T, defined extension of functionality).
- Programming and layout of the web interface for worldwide access and update of the database.
- Extension of the database content (continuous review of sorption literature) with interpretation and documentation.
- Identification and exemplarily closure of data gaps by own experiments within an experimental research program by means of batch and selected column experiments (see [3]).

ACKNOWLEDGEMENTS. Financial support by the BMBF (contract No. 02C1144) is gratefully acknowledged.

REFERENCES

- [1] Brendler, V. et al. (2004) Report FZR-409.
- [2] Brasser, T. et al. (2002) Report GRS-182.
- [3] Nebelung, C. et al. (2008) this report, p. 52.

Simultaneous detection of coexisting U(VI) compounds by TRLFS

N. Baumann

A finely ground mixture of boltwoodite ($\text{HKUO}_2\text{SiO}_4 \cdot 1.5\text{H}_2\text{O}$) and bariumuranylcarbonate ($\text{Ba}_2[\text{UO}_2(\text{CO}_3)_3] \cdot 6\text{H}_2\text{O}$) was characterized by time-resolved laser-induced fluorescence spectrometry (TRLFS) at room temperature. In the gained fluorescence signal the lifetimes of both compounds and 10 positions of their theoretically expected 12 peak maxima could be found. So it is shown that two U(VI) compounds could be proved within only one TRLFS measurement, and a contribution to assess the resolution of that method was made.

EXPERIMENTAL. Boltwoodite was synthesized using a method described by [1], bariumuranylcarbonate (BaUC) by a method described by [2]. The purity of the obtained crystals was verified by XRD and EDX measurements.

Because of the higher specific fluorescence intensity of BaUC compared to boltwoodite, the two substances were mixed in a mass ratio of 1 : 15 and finely ground with an agate mortar. The measurements were carried out with the dry powder of the mixture. The TRLFS system comprised a Nd:YAG diode laser with an excitation wavelength of 266 nm, the laser dispersion peak was avoided by using a long pass filter.

RESULTS. The acquired TRLFS spectra displayed a high signal-to-noise ratio. The deconvoluted fluorescence spectrum of the mixture (see Fig. 1) clearly shows eight emission bands at 468.8, 486.1, 499.0, 506.5, 519.6, 542.3, 566.2, and 592.8 nm and two shoulders at 527.8, and 550.5 nm; the second and the sixth peak of BaUC signal are not visible (see Tab. 1).

Based on that time-resolved measurement, the fluorescence decay function was determined (see Fig. 2). The decay curve of the signal is best described with three lifetimes: 0.77 μs , 2.8 μs , and 13.5 μs . In that case exists an excellent concordance between experimental points and fit. It is assumed that the longest lifetime t_3 is caused by BaUC, because t_3 is in same magnitude of the lifetime known from literature (see Tab. 2). Lifetime t_2 is interpreted as caused by the component boltwoodite in concordance of the results published in [3]. The shortest lifetime t_1 is assumed to be originated from a species with almost same chemical coordination, but with more water molecules in its coordination environment. This may occur on the surface of the particles.

These results presented here are an example for the possibility that the most peak positions and the lifetimes of two U(VI) compounds in one sample can be proved within one measurement by the method of time-resolved laser-induced fluorescence spectrometry.

ACKNOWLEDGEMENTS. I thank S. Amayri (Johannes Gutenberg University, Mainz) for providing the samples.

REFERENCES

- [1] Vochten, R. et al. (1997) *Can. Mineral.* **35**, 735-741.
- [2] Amayri, S. et al. (2005) *J. Solid State Chem.* **178**, 567-577.
- [3] Baumann, N. et al. (2006) *Report FZR-443*, p. 45.

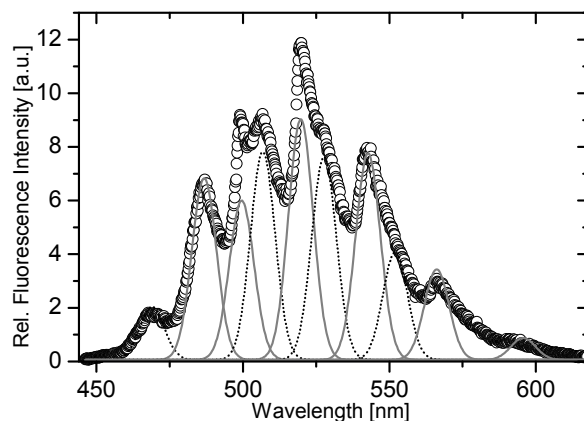


Fig. 1: Deconvoluted fluorescence spectrum of the grounded mixture. Gray - peaks caused by boltwoodite, dotted - by BaUC.

Tab. 1: Position of emission bands from the mixture in nm, in comparison to peak maxima from boltwoodite [3] and from BaUC [2].

| Peak position | Mixture | Boltwoodite | BaUC |
|-----------------|---------|-------------|-------|
| 1 st | 468.8 | | 469.9 |
| | 486.1 | 485.1 | |
| 2 nd | n. d.* | | 487.7 |
| | 499.0 | 501.5 | |
| 3 rd | 506.5 | | 507.3 |
| | 519.6 | 521.2 | |
| 4 th | 527.8 | | 528.9 |
| | 542.3 | 543.0 | |
| 5 th | 550.5 | | 552.2 |
| | 566.2 | 567.4 | |
| 6 th | n. d.* | | 570.5 |
| | 592.8 | 591.4 | |

*n. d.: not detected.

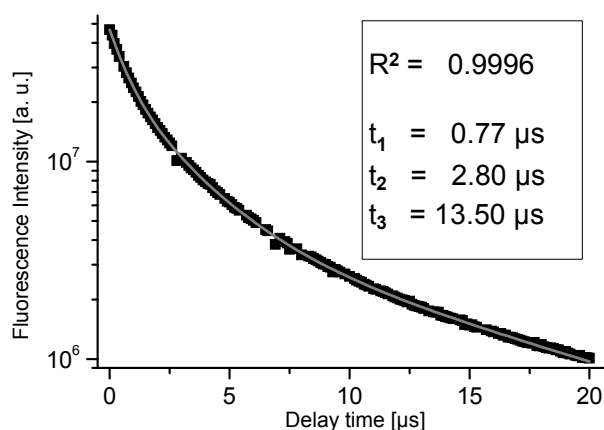


Fig. 2: Fluorescence decay of the uranium (VI) signal from the mixture.

Tab. 2: Lifetimes from the mixture, in comparison to lifetimes from boltwoodite [3] and from BaUC [2].

| Lifetime | Mixture | Boltwoodite | BaUC |
|-------------------------|---------|-------------|----------------|
| t_1 [μs] | 0.77 | 0.49 | |
| t_2 [μs] | 2.8 | 2.4 | |
| t_3 [μs] | 13.5 | | 16.3 ± 0.4 |

TRLFS fingerprinting of aluminosilicates

V. Brendler, A. Křepelová, N. Baumann, P. Trepte

TRLFS proved to be able to discriminate between aluminol and silanol surface binding sites for uranyl(VI) species on simple clay model systems: silica gel, gibbsite and kaolinite. This fingerprinting is rather based on fluorescence decay lifetimes than on emission peak maxima positions.

The U(VI) binding to complex systems such as clays, which play an important role in nuclear waste disposal design, is still to be clarified. An efficient tool to study the relevant speciation *in-situ* is required, thus TRLFS (time-resolved laser-induced fluorescence spectroscopy) was applied. Silica gel (providing higher binding site concentrations as quartz) and gibbsite were used as model substances for the investigation of silanol and aluminol binding sites in clays, respectively. Kaolinite, offering both types of surface groups, served as a further model system.

EXPERIMENTAL. Solid-liquid ratios were 0.25, 12.5, and 4.0 for silica gel, gibbsite and kaolinite, respectively. Measurements were performed in 0.1 M NaClO₄ and at uranium concentration between $5 \cdot 10^{-6}$ M and $1 \cdot 10^{-5}$ M, with the pH being varied between 4.5 and 9. For the TRLFS measurements the solid phase was centrifuged and re-suspended in a NaClO₄ solution with pH and ionic strength identical to the original but without uranium. A Nd:YAG diode laser with an excitation wavelength of 266 nm was used to study the sorbed species. Spectra were recorded by a diode array in the wavelength range between 446 and 617 nm. The delay times covered 30 ns up to 200 μ s. All measurements were performed under oxygen atmosphere and at room temperature. For more details cf. [1].

RESULTS. For silica gel, at least three U(VI) surface complexes with fluorescence decay constants τ of approximately 80 – 20 μ s, 175 μ s and 260 – 440 μ s were observable. This is very close to the values published by Gabriel et al. [2].

Concerning gibbsite, one surface species with $\tau_1 = 2.5$ μ s is present throughout the whole pH range, a second species occurs only below pH 7 (τ_2 decreasing from 22 to 10 μ s) and a third species appears at pH > 7 (τ_3 increasing from 13 to 24 μ s). The obtained lifetimes (but not the peak maxima) are contradictory to our previous work [3]. Those measurements, however, covered a much shorter time window (only 6.5 μ s compared to the 200 μ s in this work), and the sensitivity of the experimental set-up was significantly increased during the last two years.

Finally, the investigation of kaolinite revealed two surface species with lifetimes of τ_1 slightly increasing with pH from 3.6 to 4.7 μ s and τ_2 more pronounced rising from 26 to 45 μ s. For pH values below 7 this is closer to the gibbsite results, indicating that aluminol sites dominate uranyl sorption onto aluminosilicates. The lifetime results are summarized in Tab. 1.

Concerning the peak maxima (see Fig. 1), they were red-shifted compared to the free uranyl cation for all three systems: by 11 – 14 nm for the 2nd peak, by 9 – 12 nm for the 3rd peak, and by 7 – 11 nm for the 4th peak. The shifts are similar to each other (within their margins of error), with the exception of silica gel, where the shifts of the

Tab. 1: Comparison of fluorescence lifetime parameters for kaolinite and various model systems.

| System | Fluorescence lifetime [μ s] | | |
|---|----------------------------------|-----------------|-----------------|
| | 1 st | 2 nd | 3 rd |
| Silica gel ^a | 80 – 20 | 175 | 260 |
| Quartz ^d | | 170 | 360 |
| Gibbsite ^a | 2.5 | 23 – 10 | 13 – 24 |
| Gibbsite ^b | 5.6 | | |
| γ -Al ₂ O ₃ ^c | 11 | 40 | 141 |
| Kaolinite ^a | 3.6 – 4.7 | 26 – 45 | |

a) this work; b) Baumann et al. [3]; c) Froideval et al. [4]; d) Gabriel et al. [2].

long lived species (15 – 16 nm) are consistently larger than those of the short-lived ones and those of kaolinite and gibbsite. The peak positions of kaolinite (Al- and Si binding sites) are in-between those of gibbsite (Al) and silica gel (Si).

In case of UO₂²⁺ surface species, obviously lifetimes are more suitable than peak positions to discriminate contributions of aluminol and silanol surface groups to the overall sorption. The present state of knowledge indicates that aluminol sites dominate uranyl sorption onto aluminosilicates.

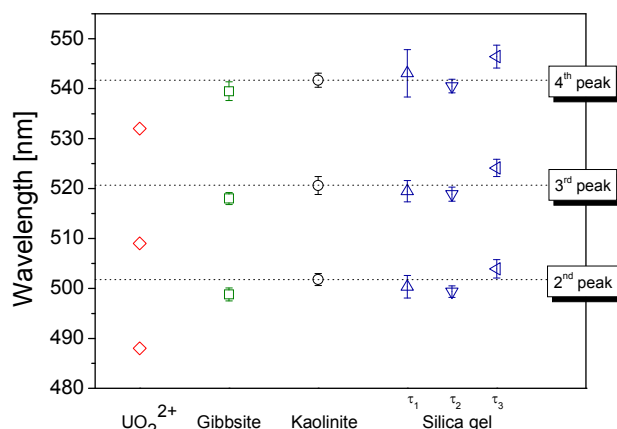


Fig. 1: Comparison of major TRLFS peak maxima for UO₂²⁺ surface species.

REFERENCES

- [1] Křepelová, A. et al. (2007) *Environ. Sci. Technol.* **41**, 6142-6147.
- [2] Gabriel, U. et al. (2001) *J. Colloid Interface Sci.* **239**, 358-368.
- [3] Baumann, N. et al. (2005) *J. Colloid Interface Sci.* **290**, 318-324.
- [4] Froideval, A. et al. (2006) *Geochim. Cosmochim. Acta* **70**, 5270-5284.

Modeling of the U(VI) sorption on mineral mixtures: Synthetic and natural sandstone

C. Nebelung, A. Richter, V. Brendler

The modeling of metal sorption on mineral mixtures requires the knowledge of the single components. All protolysis constants and surface complex formation constants of the single minerals and its mineral characterization have to be considered. The sorption can be influenced strongly even by small contents of the components. Iron is such a minor component with a high influence in the natural sandstone. The comparison between prediction and experimental results is satisfactory.

EXPERIMENTAL. The U(VI) sorption on natural and synthetic sandstone was carried out in pH (3–11) and concentration (10^{-9} M – 10^{-3} M) dependence. The sorption was measured under ambient conditions. The natural sandstone (specific surface $0.69 \text{ m}^2/\text{g}$) consists mainly of quartz. Orthoclase and iron oxides (modeled as hematite) are minor components. The synthetic sandstone I was mixed from 95 % quartz ($0.045 \text{ m}^2/\text{g}$) and 5 % muscovite containing iron ($0.88 \text{ m}^2/\text{g}$), and the synthetic sandstone II contained 90 % quartz, 5 % muscovite and 5 % hematite ($0.89 \text{ m}^2/\text{g}$). The volume to mass ratio was 12.5 g/L . The sandstone was conditioned 4 weeks with 0.1 M NaClO_4 with pH adjusting. After 5 days sorption in an overhead shaker, the solids and liquids were separated by ultra filtration (30 kD filter). The soluble uranium was measured by liquid scintillation spectroscopy. Detailed experimental conditions were given in [1].

RESULTS. The modeling was carried out with the diffuse double layer model (DDL) to predict the sorption of uranium on sandstone. For the modeling, the code MINTEQA2 (Version 4.03, US EPA May 2006) was used with thermodynamic data of aqueous and solid species from the NEA-TDB [2], solid uranium components from [3,4]. The mineralogical composition, protolysis data (pK) and surface complex formation constants (log K) were calculated for a site density of 2.31 sites/nm^2 (Tab. 1).

Tab. 1: Surface complex constants for modeling.

| pK / log K | quartz | muscovite | hematite |
|---|-------------|------------|------------|
| »XOH ₂ ⁺ | | 6.11 [7] | 7.15 [8] |
| »XO ⁻ | -7.20 [5] | -7.76 [7] | -8.45 [8] |
| »XOUO ₂ ⁺ | 0.30 [5] | -0.50 [7]* | 1.52 [8] |
| »XOUO ₂ OH | -5.65 [5] | | |
| »(XO) ₂ UO ₂ | | -5.70 [7] | |
| »(XO) ₂ UO ₂ (OH) ₃ ³⁻ | | | -22.98 [8] |
| »XO(UO ₂) ₃ (OH) ₅ | -16.75 [5]* | | |
| »XOUO ₂ CO ₃ ⁻ | 9.62 [6] | | |
| »XOHUO ₂ CO ₃ | | | 16.32 [9] |
| »XOH ₂ UO ₂ (CO ₃) ₂ ⁻ | | | 29.15 [9]* |
| »XOH ₂ UO ₂ (CO ₃) ₃ ³⁻ | | | 36.28 [9]* |

*: no influence on the sorption

The modeling of the pH dependence of U(VI) sorption on synthetic sandstone I and natural sandstone is shown in Fig. 1. The hematite hardly influences the sorption despite the small iron content. The modeling with the combination of all components gives a good agreement between sorption prediction and experiments.

In Fig. 2 the concentration dependence is described. If all solid U compounds are allowed, schoepite precipitation was predicted (black, dashed lines). Schoepite is an aged mineral and cannot be formed in five days (sorption time). If, therefore, schoepite precipitation is excluded, soddyite and metaschoepite were indicated (gray line). If schoepite and soddyite were excluded, only the precipitation of metaschoepite was calculated (black, solid lines). The predicted precipitation was found at 10^{-3} M U(VI) solution on synthetic sandstone. During the sorption on natural sandstone no precipitation was measured. The precipitation reaction may be kinetically inhibited. The uranium sorption on natural sandstone at U(VI) concentrations up to 10^{-4} M is very good predicted. At U(VI) concentrations between 10^{-9} and 10^{-6} M the measured sorption is lower for the sorption on synthetic sandstone. The principle of our sorption prediction is the superposition of simultaneous sorption and competition reactions based on mineralogical composition. With this model a good accordance with experimental values was found.

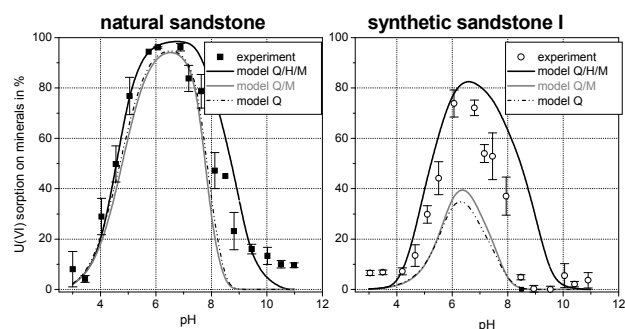


Fig. 1: Modeling of U(VI) sorption on sandstone, pH dependence ([U(VI)] = 10^{-6} M): single quartz (Q), quartz and muscovite (Q/M), and quartz, muscovite and hematite together (Q/M/H).

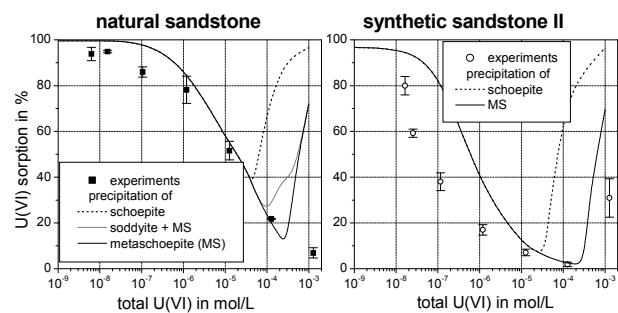


Fig. 2: Modeling of U(VI) sorption on sandstone, concentration dependence (pH=5).

ACKNOWLEDGEMENTS. Funding by the BMBF (02C1144) is gratefully acknowledged.

REFERENCES

- [1] Nebelung, C. et al. (2006) *Report FZD-459*, p. 50-51.
- [2] Guillaumont, R. et al. (2003) *Update on the chemical thermodynamics of U, Np, Pu, Am, Tc*, Elsevier, Amsterdam.
- [3] Torrero, M.E. et al. (1994) *Radiochim. Acta* **66/67**, 29.
- [4] Moll, H. et al. (1998), *J. Alloys Comp.* **271-273**, 765.
- [5] Pabalan, R.T. et al. (1998) *Adsorption of metals by geomedia*, Academic Press; San Diego.
- [6] Davis, J.A. et al. (2001) *Report NUREG/CR-6708*, U.S. NRC; Washington, DC.
- [7] Arnold, T. et al. (2001) *J. Contam. Hydrol.* **47**, 219.
- [8] Cromieres, L. (1996) Thesis, Université Paris-Sud 11, Orsay.
- [9] Turner, D.R. et al. (1996) *J. Contam. Hydrol.* **21**, 311-332.

Cesium sorption on montmorillonite and bentonite: Sorption prediction and experiments

C. Nebelung, V. Brendler

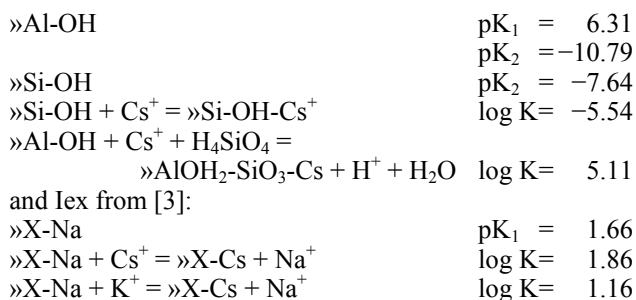
The sorption of cesium on bentonite and montmorillonite was investigated in batch experiments to understand the near-field behavior in geological nuclear repositories. The sorption was modeled using thermodynamic data of aqueous and solid species, protolysis data and surface complex formation constants from literature, and the characterization data of the solids. The predicted and experimental sorption data show a good agreement for pH dependence as well as for metal concentration dependence.

The partitioning of dissolved metals between the solution and all relevant surfaces is usually characterized by equilibrium distribution coefficients – K_D . Different physico-chemical parameters are included in this parameter. So, the K_D is very sensitive to slight changes in the system parameters such Eh, pH, specific surface area or a new mineral phase. A scientifically founded description of sorption processes at the mineral-liquid surface is possible with the surface complexation models (SCM), the ion adsorption on surface sites as complexation reaction.

EXPERIMENTAL. Sorption parameters were carried out in batch tests. The sorption on bentonite (KWK) was studied at different dry bulk densities of the clay (1.3, 1.6, 1.9 g/cm³) at pH 8 for the Cs concentration dependence (10⁻⁴ to 10⁻⁹ M). Cs sorption experiments were also carried out on the pure mineral montmorillonite (SWy-1) in 0.1 M NaClO₄. The pH dependence was measured between pH 3 and 11. The specific surface was measured by BET for bentonite 15.7 m²/g, and for montmorillonite 30.1 m²/g. Detailed experimental conditions were given in [1].

RESULTS. The modeling was carried out with the constant capacitance model (CC) and the ion exchange model (Iex) to predict the sorption of cesium on montmorillonite and bentonite. The modeling was based on the code MINTEQA2 (Version 4.03, US EPA May 2006), thermodynamic data of aqueous and solid species from the NEA-TDB [2], the mineralogical composition, protolysis data (pK) and surface complex formation constants (log K) calculated for a site density of 2.31 sites/nm².

For the modeling of Cs sorption on montmorillonite and bentonite, protolysis and surface complex formation constants were used with CC:



The modeling of the Cs sorption on montmorillonite versus pH (Fig. 1) shows a very good agreement of measured and predicted values in the case of the Iex modeling. The modeling with CC gives no congruence. Especially the

silicate complex (»AlOH₂-SiO₃-Cs) causes the high sorption prediction. For the concentration dependence (Fig. 2) a good agreement between measured and predicted values (Iex) is achieved, too. The higher sorption on montmorillonite is caused by the higher (nearly twice) specific surface. In case of sorption on bentonite at the three types of pore water the higher the pore water density, the lower the sorption was. The alkali metals in the solution compete with Cs. A light underestimation of the sorption occurred at low Cs concentrations. The prediction of the Cs sorption on bentonite and montmorillonite shows that the retention is caused by pure ion exchange.

It is possible to predict accurately the sorption with reliable pK and log K values from the literature and the exact knowledge of the actual system parameter.

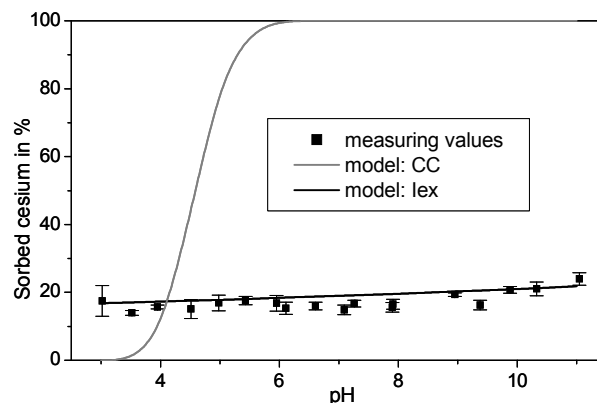


Fig. 1: Cs sorption on montmorillonite, pH dependence.

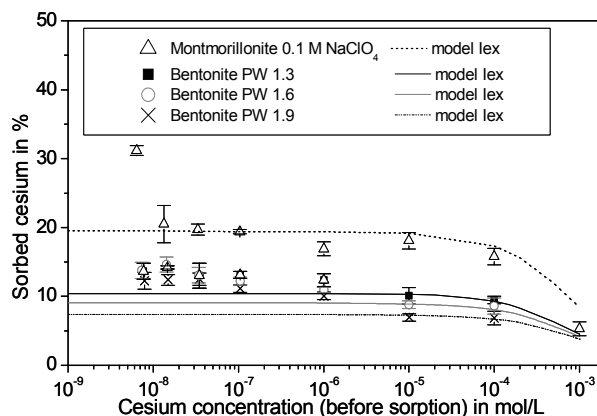


Fig. 2: Cs sorption on montmorillonite and bentonite at three pore water concentration dependence.

ACKNOWLEDGEMENTS. Funding by the European Commission (NF-PRO C2-ST-C-01) is gratefully acknowledged.

REFERENCES

- [1] Nebelung, C. et al. (2006) Report FZR-443, p. 39.
- [2] Guillaumont, R. et al. (2003) Update on the Chemical Thermodynamics of U, Np, Pu, Am, Tc, Elsevier, Amsterdam.
- [3] Hurel, C. et al. (2002) Radiochim. Acta 90, 695-698.

Selenite reduction by mackinawite, magnetite and siderite

A. C. Scheinost, H. Funke, R. Kirsch, L. Charlet¹

¹Earth and Planetary Science Department, University of Grenoble-I, Grenoble, France

Depending on Fe(II) mineral surface and pH, selenite (Se(IV)O₃²⁻) is reduced to red Se(0), gray Se(0) and to Fe(II) selenides with various structures.

The fission product ⁷⁹Se is commonly considered as one of the key risks of nuclear waste disposal sites due to its long half-life of 1.1 · 10⁶ a and due to the high environmental mobility of its anionic aqueous species. This mobility may decrease by formation of reduced Se species (oxidation states 0, -I, -II) through biotic as well as abiotic reduction mechanisms. Here we demonstrate that a range of other Fe(II)-hosting mineral phases such as mackinawite (FeS), magnetite (Fe₃O₄), and siderite (FeCO₃) are capable of reducing selenite [1].

EXPERIMENTAL. Magnetite, mackinawite and siderite samples were prepared and stored as suspensions under strictly anoxic conditions (< 1 ppmv O₂) in a Jacomex glovebox. Particle size of magnetite and mackinawite were 2 – 10 nm whereas siderite particles have a mean diameter of 3 μm. At time zero an aliquot of a Se(IV) stock solution at pH 6.0 was introduced into the glass reactor to obtain initial solution concentrations of 0.99 to 9.09 mM. After given reaction periods, a 10 mL sample of suspension was filtered through a 0.22 μm pore size membrane and analyzed for selenium concentration. The wet pastes were then transferred to XAS sample holders, shock-frozen with liquid N₂, and transported in a Dewar filled with liquid N₂ to the synchrotron facility. Se-K edge XAS spectra were collected at the ROBL beamline (ESRF, Grenoble, France) at 15 K. Following this protocol, we prevented O₂ diffusion to the sample, photo-reduction (or -oxidation) of Se by the intense X-ray beam, and excluded the thermal contributions of the Debye-Waller factor.

RESULTS. According to their white line peaks, the three mackinawite samples can be divided into two groups, sample “Mack 4 h pH 4” with a Se oxidation state of -II, and samples “Mack 4 h” and “Mack 1 d” with Se(0) (Fig. 1c). This assignment is corroborated by wavelet analysis [2]. While the three samples appear to be almost identical based on their EXAFS Fourier-transform spectra, the unfiltered EXAFS spectra show significant differences in phase shift and amplitude at low k (data not shown). For the sample at pH 4.3, these features are similar to those of tetragonal FeSe, and the features of the samples at higher pH are similar to those of nanoparticulate red Se. The small coordination numbers of the mackinawite samples for shells beyond the coordination sphere, in comparison to those of the 5-nm red Se reference, suggest that the size of structurally coherent regions is below one nanometer in the reacted samples. After 1 day reaction time, the XANES spectrum of the siderite sample is dominated by the strong white line of Se(IV) (“B” in Fig. 1e), and the EXAFS Fourier-transform shows the presence of an oxygen coordination shell at about 1.4 Å (Fig. 1f), hence unreduced selenite is still present after one day. A small shoulder in the edge, however, with an inflexion point at 12656.0 eV (“A” in

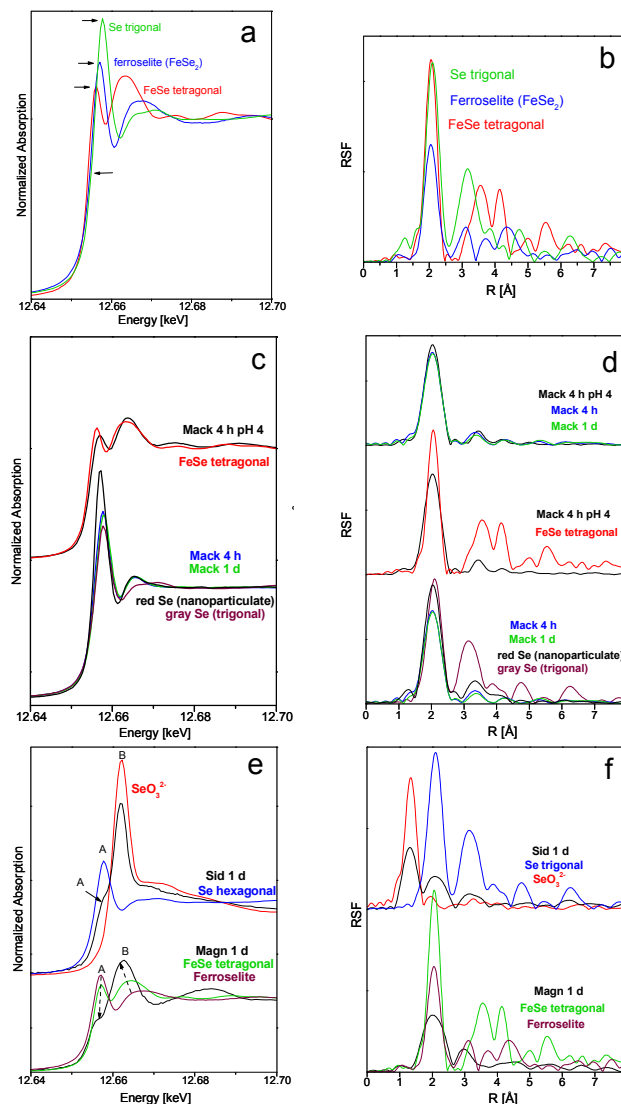


Fig. 1: Se K-edge XANES (a,c,e) and EXAFS spectra (b,d,f) of redox samples and of selected references. (a,b) Trigonal Se, ferroselite (FeSe₂) and tetragonal FeSe. (c,d) Selenite reduced by nanoparticulate mackinawite (FeS). (e, f) Selenite reduced by siderite (FeCO₃) and by nanoparticulate magnetite (Fe₃O₄).

Fig. 1e), and the EXAFS fit result with a 0.6 Se atoms at 2.38 Å suggests partial reduction to elemental Se. For the magnetite sample, the XANES edge position indicates oxidation state -II (Fig. 1e). The narrow peak typical for FeSe phases is not present, however, and appears only as a shoulder in the edge (labeled “A” in Fig. 1e). EXAFS Fourier-transform does not reveal any traces of an oxygen shell (Fig. 1f), indicating a complete reduction of selenite. The closest match of Se(-II) structures is trigonal Fe^{II}₅Fe^{III}₂Se₈, which has one Fe atom at 2.33 Å, followed by four Fe atoms at distances from 2.47 to 2.54 Å and 12 Se atoms at 3.54 – 3.62 Å [3].

REFERENCES

- [1] Scheinost, A. C. et al. (2008) *Environ. Sci. Technol.*, in press.
- [2] Funke, H. et al. (2008) this report, p. 55.
- [3] Andresen, A. F. et al. (1964) *J. Phys. IV* **25**, 574-578.

Identification of selenium redox products by EXAFS wavelet analysis

H. Funke, A. C. Scheinost

A new type of application of the wavelet transform to the analysis of EXAFS data is presented. A unique correlation of the sorption products of reduced Se species on Fe nanoparticles with reference substances is demonstrated by comparison of their wavelet transforms.

The reduction from soluble selenate (Se(VI)) or selenite (Se(IV)) species to elemental Se and iron selenides of low solubility by Fe containing minerals (e.g. mackinavite (FeS), magnetite (Fe₃O₄)) is in detail examined by Scheinost et al. [1,2]. The adequate method for this analysis is the X-ray absorption spectroscopy (XANES and EXAFS). The radioecological aspect of these investigations is well founded on the fact that on the one hand selenium may be arise as a long lived radioactive decay product, and on the other hand that the described reduction process changes the solubility behavior of the Se species substantially. In this report the wavelet analysis of the available EXAFS spectra is elucidated.

WAVELET ANALYSIS. The wavelet analysis of EXAFS spectra is developed in [3], and an extended description of their uncertainty properties is given in [4]. The wavelet transform of the k^n weighted EXAFS spectrum is given as:

$$W_{\chi}^w(k, r) = \sqrt{2r} \int_{-\infty}^{+\infty} \chi(k') k'^n \psi^*(2r(k' - k)) dk'. \quad (1)$$

In the present case the “mother” wavelet function is the Morlet wavelet

$$\psi(k) = \frac{1}{\sqrt{2\pi\sigma}} \exp(i\eta k) \cdot \exp\left(\frac{-k^2}{2\sigma^2}\right) \quad (2)$$

with the parameters, $\eta = 30$, $\sigma = 0.167$, ($\eta\sigma = 5$) which are values optimized to the distances of interest.

The goal of this present wavelet analysis is the answer of the question: Is the 1st shell maximum in the Fourier magnitude of the selenium K edge EXAFS spectra of the Fe nanoparticles with sorbed reduced Se dominated by Fe or by Se? The distance of the Fe respectively Se shell is $R \approx 2 \text{ \AA}$ (not phase corrected).

This wavelet analysis is performed by means of a comparison of wavelet transformations of well-known reference spectra with spectra, which contain partially unknown characteristics (in the wavevector space).

In earlier cases, e.g. [3], of EXAFS wavelet analyses one spectrum was evaluated to search two different elements in the same distance. In this situation the (usual) k weighting of 3 was chosen.

In the present case the weight $k = 1$ is more adapted for two reasons. First, the maximum of the backscattering amplitudes for Se arise at higher values of k than the amplitudes for Fe. The pure Se trigonal spectrum shows its amplitude maximum at $k \approx 7.7 \text{ \AA}^{-1}$.

Second, the FeSe reference, together with the corresponding redox species, shows in its 1st shell maxima Fe back scatterers with an incorporation of about $\frac{1}{4}$ Se atoms in nearly the same distance. This leads to a negative interference of the backscattering signals between the mean component Fe and the Se incorporation. A higher k weighting will amplify the Se influence on the Fe backscatterer am-

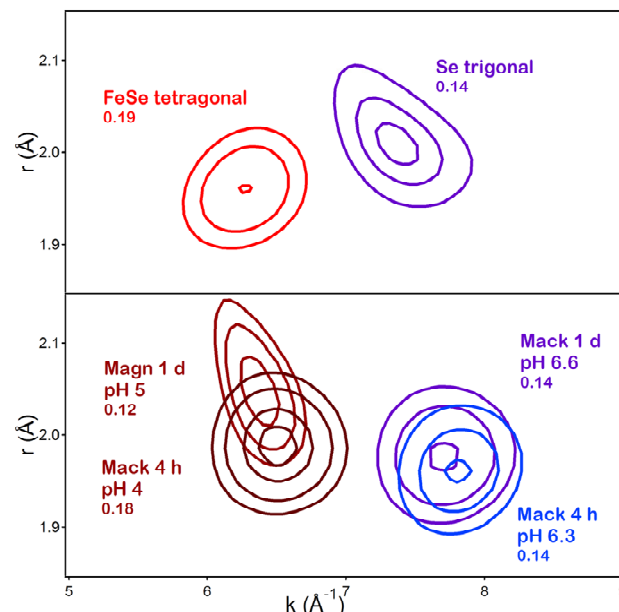


Fig. 1: Wavelet analysis of Se-K EXAFS spectra of references (top) and samples (bottom). The 1st shell maxima of Fe and Se backscatterers are obtained in different regions in the k space. Values of peak heights are given below the sample labels.

plitude which represents an unwanted falsification of the examined effect.

Remark: Due to the fact that wavelet transforms analyzes the signal parallel in r and k space, this example shows that the comprehension of the k weighting in the wavelet analysis of the EXAFS spectrum is an important step.

RESULTS. The maxima of the two references spectra FeSe tetragonal (Fe dominated) and Se trigonal (pure Se) are compared exemplarily with four selenium reduction products: mackinavite (Mack) and magnetite (Magn) minerals with different absorption times and different pH values:

- Magn 1d: pH 5, sorption on Magn, oxid. state –II,
- Mack 4h: pH 4, sorption on Mack, oxid. state –II,
- Mack 1d: pH 6.6, sorption on Mack, oxid. state 0,
- Mack 4h: pH 6.3, sorption on Mack, oxid. state 0.

The wavelet analysis, presented in Fig. 1, shows unambiguously that selenium is coordinated predominantly to Fe atoms for magnetite and mackinavite in the oxidation states –II (lower pH) and coordinated to Se for mackinavite in the oxidation states 0 (higher pH). This result is independent from the sorption time.

REFERENCES

- [1] Scheinost, A. C. et al. (2008) *Environ. Sci. Technol.*, in press.
- [2] Scheinost, A. C. (2008) this report, p. 54.
- [3] Funke, H. et al. (2005) *Phys. Rev B* **71**, 094110.
- [4] Funke, H. et al. (2007) *J. Synchrotron Rad.* **14**, 426-432.

Sorption of uranium(VI) on multiwall carbon nanotubes

A. Schierz, H. Zänker, G. Bernhard

The influence of acid treatment of multiwall carbon nanotubes on the sorption of U(VI) was studied in batch experiments. Results showed that the acid treatment of carbon nanotubes has a positive effect on both the sorption capacity and the sorption affinity.

Carbon nanotubes (CNTs) are attracting the attention of many scientists due to their unique structural, mechanical, electronic, chemical and biological properties [1]. Acid treatment was recommended as a method of purification [2]. Additionally, the oxidation causes chemical and/or structural changes on CNTs, which modify their properties and offer new applications.

Due to their hollow and nanosized structure, the use of CNTs as an adsorbent for pollutants such as Cd^{2+} or Pb^{2+} [3,4] has been considered. These studies suggested that CNTs may be a promising adsorbent for use in environmental protection and for drinking water purification. The high cost of CNTs still limits their practical use. In this work the influence of acid treatment on the U(VI) sorption properties of CNTs is investigated.

EXPERIMENTAL. The raw material (multiwall carbon nanotubes, Ilo-litech, Germany) was dispersed in $\text{HNO}_3/\text{H}_2\text{SO}_4$ (conc.; 3 : 1). The mixture was refluxed for 3 h and stirred under ultrasonication for 16 h at 70 °C. The product, the treated CNTs, was washed and dried at 90 °C.

Two series of batch experiments with the pristine and the modified CNTs were carried out: variation of pH and U(VI) concentration and/or mass-volume (m/V), respectively. The CNTs were conditioned in 0.1 M NaClO_4 with pH adjustment for 24 h under air atmosphere. After uranium addition the samples were equilibrated for 48 h and subsequently centrifuged (60 min, 170000 g). Aliquots of the supernatant were prepared for ICP-MS measurements. For studying the pH dependence the pH value of the samples were adjusted to a pH range of 1 – 11 ($\Delta \text{pH} = 1$).

RESULTS AND DISCUSSION. In this work, the sorption of U(VI) on CNTs was investigated for the first time. The acid treatment has a great impact on the adsorption capacity of CNTs for U(VI) at different pH values. The sorption capacity of the CNTs increases from 2 mg/g to 16 mg/g at pH 4 due to the higher surface functionalization by acidic groups introduced by nitric acid oxidation (Fig. 1). Both the Langmuir sorption isotherm model (correlation coefficient $R^2 > 0.98$) and the Freundlich model ($R^2 > 0.91$) describe the experimental data at different pH values adequately. Under the given conditions, precipitation of U(VI) from solution could be excluded. Consequently, the major adsorption mechanism is obviously surface complexation of the U(VI). It is well known that U(VI) forms strong complexes with carboxylic acid groups [5] which have been identified as the major functional surface groups of our modified CNTs by FT-IR spectroscopy.

In Fig. 2, the U(VI) sorption on pristine and modified CNTs is shown as a function of pH, it exhibits a characteristic shape. It becomes apparent that the U(VI) sorption edge is shifted to lower pH values due to the modification. The observed uptake of U(VI) by the modified CNTs

is most likely due to binding with carboxylic acid groups capable of ionization at the studied pH range. The percentage uptake decreases with decreasing pH based on the competition of uranyl species with hydronium ions for the binding sites. Furthermore, we observed a sharp decrease of the extent of sorption for both sorbents above pH 8 due to the strong uranium-carbonate complexation. In conclusion, the results showed that sorption characteristics are strongly effected by surface oxidation.

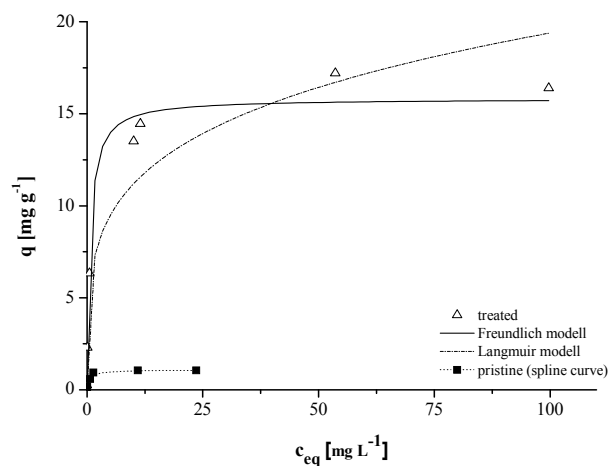


Fig. 1: Sorption isotherms of U(VI) on pristine and modified CNTs ($c_{\text{CNT}} = 25 - 1200 \text{ mg} \cdot \text{L}^{-1}$, $c_{\text{total,U(VI)}} = 10^{-7} - 5 \cdot 10^{-4} \text{ M}$, $I_{\text{NaClO}_4} = 0.1 \text{ M}$, $p_{\text{CO}_2} = 10^{-3.5} \text{ atm}$).

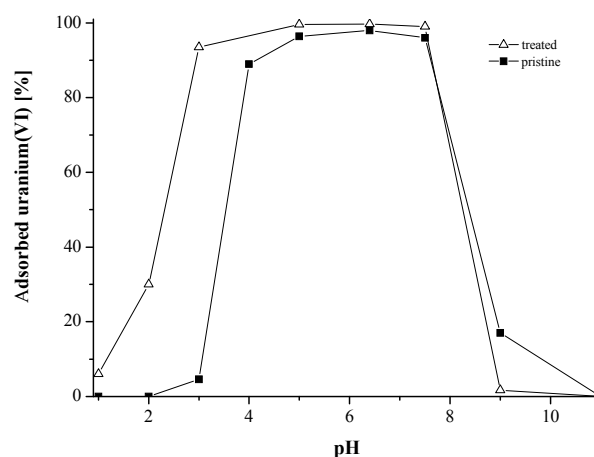


Fig. 2: pH dependence of U(VI) sorption on CNTs ($c_{\text{CNT}} = 1 \text{ g} \cdot \text{L}^{-1}$, $c_{\text{total,U(VI)}} = 10^{-6} \text{ M}$, $I_{\text{NaClO}_4} = 0.1 \text{ M}$, $p_{\text{CO}_2} = 10^{-3.5} \text{ atm}$).

REFERENCES

- [1] Tasis, D. et al. (2003) *Chem.-Eur. J.*, **9**, 4001-4008.
- [2] Chiang, I.W. et al. (2001) *J. Phys. Chem. B*, **105**, 1157-1161.
- [3] Li, Y. H. et al. (2002) *Chem. Phys. Lett.*, **357**, 263-266.
- [4] Li, Y. H. et al. (2003) *Carbon*, **41**, 2787-2792.
- [5] Moll, H. et al. (2003) *Radiochim. Acta*, **91**, 11-20.

Existence of colloidal uranium(IV) in near-neutral hydrogen carbonate solutions

I. Dreissig, S. Weiß, H. Zänker, G. Bernhard

Near-neutral solutions of uranium(IV) and NaHCO_3 were studied by light scattering. Stable U(IV) colloids were formed in the presence of silicate. ICP/MS analyses before and after ultrafiltration confirmed the existence of colloidal U(IV).

Uranium(IV) is usually regarded as sparingly soluble at near-neutral pH values. It should, therefore, be immobile in anoxic groundwaters. However, it has been shown that UO_2 is able to form stable colloids (nanoparticles) [1] and the question arises if such colloids might counteract the immobility of U(IV) in the nature. Hitherto, UO_2 colloids have only been observed at pH values of < 3 . In this pH region the UO_2 colloids are electrostatically stabilized; a zeta potential of +35 mV was found for pH 2.5 [1] were the colloidal UO_2 suspensions were stable over years. The isoelectric point (IEP) of the colloids was at pH 6.9, i.e. the UO_2 colloids possess their stability minimum in the typical pH range of natural waters.

UO_2 colloids, even if they are formed by a natural process, should immediately aggregate and sediment under normal groundwater conditions. In [2] we tried to shift the zeta potential by the addition of silicate, an anion ubiquitous in natural waters. With the presence of $3.5 \cdot 10^{-3}$ M silicate, we found zeta potentials of -40 mV for the UO_2 colloids in the near-neutral pH region. The IEP was at pH = 3.2. This raises the question if there may exist electrostatically stabilized U(IV) colloids in the environmentally relevant pH range. However, the generation of such U(IV) colloids from strongly acidic solutions by increasing the pH failed, presumably because we always had to pass through the pH of the IEP at 3.2 where the colloids aggregate. This aggregation seems to be irreversible, i.e. the aggregates formed at the IEP did not re-dissolve, even though the electrostatic charge of the aggregates became high (strongly negative) in the near-neutral region.

This made us ask ourselves if silicate-stabilized colloids might be producible by U(VI) reduction in alkaline solution and titration toward the near-neutral region from the alkaline side of the pH scale.

EXPERIMENTAL. The galvanostatic reduction of a 20 mM $\text{UO}_2(\text{ClO}_4)_2$ solution in 1 M NaHCO_3 was carried out at a current of 10 mA in an electrochemical cell (designed by A. Ikeda). The reduction was completed after about five hours. Aliquots of the stock solution thereby produced were diluted by a factor of 20 by four different aquatic solutions (*Experiments A through D*) and afterwards neutralized with perchloric acid. The diluents were

- *Experiment A*: Degassed Membrapure water
- *Experiment B*: 1 M NaHCO_3 .
- *Experiment C*: 3 mM silicate
- *Experiment D*: 3 mM silicate in 1 M NaHCO_3 .

The occurrence of colloids after dilution or after neutralization was detected by light scattering with a BI-90 photon correlation spectroscope (PCS) from Brookhaven Instruments Corp. as well as by ultrafiltration with 3-kD filters plus ICP-MS analysis of the filtrates. All solutions were prepared and handled in a glove box under nitrogen atmosphere with < 10 ppm O_2 .

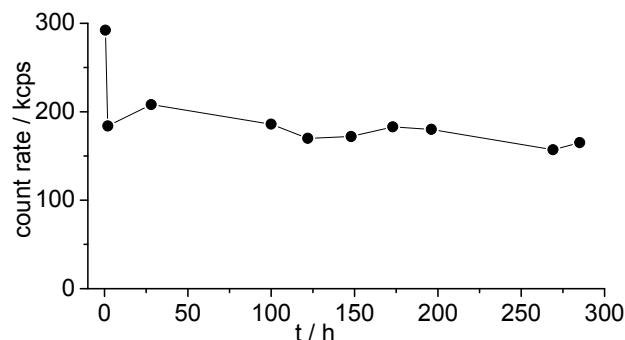


Fig. 1: Count rate alteration of *Exp. C* at pH 7.3.

RESULTS. No precipitates or colloids were observed in *Experiments (Exp.) B and D*. Obviously, the high carbonate concentrations stabilized the dissolved U(IV) as carbonate complexes in these experiments. A dark green precipitate, which turned into dark brown within a week, but no colloids were generated in *Exp. A*. Here, the U(IV) carbonate complexes were obviously destroyed due to the dilution. However, U(IV) colloids were found in *Exp. C*, both, after dilution and after neutralization. The solutions were optically clear but the scattered light intensity (count rate) showed a level of about 200 kcps. This is about 100 times the scattered light intensity of Membrapure water. Figure 1 gives the course of the scattered light intensity within 300 h. It demonstrates the relatively high stability of the colloids. After longer periods of time the colloids finally disappeared. However, this seemed to be rather due to uranium oxidation than to aggregation and sedimentation. The appearance of uranium(VI) in the solution could also be detected by UV-vis spectrometry after a few days.

The specification of the stable colloids of *Exp. C* as U(IV) colloids was confirmed by the ultrafiltration experiments. They resulted in a decrease of the uranium concentration from 1 to 0.024 M and of the silicon concentration from 3 to 1.78 M. This demonstrates that almost all the uranium and also a significant fraction of the silicon was in a colloid-borne (i.e. filterable) form. According to PCS, the colloid particles have a size of roughly 200 nm.

CONCLUSIONS. Uranium(IV) forms truly dissolved carbonate complexes in carbonate solutions of high concentration which do not precipitate under our conditions (*Exp. B and D*). Dilution with water results in the destruction of these complexes i.e. in precipitation (*Exp. A*). However, the presence of silicate can prevent the formation of a bulk precipitate and stabilize the produced solid phase as colloids (*Exp. C*). We assume that this is attributable to a shift of the zeta potential toward more negative values. Measurements of the zeta potential on these U(IV) colloids are in preparation.

ACKNOWLEDGEMENTS. The authors are grateful to A. Ikeda for supporting them in electrochemical uranium reduction and for fruitful discussions.

REFERENCES

- [1] Weiß, S. et al. (2007) Report FZD-459, p. 61.
- [2] Weiß, S. et al. (2008) this report, p. 58.

Investigations of the interaction of colloidal U(IV) with silicate

S. Weiß, H. Zänker

Uranium is usually considered to be immobile in anoxic waters because it is in the tetravalent form under reducing conditions which is sparingly soluble. However, the question arises if this immobility can be counteracted by colloids of U(IV). The formation of such colloids in acidic solutions and the influence of silicate on them is tested.

EXPERIMENTAL. All experiments were performed under nitrogen atmosphere with < 10 ppm O_2 in degassed water to avoid U(IV) oxidation. The ionic strength was 0.2 M $HClO_4/NaClO_4$. For the electrochemical preparation of $UO_2(am)$ see [1]. Silica was added by appropriate volumes of tetramethylorthosilicate (TMOS) which hydrolyses to orthosilicic acid [2]. U(IV) to Si ratios were varied from $1 : 1$ to $1 : 10$. The silica and uranium concentrations did not exceed $3.5 \cdot 10^{-3}$ M and 10^{-3} M, respectively. Two kinds of experiments were done: (1) co-precipitation of U(IV) and Si, and (2) adding of Si 24 hours after U(IV) precipitation. The uranium and silicon contents after 10 kD filtration (Centricon, Millipore) at different pH values were analyzed by ICP-MS. Zeta potential measurements of a co-precipitate were done by laser Doppler velocimetry (Zetasizer Nano ZS, Malvern Instruments) according to a procedure described in [3].

RESULTS. Figure 1 shows the typical behavior of U and Si in solutions on filtration at the different pH values in a co-precipitation experiment. At $pH < 2$ all of the U and Si was soluble and passed the filter membranes completely. The generation of colloidal U(IV) started at $pH > 2$ when the thermodynamic solubility of $UO_2(am)$ was exceeded. The uranium content in the filtrates decreased to concentrations close to the detection limit in a narrow pH range with the occurrence of U(IV) colloids. The Si content of the filtrates was constant at $pH > 4$.

Sorption of Si was also observed in the sorption experiments (not given here), but the amount of sorbed silica was independent of the pH in the pH range 2 – 9.

The molar ratios U(IV) : Si in the solutions and precipitates of all experiments are listed in Tab. 1. With the same U(IV) : Si ratios in solution, a significantly higher content of Si was found in the precipitates of the co-precipitation experiments. Freshly precipitated $UO_2(am)$ seems to offer a higher surface area for the sorption of Si than the 24 h old precipitate in the sorption experiments does.

The Smoluchowski zeta potential of a co-precipitate (with U(IV) : Si = $1 : 86$) was measured and compared with the results of pure $UO_2(am)$ from [4] (Fig. 2). The isoelectric point (IEP) is shifted from $pH 6.9$ to 3.2 in the presence of Si. Obviously, the adsorbed silica forms a layer on the surface of the colloidal U(IV) which is responsible for the change of the IEP. The IEP of 3.2 is close to $pH 2 \pm 0.5$ found for various types of silica [4].

CONCLUSIONS. There is a strong interaction between the U(IV) colloids and the silicate. It shifts the IEP away from the near-neutral pH range and results in a significant particle charge at $pH 7$. This allows to speculate on the possible existence of electrostatically stabilized U(IV) colloids in the environmentally relevant pH range which, however, could not be proved by these experiments. The

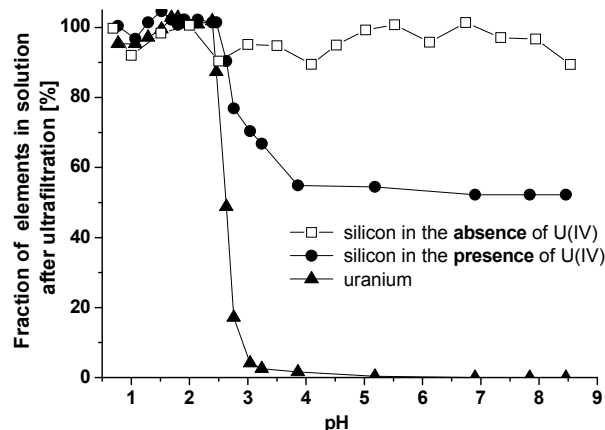


Fig. 1: Fractions of U and Si in the ultrafiltrates vs. pH of a co-precipitation experiment with U(IV):Si = $1 : 4$ in solution.

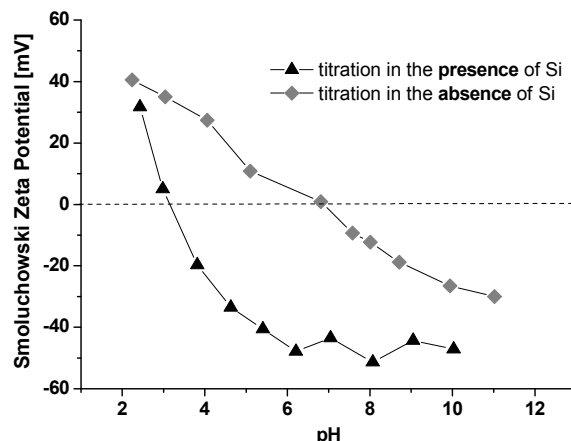


Fig. 2: Zeta potential of uraninite in the absence and the presence of Si (U(IV):Si in the precipitate: $1 : 1,86$).

Tab. 1: Molar ratios U(IV):Si in the solutions and the precipitates.

| Experiment | Molar ratio U(IV):Si | |
|------------------|----------------------|------------------|
| | in solution* | in precipitate** |
| Sorption | $1 : 3$ | $1 : 1.14$ |
| | $1 : 4$ | $1 : 1.03$ |
| Co-precipitation | $1 : 1$ | $1 : 0.62$ |
| | $1 : 4$ | $1 : 1.86$ |
| | $1 : 10$ | $1 : 1.76$ |

*before precipitation; **measured at $pH > 8$.

nature of the interaction between silicate and U(IV) is not yet known. It may be both adsorption or the formation of a coffinite ($USiO_4$) precursor. EXAFS experiments to elucidate the local structure around U(IV) in the precipitates of all experiments and using synthetic uraninite and coffinite as reference compounds are in preparation.

ACKNOWLEDGEMENTS. The authors thank T. Meissner and A. Potthoff (Fraunhofer IKTS) for performing the titrations and zeta potential measurements.

REFERENCES

- [1] Weiß, S. et al. (2004) *Report FZR-419*, p. 13.
- [2] Jensen, M.P. et al. (1996) *Radiochim. Acta* **72**, 143-150.
- [3] Weiß, S. et al. (2006) *Report FZD-459*, p. 61.
- [4] Iler, R. K. (1979) *The chemistry of silica*, Wiley, New York.

Curium(III) speciation during the precipitation process of calcium carbonate

H. Moll, G. Bernhard

The Cm(III) speciation was investigated during the calcium carbonate precipitation process using TRLFS. As a function of the reaction time, three different species could be identified. A combination of incorporation and sorption during the Cm(III) co-precipitation process with calcium carbonate was observed.

For an improved understanding of the radionuclide retardation process in nuclear waste repositories it is necessary to know the speciation of released actinides, for example during the co-precipitation process with solids. Calcium carbonate (vaterite/calcite) is one example because it is omnipresent in the geosphere and also a constituent of bentonite backfill materials which will be used in the storage of nuclear waste canisters in the bedrock.

EXPERIMENTAL. The experiments were performed in a glove box under N₂ atmosphere at 25 °C. Analytical grade 1 M NaClO₄ was used as a background electrolyte. The test samples contained 3 · 10⁻⁷ M Cm(III) and 0.02 M CO₃²⁻ at a pH of 10.4. The calcium concentration was stepwise increased from 5 · 10⁻⁵ to 1 · 10⁻³ M in time intervals of approximately 1 h. All samples were stirred while measuring the Cm(III) fluorescence. The time dependence of the emission spectrum was investigated up to 1080 h in short intervals. Details on the experimental set-up of the laser equipment are summarized in [1].

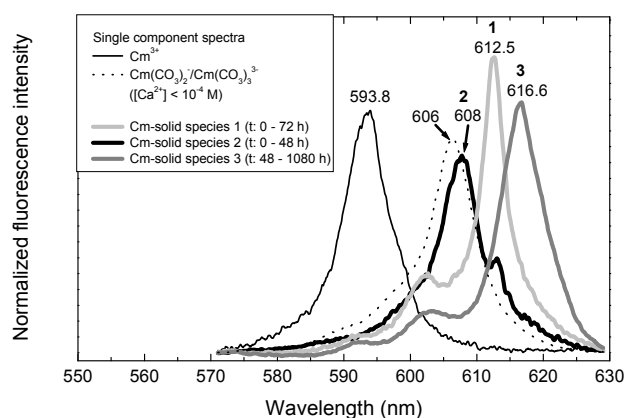


Fig. 1: Fluorescence spectra of the single components identified during the Cm(III) calcium carbonate co-precipitation process.

RESULTS. In samples at [Ca²⁺] ≤ 1 · 10⁻⁴ M, the emission maximum at 606.2 nm (see Fig. 1) and the mono-exponential fluorescence decay with the fluorescence lifetime of 137 ± 2 μs indicate a fast ligand exchange between Cm(CO₃)₂²⁻ and Cm(CO₃)₃³⁻ compared to the fluorescence decay rate of the excited Cm(III) [2]. At [Ca²⁺] ≥ 5 · 10⁻⁴ M a co-precipitation process of Cm(III) with calcium carbonate was observed. At contact times < 24 h, the fluorescence spectra are dominated by the narrow, red shifted emission band at 612.5 nm (Fig. 1). The Cm-solid species 1 is characterized by a long fluorescence lifetime of 1273 ± 30 μs and was not observed before. By applying the Kimura-Choppin equation [3] this indicates that Cm(III) has lost its complete hydration sphere and is already incorporated into the calcium carbonate seed crystal structure. According to Tsuno et al. [4], incorporation into a polymorph vaterite phase could explain this narrow

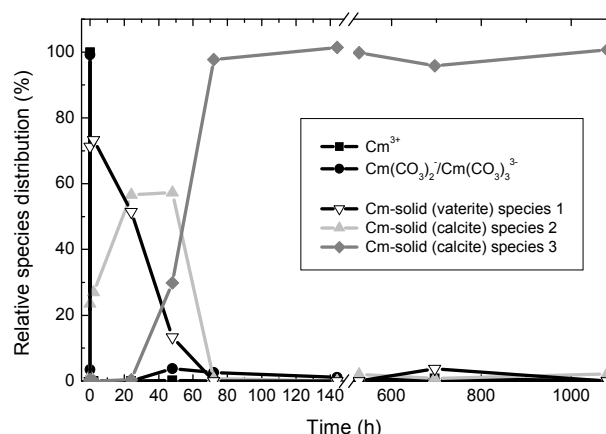


Fig. 2: Time dependent Cm(III) speciation during the Cm(III) calcium carbonate co-precipitation, as derived by peak deconvolution using factor analysis.

and red shifted emission band. The crystallization of calcium carbonate can be described by a fast formation of vaterite followed by a transformation in calcite after approximately 8 hours [4].

At contact times between 0 and 48 h, the increased influence of a second Cm(III)-solid species was observed (Fig. 1, 2). Species 2 shows an emission maximum at 608 nm with a shorter fluorescence lifetime of 277 ± 32 μs. Cm-solid species 2, is equivalent to the species 1 described in reference [5]. At this stage, our findings might indicate a combination of incorporation and sorption of Cm(III) species during the calcium carbonate precipitation.

At contact times > 48 h (Fig. 1, 2), the time dependence of the fluorescence emission spectra indicated that the Cm(III)-solid species 3, emission maximum at 616.6 nm and lifetime of 1334 ± 21 μs, dominates. This species is equivalent to the species 2 described in reference [5] and shows the incorporation of Cm(III) in the calcite lattice.

In contrast to [5], a much faster incorporation, within a few hours, of aqueous Cm(III)-carbonato species into the calcium carbonate lattice was observed. The Cm(III)-solid species 3 (Fig. 1) exhibits at 616.6 nm with full width at half maximum of 7.7 nm a broader fluorescence emission band as the Cm(III)-solid species 1. The possibility of two incorporation sites having emission maxima at 617 and 624 nm at T < 20 K according to Stumpf et al. [6] was tested. As a result, the broader emission band at 616.6 nm could be as well fit with two species at 616 and 621 nm which points also to the occurrence of two calcite incorporation species.

REFERENCES

- [1] Moll, H. et al. (2008) *BioMetals*, in press.
- [2] Vercouter, T. et al. (2005) *Inorg. Chem.* **44**, 5833-5843.
- [3] Kimura, T. et al. (1994) *J. Alloys Comp.* **213/214**, 313-317.
- [4] Tsuno, H. et al. (2001) *Bull. Chem. Soc. Jpn.* **74**, 479-486.
- [5] Stumpf, T. et al. (2002) *J. Colloid Interface Sci.* **249**, 119-122.
- [6] Stumpf, T. et al. (2007) *MIGRATION'07, Abstracts*, p. 172-173.

Simultaneous determination of beta nuclides by liquid scintillation spectrometry

P. Jähnigen, C. Nebelung, G. Bernhard

Many beta nuclides, released by weapon tests, from nuclear power plants or nuclear fuel reprocessing facilities, are radiotoxic even in small concentrations. Therefore, the determination of radionuclides in environmental samples at low levels is important. A useful method is the simultaneous measurement of the nuclides by recording and analyzing the liquid scintillation spectra [1]. The nuclides ^3H (18.6 keV), ^{14}C (156.5 keV), ^{55}Fe (231.4 keV), ^{60}Co (2823.9 keV), ^{90}Sr (^{90}Sr : 546.0 keV, ^{90}Y : 2280.1 keV), ^{99}Tc (293.7 keV), ^{137}Cs (1175.6 keV) were measured in various combinations of mixtures as well as with the TriCarb 3100 TR (Perkin Elmer). Up to three nuclides in one sample were determined with a good accuracy even for large activity differences and beta energies close together.

EXPERIMENTAL. First, it is necessary to generate quench curves for each nuclide to calculate the dpm (disintegrations per minute) from the measured cpm (counts per minute). With this quench curves, double and triple labeled mixture can be determined. These mixtures were prepared from the standard solution of each nuclide with 5 mL of liquid scintillation cocktail (Ultima Gold, Packard Instrument). Four samples were prepared for each combination, measuring time was 5 min.

RESULTS. Figures 1 and 2 summarize the beta spectra of the doubly labeled samples with equal activities. ^{14}C has been detected up to 120 keV. The high energetic nuclides ^{137}Cs , ^{99}Tc , ^{60}Co , and ^{90}Sr can be measured up to 560 keV, 230 keV, 350 keV and 1400 keV, respectively. In the spectrum of ^{55}Fe and ^3H no separation of both nuclides in the shape of the spectrum up to 12 keV is visible [2]. The measured maximal energy is lower than the theoretical maximum. The deviation from the expected activities is $< 3.2\%$ for equal activities, and $< 3.0\%$ for activity ratios up to 1 : 50.

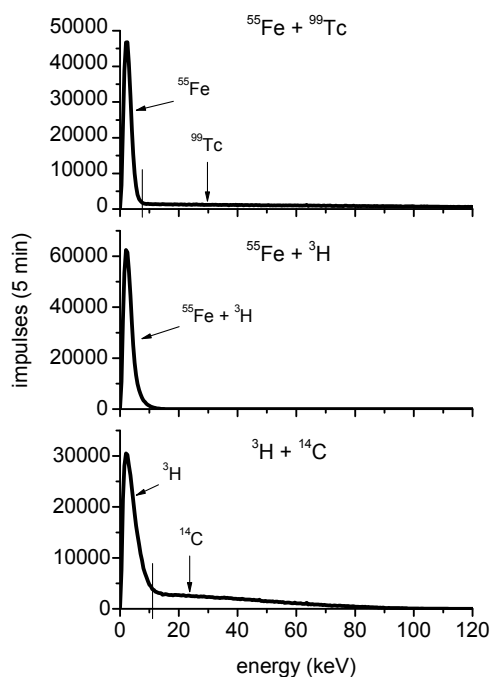


Fig. 1: Beta spectra of double labeled samples (1 kBq per nuclide, $^{55}\text{Fe} + ^3\text{H}$, $^{55}\text{Fe} + ^{99}\text{Tc}$, $^3\text{H} + ^{14}\text{C}$).

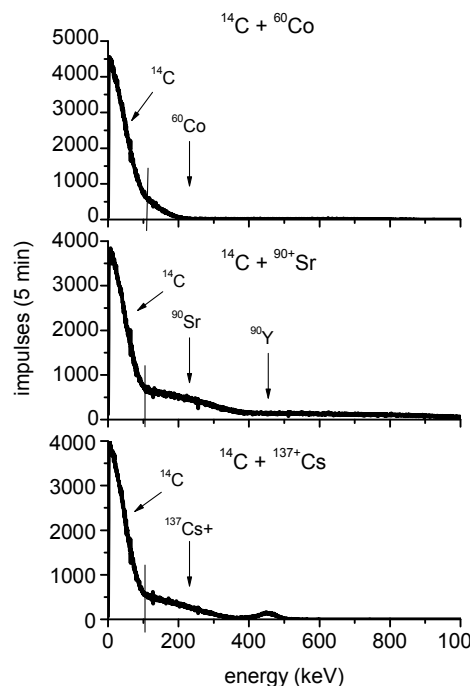


Fig. 2: Beta spectra of double labeled samples (1 kBq per nuclide, $^{14}\text{C} + ^{137}\text{Cs}$, $^{14}\text{C} + ^{90}\text{Sr}$, $^{14}\text{C} + ^{60}\text{Co}$).

Figure 3 displays the beta spectra of triple labeled samples. The low energy nuclides ^3H and ^{55}Fe are well visible in the beta spectra. The transition between middle energetic (^{14}C , ^{99}Tc) and high energetic nuclides (^{137}Cs , ^{60}Co , ^{90}Sr) is better seen in the enlargement. The deviation from the expected activities is $< 2.0\%$ (identical activities) and $< 2.6\%$ for activity ratios up to 1 : 50.

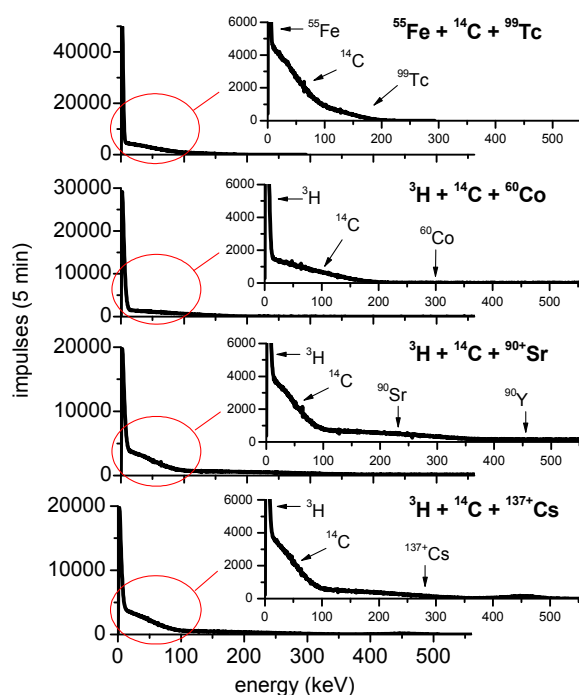


Fig. 3: Beta spectra of triple labeled samples (1 kBq per nuclide).

REFERENCES

- [1] Kopitz, J. et al. (2006) *Application Notes*, Perkin-Elmer.
- [2] Jähnigen, P. (2007) Thesis, Dresden University of Technology, Dresden.

The problem of radioactivity in process waters of geothermal plants

S. Gester, V. Brendler, M. Köhler,¹ D. Degering¹

¹Verein für Kernverfahrenstechnik und Analytik Rossendorf e.V. (VKTA), Dresden, Germany

Research activities belonging to the long-term operational safety of geothermal plants are pointing to increased concentrations of several radionuclides in raised geothermal waters.

The currently increased use of renewable energy sources also features new problems. At the geothermal power plant Neustadt-Glewe, it was detected that process waters contained increased concentrations of radionuclides (especially radium in absence of the mother nuclide thorium), whereas the specific activities of these nuclides in the corresponding decay chain in the reservoir rock followed normal patterns (Tab. 1 and Fig. 1). Our goal was the identification of the source and of underlying interaction processes taking place in the aquifer. With simultaneous consideration of physical models, e.g. transport and α -recoil [1], a further insight should be obtained with geochemical speciation modeling.

Tab. 1: Activities of radium nuclides in several samples from the geothermal plant Neustadt-Glewe.

| Sample | Nuclide | Activity |
|----------------|----------------------|----------------|
| process water | Ra-224 | 8.2 – 9.6 Bq/L |
| | Ra-226 | 6.9 – 8.1 Bq/L |
| | Ra-228 | 8.7 – 9.7 Bq/L |
| reservoir rock | Ra-226 ^{*)} | 3.3 – 99 Bq/kg |
| | Ra-228 ^{*)} | 5.0 – 71 Bq/kg |

^{*)} in radioactive equilibrium within the corresponding decay chain

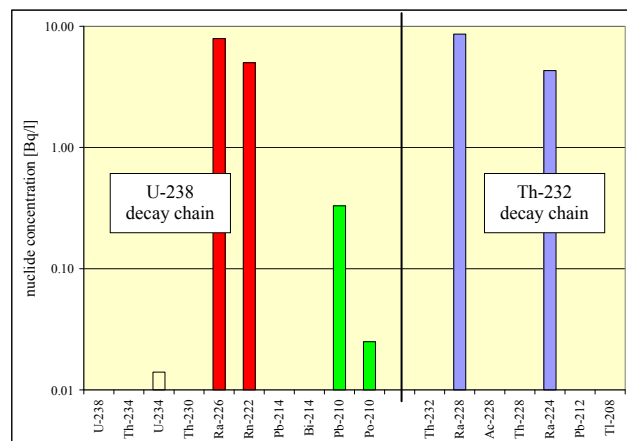


Fig. 1: Radionuclide concentrations in process waters from the geothermal plant Neustadt-Glewe.

DATABASE AND MODELING. An evaluation of the accomplished analyses of geothermal waters from the Neustadt-Glewe site [2] yielded a high salinity (salt content about 230 g/L, ionic strength about 4.1 M). This implied the use of the Pitzer model in speciation calculations with EQ3/6 [3], since other models, like Debye-Hückel, Davies or SIT, do not adequately describe the ion-ion interactions in such brines resulting in incorrect activity coefficients. Furthermore, it could be estimated from the analytical data that dissolved species and solid phases should be taken into consideration in modeling calculations.

The existing Pitzer data base of EQ3/6 lacked of information about radium and its compounds, hence, the focus was on the literature research of thermodynamic param-

eters ($\Delta_f G^0$, $\Delta_f H^0$, S_f^0 , C_p^0 , $\log K$) and Pitzer parameters ($\alpha^{(n)}$, $\beta^{(n)}$, C^Φ , Θ , Ψ) as well as of data concerning the temperature dependence of these parameters because the geothermal waters in the aquifer of Neustadt-Glewe have a temperature of about 100 °C.

During the literature search it became clear that experimental data from radium compounds are rare and suitable Pitzer parameters only exist for radium sulfate (RaSO_4) [4]. Therefore, the required parameters have been obtained in general from estimation and extrapolation of data from analogous alkaline earth metal compounds of Ca, Sr and Ba.

The collected data were implemented in the Pitzer data base of EQ3/6, and a project specific geothermic data base was established thereof.

RESULTS AND DISCUSSION. At the current status of the geochemical modeling without an implementation of a model for solid solutions, the interpretation of the speciation calculations demonstrates a saturation of the process waters from Neustadt-Glewe with the minerals bassanite ($\text{CaSO}_4 \cdot 0.5\text{H}_2\text{O}$), gypsum ($\text{CaSO}_4 \cdot 2\text{H}_2\text{O}$), strontianite (SrCO_3) and celestite (SrSO_4), as well as a supersaturation with anhydrite (CaSO_4) by the factor of 3.3 and with barite (BaSO_4) by the factor of 5.7. These results agree with the observations of Kühn et al. [5]. The precipitation of barite leads to the simultaneous deposition of radium and to the formation of mixed crystals of radiobarite ($\text{Ba,Ra}(\text{SO}_4)$). If a near ideal behavior for radium in the solid solution is assumed and the activity coefficients of radium and barium are almost the same, then it follows that the saturation of radium in the process water is one order of magnitude higher as it would be theoretically expected.

In summary, it could be stated that the increased concentrations of radium nuclides found in the geothermal process waters of Neustadt-Glewe were caused to a lesser extend by dissolution processes. The dominant process of the radium release seems to be the α -recoil effect.

ACKNOWLEDGEMENTS. This work was financially supported by the Federal Ministry for the Environment, Nature Conservation and Nuclear Safety (BMU).

REFERENCES

- [1] Porcelli, D. et al. (2003) *Rev. Mineral. Geochem.* **52**, 317-361.
- [2] Kellner, T. (2004) *Übersicht und Wertung der bisher am Standort Neustadt-Glewe durchgeführten Analytik von Fluid, Feststoffen, Mikrobiologie*, Geothermie Neubrandenburg GmbH, Neubrandenburg.
- [3] Wolery, T.J. (1992) *UCRL-MA-110662 Part I*, Lawrence Livermore National Laboratory, Livermore.
- [4] Paige, C.R. et al. (1998) *Geochim. Cosmochim. Acta* **62**, 15-23.
- [5] Kühn, M. et al. (1997) *Grundwasser* **97**, 111-117.

- ▶ Articles (peer-reviewed)
- ▶ Abstracts, proceedings, reports
- ▶ Lectures, oral presentations
- ▶ Posters
- ▶ Awards, research fellowships
- ▶ Patent
- ▶ Theses
- ▶ Diploma
- ▶ Work placements

► Articles (peer-reviewed)

- Bernhard, G.; Geipel, G.
Bestimmung der Bindungsform des Urans in Mineralwässern
Vom Wasser 1053, 7-10 (2007).
- Billard, I.; Gaillard, C.; Hennig, C.
Dissolution of UO₂, UO₃ and of some lanthanide oxides in BumimTf2N: Effect of acid and water and formation of UO₂(NO₃)₃⁻
Dalton Transactions 37, 4214-4221 (2007).
- Charlet, L.; Scheinost, A. C.; Tournassat, C.; Greneche, J.; Géhin, A.; Fernández-Martínez, A.; Coudert, S.; Tisserand, D.; Brendle, J.
Electron transfer at the mineral/water interface: Selenium reduction by ferrous iron sorbed on clay
Geochimica et Cosmochimica Acta 71, 5731-5749 (2007).
- Creamer, N. J.; Mikheenko, I. P.; Deplanche, K.; Yong, P.; Wood, J.; Pollmann, K.; Macaskie, L. E.; Selenska-Pobell, S.
A novel hydrogenation and hydrogenolysis catalyst using palladized biomass of gram negative and gram positive bacteria
Advanced Materials Research 20-21, 603-606 (2007).
- Creamer, N.; Mikheenko, I.; Yong, P.; Deplanche, K.; Sanyahumbi, D.; Wood, J.; Pollmann, K.; Merroun, M.; Selenska-Pobell, S.; Macaskie, L.
Novel supported Pd hydrogenation bionanocatalyst for hybrid homogeneous/heterogeneous catalysis
Catalysis Today 128, 80-87 (2007).
- Fillaux, C.; Berthet, J.-C.; Conradson, S. D.; Guilbaud, P.; Guillaumont, D.; Hennig, C.; Moisy, P.; Roques, J.; Simoni, E.; Shuh, D. K.; Tyliczszak, T.; Castro-Rodriguez, I.; Den Auwer, C.
Combining theoretical chemistry and XANES multi-edge experiments to probe actinide valence states
Comptes Rendus Chimie 10, 859-871 (2007).
- Foerstendorf, H.; Seidel, W.; Heim, K.; Bernhard, G.
Identification of actinide molecule complexes: A new vibrational spectroscopic approach at the free electron laser facility FELBE
Journal of Nuclear Materials 366, 248-255 (2007).
- Funke, H.; Chukalina, M.; Scheinost, A. C.
A new FEFF-based wavelet for EXAFS data analysis
Journal of Synchrotron Radiation 14, 426-432 (2007).
- Gaillard, C.; Chaumont, A.; Billard, I.; Hennig, C.; Ouadi, A.; Wipff, G.
Uranyl coordination in ionic liquids: The competition between ionic liquid anions, uranyl counterions, and Cl⁻ anions investigated by extended X-ray absorption fine structure and UV-visible spectroscopies and molecular dynamics simulations
Inorganic Chemistry 46, 4815-4826 (2007).
- Ghabbour, E.; Scheinost, A. C.; Davies, G.
XAFS studies of cobalt(II) binding by solid peat and soil-derived humic acids and plant-derived humic acid-like substances
Chemosphere 67, 285-291 (2007).
- Glorius, M.; Moll, H.; Bernhard, G.
Complexation of uranium(VI) with aromatic acids in aqueous solution – A comparison of hydroxamic acids and benzoic acid
Radiochimica Acta 95, 151-157 (2007).
- Großmann, K.; Arnold, T.; Krawczyk-Bärsch, E.; Diessner, S.; Wobus, A.; Bernhard, G.; Krawitz, R.
Identification of fluorescent U(V) and U(VI) microparticles in a multispecies biofilm by confocal laser scanning microscopy and fluorescence spectroscopy
Environmental Science & Technology 41, 6498-6504 (2007).
- Günther, A.; Geipel, G.; Bernhard, G.
Complex formation of uranium(VI) with the amino acids L-glycine and L-cysteine: A fluorescence emission and UV-vis absorption study
Polyhedron 26, 59-65 (2007).
- Hennig, C.
Evidence for double-electron excitations in X-ray absorption spectra of actinides
Physical Review B 75 Art. No. 035120-1-7 (2007).
- Hennig, C.; Schmeide, K.; Brendler, V.; Moll, H.; Tsushima, S.; Scheinost, A. C.
EXAFS investigation of U(VI), U(IV) and Th(IV) sulfato complexes in aqueous solution
Inorganic Chemistry 46, 5882-5892 (2007).

- Ikeda, A.; Hennig, C.; Tsushima, S.; Takao, K.; Ikeda, Y.; Scheinost, A. C.; Bernhard, G.
A comparative study of U(VI) and U(V) carbonato complexes in aqueous solution
Inorganic Chemistry 46, 4212-4219 (2007).
- Jroundi, F.; Merroun, M.; Arias, J. M.; Rossberg, A.; Selenska-Pobell, S.; González-Muñoz, M. T.
Spectroscopic and microscopic characterization of uranium biomineralization in *Myxococcus xanthus*
Geomicrobiology Journal 24, 441-449 (2007).
- Koban, A.; Bernhard, G.
Uranium(VI) complexes with phospholipid model compounds – A laser spectroscopic study
Journal of Inorganic Biochemistry 101, 750-757 (2007).
- Křepelová, A.; Brendler, V.; Sachs, S.; Baumann, N.; Bernhard, G.
U(VI)-kaolinite surface complexation in absence and presence of humic acid studied by TRLFS
Environmental Science & Technology 41, 6142-6147 (2007).
- Martin, P.; Grandjean, S.; Valot, C.; Carlot, G.; Ripert, M.; Blank, P.; Hennig, C.
XAS study of (U1-yPuy)O₂ solid solutions
Journal of Alloys and Compounds 444/445, 410-414 (2007).
- Merroun, M.; Rossberg, A.; Hennig, C.; Scheinost, A. C.; Selenska-Pobell, S.
Spectroscopic characterization of gold nanoparticles formed by cells and S-layer protein of *Bacillus sphaericus* JG-A12
Materials Science and Engineering C – Biomimetic And Supramolecular Systems 27, 188-192 (2007).
- Merroun, M.
Interactions between metals and bacteria: fundamental and applied research
Communicating Current Research and Educational Topics and Trends in Applied Microbiology (Mendez-Vilas, A. ed.), Microbiology Series No. 1, Vol. 1, Formatex, Badajoz, 108-119 (2007).
- Meybohm, A.; Ulrich, K.-U.
Response of drinking-water reservoir ecosystems to decreased acidic atmospheric deposition in central Europe II. Signs of biological recovery
Water, Air & Soil Pollution 7, 275-284 (2007).
- Mibus, J.; Sachs, S.; Nebelung, C.; Bernhard, G.
Migration of uranium (IV)/(VI) in the presence of humic acids in quartz sand: A laboratory column study
Journal of Contaminant Hydrology 89, 199-217 (2007).
- Moll, H.; Bernhard, G.
Complex formation of curium(III) with amino acids of different functionalities: L-threonine and O-phospho-L-threonine.
Journal of Coordination Chemistry 60, 1795-1807 (2007).
- Moll, H.; Bernhard, G.
Complexation of curium(III) with L2-amino-butyric acid investigated by time-resolved laser-induced fluorescence spectroscopy (TRLFS).
Journal of Radioanalytical and Nuclear Chemistry 274, 603-608 (2007).
- Nebelung, C.; Baraniak, L.
Simultaneous determination of ²²⁶Ra, ²³³U and ²³⁷Np by liquid scintillation spectrometry
Applied Radiation and Isotopes 65, 209-217 (2007).
- Nedelkova, M.; Merroun, M.; Rossberg, A.; Hennig, C.; Selenska-Pobell, S.
Microbacterium isolates from the vicinity of a radioactive waste depository and their interactions with uranium
FEMS Microbiology Ecology 59, 694-705 (2007).
- Nikitenko, S. I.; Hennig, C.; Grigoriev, M. S.; Le Naour, C.; Cannes, C.; Trubert, D.; Bossé, E.; Berton, C.; Moisy, P.
Structural and spectroscopic studies of the complex [BuMeIm]₂[UCl₆] in the solid state and in hydrophobic room temperature ionic liquid [BuMeIm][Tf₂N]
Polyhedron 26, 3136-3142 (2007).
- Opel, K.; Weiß, S.; Hübener, S.; Zänker, H.; Bernhard, G.
Study of the solubility of amorphous and crystalline uranium dioxide by combined spectroscopic methods
Radiochimica Acta 95, 143-149 (2007).
- Pollmann, K.; Matys, S.
Construction of an S-layer protein exhibiting modified self-assembling properties and enhanced metal binding capacities
Applied Microbiology and Biotechnology 75, 1079-1085 (2007).

- Sachs, S.; Brendler, V.; Geipel, G.
Uranium(VI) complexation by humic acid under neutral pH conditions studied by laser-induced fluorescence spectroscopy
Radiochimica Acta 95, 103-110 (2007).
- Schimmack, W.; Gerstmann, U.; Schultz, W.; Geipel, G.
Long-term corrosion and leaching of depleted uranium (DU) in the soil
Radiation and Environmental Biophysics 46, 221-227 (2007).
- Servaes, K.; Hennig, C.; Billard, I.; Gaillard, C.; Binnemans, K.; Görller-Walrand, C.; van Deun, R.
Speciation of uranyl nitrate complexes in acetonitrile and in the ionic liquid 1-butyl-3-methylimidazolium bis(trifluoromethylsulfonyl)imide
European Journal of Inorganic Chemistry 5120-5126 (2007).
- Soldatov, A. V.; Lamoen, D.; Konstantinovic, M. J.; van den Berghe, S.; Scheinost, A. C.; Verwerft, M.
Local structure and oxidation state of uranium in some ternary oxides: X-ray absorption analysis
Journal of Solid State Chemistry 180, 53-60 (2007).
- Tsushima, S.
Hydration and water exchange mechanism of the UO_2^{2+} ion revisited: The validity of the "n+1" model
Journal of Physical Chemistry A 111, 3613-3617 (2007).
- Tsushima, S.; Rossberg, A.; Ikeda, A.; Müller, K.; Scheinost, A. C.
Stoichiometry and structure of uranyl (VI) hydroxo dimer and trimer complexes in aqueous solution
Inorganic Chemistry 46, 10819-10826 (2007).
- Voigt, W.; Brendler, V.; Marsh, K.; Rarey, R.; Wanner, H.; Gaune-Escard, M.; Cloke, P.; Vercouter, Th.; Bastrakov, E.; Hagemann, S.
Quality assurance in thermodynamic databases for performance assessment studies in waste disposal
Pure and Applied Chemistry 79, 883-894 (2007).

► Abstracts, proceedings, reports

- Baumann, N.; Arnold, T.; Foerstendorf, H.; Read, D.; Black, S.; Massanek, A.
Fingerprinting of a thin secondary mineral film on DU
Geochimica et Cosmochimica Acta 71, A66 (2007).
- Den Auwer, C.; Guilbaud, P.; Guillaumont, D.; Moisy, P.; Digiandomenico, V.; Le Naour, C.; Trubert, D.; Simoni, E.; Hennig, C.; Scheinost, A. C.; Conradson, A. D.
Molecular characterization of actinide oxocations from protactinium to plutonium
XAFS-13, 13th International Conference on X-ray Absorption Fine Structure, July 09-14, 2006, Stanford, USA. AIP Conference Proceedings, Vol. 882 (Hedman, B.; Pianetta, P. eds.), AIP, Melville, 184-186 (2007)
- Den Auwer, C.; Guilbaud, P.; Guillaumont, D.; Moisy, P.; Fillaux, C.; Naour, C. L.; Trubert, D.; Simoni, E.; Digiandomenico, V.; Hennig, C.; Scheinost, A. C.; Conradson, S. D.
Characterisation of heavy cations from dysprosium to plutonium
Speciation Techniques and Facilities for Radioactive Materials at Synchrotron Light Sources, Workshop Proceedings, September 18-20, 2006, Karlsruhe, Germany, OECD Publications, Paris, 23-30 (2007).

- Funke, H.; Chukalina, M.; Voegelin, A.; Scheinost, A. C.
Improving Resolution in k and r Space: A FEFF-based Wavelet for EXAFS Data Analysis
XAFS-13, 13th International Conference on X-ray Absorption Fine Structure, July 09-14, 2006, Stanford, USA. AIP Conference Proceedings, Vol. 882 (Hedman, B.; Pianetta, P. eds.), AIP, Melville, 72-74 (2007).
- Funke, H.; Hennig, C.; Scheinost, A. C.
The structure of soddyite-EXAFS shell fitting and wavelet analysis
Speciation Techniques and Facilities for Radioactive Materials at Synchrotron Light Sources, Workshop Proceedings, September 18-20, 2006, Karlsruhe, Germany, OECD Publications, Paris, 211 (2007).
- Funke, H.; Chukalina, M.; Scheinost, A. C.
Application of wavelet transform to extended X-ray absorption spectroscopy
Mathematical Methods and Computational Techniques in Research and Education (Dondon, P.; Mladenov, V.; Impedovo, S.; Cepisca, S. eds.), WSEAS Press, 117-121 (2007).
- Gaillard, C.; Billard, I.; Mekki, S.; Ouadi, A.; Hennig, C.; Denecke, M. A.
Combined techniques for studying actinide complexes in room temperature ionic liquids
Speciation Techniques and Facilities for Radioactive Materials at Synchrotron Light Sources, Workshop Proceedings, September 18-20, 2006, Karlsruhe, Germany, OECD Publications, Paris, 13-20 (2007).
- Geipel, G.; Baumann, N.; Arnold, T.; Bernhard, G.; Gerstmann, U.; Schimmack, K.; Read, D.
Mobilisation and speciation of depleted uranium in water and soils
Geochimica et Cosmochimica Acta 71, A314 (2007).
- Geissler, A.; Selenska-Pobell, S.
Bacterial response to sodium and uranyl nitrate treatments of uranium mining waste samples
Biospektrum Sonderausgabe, VAAM-Jahrestagung, April 01-04, 2007, Osnabrück, Germany, Elsevier, Heidelberg, 192 (2007).
- Hennig, C.; Schmeide, K.; Brendler, V.; Moll, H.; Tsushima, S.; Scheinost, A. C.
The structure of uranyl sulfate in aqueous solution – Monodentate versus bidentate coordination
XAFS-13, 13th International Conference on X-ray Absorption Fine Structure, July 09-14, 2006, Stanford, USA. AIP Conference Proceedings, Vol. 882 (Hedman, B.; Pianetta, P. eds.), AIP, Melville, 262 (2007).
- Hennig, C.; Schmeide, K.; Brendler, V.; Moll, H.; Tsushima, S.; Scheinost, A. C.
EXAFS investigation of U(VI), U(IV) and Th(IV)sulfato complexes in aqueous solution
Speciation Techniques and Facilities for Radioactive Materials at Synchrotron Light Sources, Workshop Proceedings, September 18-20, 2006, Karlsruhe, Germany, OECD Publications, Paris, 33 (2007).
- Hennig, C.
Double-electron excitations in L edge X-ray absorption spectra of actinides
Speciation Techniques and Facilities for Radioactive Materials at Synchrotron Light Sources, Workshop Proceedings, September 18-20, 2006, Karlsruhe, Germany, OECD Publications, Paris, 219-224 (2007).
- Hennig, C.; Fahmy, K.; Merroun, M.; Pollmann, K.; Raff, J.; Savchuk, O.; Selenska-Pobell, S.
Bacterial S-layers as template for the formation of Pd nanoclusters
ESRF Highlights 2007, ESRF, Grenoble, 83-84 (2007).
- Herrmannsdörfer, T.; Bianchi, A. D.; Papageorgiou, T. P.; Pobell, F.; Wosnitza, J.; Pollmann, K.; Merroun, M.; Raff, J.; Selenska-Pobell, S.
Magnetic properties of transition-metal nanoclusters on a biological substrate
Journal of Magnetism and Magnetic Materials 310, E821-E823 (2007).
- Ikeda, A.; Hennig, C.; Rossberg, A.; Scheinost, A. C.; Bernhard, G.; Takao, K.; Ikeda, Y.
A comparative study of U(V)O₂⁺ and U(VI)O₂²⁺ carbonato complexes in aqueous solution.
Speciation Techniques and Facilities for Radioactive Materials at Synchrotron Light Sources, Workshop Proceedings, September 18-20, 2006, Karlsruhe, Germany, OECD Publications, Paris, 225-232 (2007).

- Li, B.; Foerstendorf, H.; Raff, J.; Bernhard, G.
FT-IR investigation of the uranium S-layer interaction in aqueous solutions
Geochimica et Cosmochimica Acta 71, A567 (2007).
- Merroun, M.; Geissler, G.; Raff, J.; Hennig, C.; Selenska-Pobell, S.
Interaction mechanisms of bacterial strains isolated from uranium mining waste piles with U and Pb
Biospektrum Sonderausgabe, VAAM-Jahrestagung, April 01-04, 2007, Osnabrück, Germany, Elsevier, Heidelberg, Germany, 193 (2007).
- Merroun, M.; Geissler, G.; Nedelkova, M.; Selenska-Pobell, S.
Interactions of U(VI) and Eu(III) with natural bacterial isolates
Geochimica et Cosmochimica Acta 71, A656 (2007).
- Moll, H.
Interactions of microbes found at Äspö underground lab with actinides such as curium, plutonium and uranium
2nd Annual Workshop of the IP FUNMIG, November 21-23 2006, Stockholm, Sweden, 131-137 (2007).
- Müller, K.; Foerstendorf, H.; Bernhard, G.
Infrared spectroscopic identification of aqueous uranium(VI) species
Geochimica et Cosmochimica Acta 71, A694 (2007).
- Nebelung, C.; Brendler, V.; Richter, A.; Bernhard, G.
Uranium(VI)-Sorption an natürlichem und synthetischem Sandstein
Wissenschaftsforum Chemie 2007 – Energie, Materialien, Synthese, September 16-19, 2007, Ulm, Germany, GdCh, Frankfurt am Main 173 (2007).
- Reitz, T.; Geissler, A.; Merroun, M.; Selenska-Pobell, S.
Crenarchaeota 1.1b and Firmicutes consortium recovered from a uranyl nitrate treated uranium waste sample and its possible role against the toxicity of uranium
Biospektrum Sonderausgabe, VAAM-Jahrestagung, April 01-04, 2007, Osnabrück, Germany, Elsevier, Heidelberg, Germany, 193 (2007).
- Reitz, T.; Geissler, A.; Merroun, M.; Selenska-Pobell, S.
Interactions of U(VI) with members of a microbial consortium recovered from a uranium mining waste pile
37th Journées des Actinides, Sesimbra, Portugal, March 24-27, 2007, 56 (2007).
- Richter, A.; Nebelung, C.; Brendler, V.
U(VI) sorption on sandstone: Experiments and modeling
Geochimica et Cosmochimica Acta 71, A838 (2007).
- Rossberg, A.; Ulrich, K.-U.; Scheinost, A. C.
The molecular topology of uranium(VI) bonding to iron and aluminium oxyhydroxide nanoclusters revisited by EXAFS spectroscopy
Speciation Techniques and Facilities for Radioactive Materials at Synchrotron Light Sources, Workshop Proceedings, September 18-20, 2006, Karlsruhe, Germany, OECD Publications, Paris, 281 (2007).
- Sachs, S.; Křepelová, A.; Schmeide, K.; Koban, A.; Günther, A.; Mibus, J.; Brendler, V.; Geipel, G.; Bernhard, G.
Joint Project: Migration of actinides in the system clay, humic substance, aquifer – Migration behavior of actinides (uranium, neptunium) in clays: Characterization and quantification of the influence of humic substances
FZD-460, Technical Report Forschungszentrum Dresden-Rossendorf, Dresden, Germany (2007).
- Scheinost, A. C.; Charlet, L.
Selenite reduction by nano-crystalline green rust, magnetite, siderite and mackinawite: EXAFS identification of Se species
Geochimica et Cosmochimica Acta 71, A886 (2007).
- Scheinost, A. C.; Hennig, C.; Funke, H.; Rossberg, A.; Oehme, W.; Dienel, S.; Claussner, J.; Proehl, D.; Bernhard, G.
Rossendorf Beamline at ESRF: An XAS experimental station for actinide research
Speciation Techniques and Facilities for Radioactive Materials at Synchrotron Light Sources, Workshop Proceedings, September 18-20, 2006, Karlsruhe, Germany, OECD Publications, Paris, 141-150 (2007).

- Servaes, K.; Hennig, C.; Görrler-Walrand, C.
EXAFS and UV-VIS investigation of the first co-ordination sphere of the uranyl ion in $\text{UO}_2(\text{NO}_3)_2(\text{TBP})_2$
Speciation Techniques and Facilities for Radioactive Materials at Synchrotron Light Sources, Workshop Proceedings, September 18-20, 2006, Karlsruhe, Germany, OECD Publications, Paris, 293-300 (2007).
- Tsushima, S.; Scheinost, A. C.
Hydration of U(VI,V) and Np(VI) Ions Revisited
Speciation Techniques and Facilities for Radioactive Materials at Synchrotron Light Sources, Workshop Proceedings, September 18-20, 2006, Karlsruhe, Germany, OECD Publications, Paris, 313-318 (2007).
- Ulrich, K.-U.; Zänker, H.
Kolloidgetragener Transport von Uran und anderen radiotoxischen Schwermetallen in oxischen Bergwerkswässern
Final Report of DFG Research Project ZA 238/2-1 and 2-2, Technical Report Forschungszentrum Dresden-Rossendorf, Dresden, Germany (2007).
- Zänker, H.; Ulrich, K.-U.; Opel, K.; Brendler, V.
Der Einfluss von Kolloiden auf den Urantransport in radioaktiven Endlagern und in stillgelegten Uranbergwerken - Ein kritischer Vergleich
Wasser 2007. Jahrestagung der Wasserchemischen Gesellschaft, GDCh, May 14-16, 2007, Passau, Germany, 68-71 (2007).
- Zänker, H.; Ulrich, K.-U.; Opel, K.; Brendler, V.
The role of colloids in uranium transport: A comparison of nuclear waste repositories and abandoned uranium mines
Proceedings of the IMWA Symposium 2007, Water in Mining Environments, May 27-31, 2007, Cagliari, Italy, 127-131 (2007).

► Lectures, oral presentations

- Barkleit, A.; Moll, H.; Bernhard, G.
Reaction of uranium(VI) with lipopoly-saccharide – A laser spectroscopic study
Migration 2007, 11th Conference on the Chemistry and Migration Behaviour of Actinides and Fission Products in the Geosphere, August 26-31, 2007, Munich, Germany.
- Baumann, N.; Arnold, T.; Read, D.
Uranium ammunition in soil
Protecting Water Bodies from Negative Impacts of Agriculture Loads and Fate of Fertiliser Derived Uranium, June 04-06, 2007, Braunschweig, Germany.
- Bernhard, G.; Geipel, G.
Uran – Bindungsform und Toxizität
Workshop "Heinrichsquelle Nürtingen", March 19, 2007, Nürtingen, Germany.
- Brendler, V.
Nukleare Endlager – und was die Radiochemie dazu beiträgt
Tag des offenen Labors, May 12, 2007, FZD, Dresden, Germany.
- Foerstendorf, H.
Schwingungsspektroskopische Analyse von Actinylkomplexen in wässrigen Lösungen und an festen Oberflächen
Institutskolloquium des Instituts für Interdisziplinäre Isotopenforschung Leipzig, February 26, 2007, Leipzig, Germany.
- Foerstendorf, H.
Ein Schwermetall sieht (infra-)rot
Tag des offenen Labors, May 12, 2007, FZD, Dresden, Germany.
- Funke, H.; Chukalina, M.; Scheinost, A. C.
Application of wavelet transform to extended X-ray absorption spectroscopy
WAMUS07 – 7th WSEAS International Conference on Wavelet Analysis & Multirate Systems, October 13-15, 2007, Arcachon, France.
- Geipel, G.
Uran – Bindungsformen und Toxizität
ISS Kolloquium, May 08, 2007, Neuherberg, Germany.

- Geipel, G.; Baumann, N.; Arnold, T.; Bernhard, G.; Gerstmann, U.; Schimmack, K.; Read, D.
Model studies with DU to assess the mobilisation and speciation of U in soils
International Symposium Protecting Water Bodies from Negative Impacts of Agriculture, June 04-06, 2007, Braunschweig, Germany.
- Geipel, G.; Baumann, N.; Arnold, T.; Bernhard, G.; Gerstmann, U.; Schimmack, K.; Read, D.
Mobilisation and speciation of depleted uranium in water and soils
17th Annual V.M. Goldschmidt Conference 2007, August 19-24, 2007, Cologne, Germany.
- Geipel, G.; Bernhard, G.
Bestimmung der Bindungsform des Urans in kontaminierten Wässern
Workshop "Heinrichsquelle Nürtingen", March 19, 2007, Nürtingen, Germany.
- Geissler, A.; Merroun, M.; Geipel, G.; Reuther, H.; Selenska-Pobell, S.
Bacterial responses to uranyl and sodium nitrate treatments and fate of the added U(VI) in uranium mining waste piles
BAGECO 9 – 9th Symposium on Bacterial Genetics and Ecology, June 23-27, 2007, Wernigerode, Germany.
- Glorius, M.
Actinides in biosystems – Complexation studies with relevant bioligands
University of Cologne, Institut für theoretische Chemie, June 28-29, 2007, Cologne, Germany.
- Günther, A.
Boden-Pflanzen Transfer von U(VI) – Anwendung mikroskopischer und spektroskopischer Methoden zur Charakterisierung der chemischen Speziation
Workshop "Uran in Böden", December 04, 2007, Freiberg, Germany.
- Hennig, C.
Complex structure and species distribution of U(VI) chloride in aqueous and nonaqueous solutions
Institute de Physique Nucleaire, Groupe de Radiochimie, December 13, 2007, Orsay, France.
- Hennig, C.
Die Koordination von Uran-Spezies in Lösungen – Eine Analyse mit EXAFS Spektroskopie
Bundesanstalt für Materialforschung und -prüfung, June 05, 2007, Berlin, Germany.
- Hennig, C.
The structure of actinides in solution – An investigation with XAFS spectroscopy
Workshop on Structural Chemistry of Actinide and Lanthanide Inorganic Compounds, September 29- October 01, 2007, Tsarskoe Selo, St. Petersburg, Russia.
- Hennig, C.; Ikeda, A.; Rossberg, A.; Funke, H.; Scheinost, A. C.
Investigation of actinides in solution under controlled redox conditions
ESRF Beamline Review Panel Meeting, November 06-07, 2007, Grenoble, France.
- Hennig, C.; Schmeide, K.; Brendler, V.; Moll, H.; Tsushima, S.; Ikeda, A.; Scheinost, A. C.; Skanthakumar, S.; Wilson, R.; Soderholm, L.; Servaes, K.; van Deun, R.; Görller-Walrand, C.
Structure and speciation of U(VI) sulfate in aqueous solution
Migration 2007, 11th Conference on the Chemistry and Migration Behaviour of Actinides and Fission Products in the Geosphere, August 26-31, 2007, Munich, Germany.
- Ikeda, A.
Recent achievement on actinide chemistry at FZD: Short introduction about electro-chemical and structural study of uranium and neptunium in solution.
Internal Seminar at the Synchrotron Radiation Research Center, Japan Atomic Energy Agency, November 29, 2007, Hyogo, Japan.
- Joseph, C.
Charakterisierung des Opalinus-Tones und erste Ergebnisse zur U(VI)-Komplexierung mit Huminsäure-Modellliganden
Workshop des Verbundprojektes Wechselwirkung und Transport von Actiniden im natuerlichen Tongestein unter Berücksichtigung von Huminstoffen und Tonorganika, April 02-03, 2007, Potsdam, Germany.
- Krawczyk-Bärsch, E.; Arnold, T.; Großmann, K.
Determination of structural components, e.g. exopolymeric substances (EPS) within bio-films and their effect on the immobilisation of actinides (U) - Determination of pH, Eh, and dissolved oxygen and their influence on the actinide speciation
3rd Semi-Annual RTDC-2 meeting of FUNMIG, August 26, 2007, Munich, Germany.

- Křepelová, A.
Einfluss von HS auf die U(VI)- und Am(III) Sorption an Kaolinit: TRLFS Untersuchungen
Workshop zum Forschungsvorhaben "Wechselwirkung und Transport von Actiniden im natürlichen Tongestein unter Berücksichtigung von Huminstoffen und Tonorganika", April 02-03, 2007, Potsdam, Germany.
- Merroun, M.; Rossberg, A.; Hennig, C.; Selenska-Pobell, S.
Molecular scale characterization of speciation of uranium(VI) associated with bacterial strains isolated from extreme habitats
BAGECO 9 – 9th Symposium on Bacterial Genetics and Ecology, June 23-27, 2007, Wernigerode, Germany.
- Müller, K.; Foerstendorf, H.; Bernhard, G.
Infrared spectroscopic identification of aqueous uranium(VI) species
17th Annual V.M. Goldschmidt Conference 2007, August 19-24, 2007, Cologne, Germany.
- Nebelung, C.; Brendler, V.; Richter, A.; Bernhard, G.
Uranium(VI)-Sorption an natürlichem und synthetischem Sandstein
Wissenschaftsforum Chemie 2007, September 16-19, 2007, Ulm, Germany.
- Pollmann, K.; Raff, J.; Merroun, M.; Selenska-Pobell, S.; Herrmannsdorfer, T.
Development of novel nanomaterials based on self-organising bacterial S-layer proteins
NanoBio-Europe 2007, June 13-15, 2007, Münster, Germany.
- Raditzky, B.; Eilzer, M.
Binding properties of a phosphonate clip towards nucleic acid building blocks
4th SUPRAPHONE Meeting, May 31- June 03, 2007, Lipari, Italy.
- Raff, J.
Biofilme in Natur und Gesellschaft
Tag des offenen Labors, May 12, 2007, FZD, Dresden, Germany.
- Raff, J.
Bio-nanotechnology/Nanocluster dank Bakterien
Vortrag zum Besuch von Schülern der 11. und 12. Klasse (Chemie-LK) des Gymnasiums Radeberg, January 18, 2007, FZD, Dresden, Germany.
- Raff, J.
Gründungsidee und Geschäftskonzept - BIOREM
FutureSAX-Businessplan-Wettbewerb, April 19, 2007, Leipzig, Germany.
- Raff, J.; Pollmann, K.
Bakterielle Hüllproteine (S-Layer) als Werkzeug für die Entwicklung nanoskaliger Katalysatoren, Biosensoren und Filtermaterialien
Innovationsforum "REDUPHARM", September 07, 2007, Dessau, Germany.
- Reitz, T.; Geissler, A.; Merroun, M.; Selenska-Pobell, S.
Interactions of U(VI) with members of a microbial consortium recovered from a uranium mining waste pile
37th Journées des Actinides, , March 24-27, 2007, Sesimbra, Portugal.
- Richter, A.; Nebelung, C.; Brendler, V.
U(VI) sorption on sandstone: Experiments and modeling
17th Annual V.M. Goldschmidt Conference 2007, August 19-24, 2007, Cologne, Germany.
- Scheinost, A. C.
Synchrotron research in environmental chemistry: Linking space, time, redox and biota
Kolloquium, June 13, 2007, Leipzig, Germany.
- Scheinost, A. C.
Environmental soil chemistry with synchrotron methods
Seminar-Vortrag am Institut für Ökologie der TU Berlin, April 24, 2007, Berlin, Germany.
- Scheinost, A. C.; Charlet, L.
Selenite reduction by green rust, magnetite, siderite and mackinawite: EXAFS identification of Se species
17th Annual V.M. Goldschmidt Conference 2007, August 19-24, 2007, Cologne, Germany.
- Schierz, A.; Zaenker, H.; Bernhard, G.
Sorption of U(VI) on multiwall carbon nanotubes
Aquatic Nanoscience and Nanotechnology, December 09-11, 2007, Vienna, Austria.
- Schmeide, K.; Joseph, C.; Raditzky, B.
Spektroskopische Untersuchung der Uran(IV)- und Uran(VI)-Komplexierung mit organischen Modellliganden
Workshop zum Forschungsvorhaben "Wechselwirkung und Transport von Actiniden im natürlichen Tongestein unter Berücksichtigung von Huminstoffen und Tonorganika", October 11-12, 2007, Saarbrücken, Germany.

- Selenska-Pobell, S.
Microbial response to U(VI) and nitrate treatments of uranium mining waste pile samples
Winter-Spring 2007 Seminar Series, January 31-Februaury 02, 2007, Utrecht, The Netherlands.
- Selenska-Pobell, S.
Bacteria-based nanoscaled materials
Institut für Neue Materialien GmbH, February 23, 2007, Saarbrücken, Germany.
- Selenska-Pobell, S.
Novel S-layer supported Pd bionanocatalysts
Institute of Molecular Biology, September 26, 2007, Sofia, Bulgaria.
- Selenska-Pobell, S.
Biogeochemical changes in uranium wastes induced by increased U(VI) and nitrate concentrations
Institute of Microbiology, November 02, 2007, Prague, Czech Republic.
- Tsushima, S.
Combining DFT calculations , EXAFS, IR, and UV-vis spectroscopy
ACTINET workshop "How can we improve coupling theoretical chemistry with X-ray absorption spectroscopy?", October 11-12, 2007, Avignon, France.
- Tsushima, S.; Hennig, C.; Ikeda, A.; Rossberg, A.; Scheinost, A. C.
Structures of actinide complexes: combining DFT calculations, EXAFS spectroscopy, and thermodynamic speciation
American Chemical Society 234th National Meeting, Symposium: Computational Actinide and Transactinide Chemistry: Progress and Perspectives, August 19-23, 2007, Boston, USA.
- Tsushima, S.; Hennig, C.; Ikeda, A.; Scheinost, A. C.
Uranium redox chemistry and its importance in nuclear waste disposal
American Chemical Society 234th National Meeting, Symposium: Computational Electrochemistry for New Energy, August 19-23, 2007, Boston, USA.
- Zänker, H.
Die Welt der vernachlässigten Dimensionen
Lange Nacht der Wissenschaft, June 29, 2007, Dresden, Germany.
- Zänker, H.; Opel, K.; Weiß, S.; Hübener, S.; Bernhard, G.
Investigations into the formation of real colloids and pseudocolloids of uranium(IV)
Migration 2007, 11th Conference on the Chemistry and Migration Behaviour of Actinides and Fission Products in the Geosphere, August 26-31, 2007, Munich, Germany.
- Zänker, H.; Schierz, A.
The influence of natural and manufactured nanoparticles on heavy metal behavior in natural waters
Aquatic Nanoscience and Nanotechnology December 09.-11, 2007, Vienna, Austria.
- Zänker, H.; Ulrich, K.-U.; Opel, K.; Brendler, V.
Der Einfluss von Kolloiden auf den Urantransport in radioaktiven Endlagern und in stillgelegten Uranbergwerken - Ein kritischer Vergleich
Wasser 2007. Jahrestagung der Wasserchemischen Gesellschaft, GDCh, May 14-16, 2007, Passau, Germany.
- Zänker, H.; Ulrich, K.-U.; Opel, K.; Brendler, V.
The role of colloids in uranium transport: A comparison of nuclear waste repositories and abandoned uranium mines
IMWA Symposium 2007, Water in Mining Environments, May 27-31, 2007, Cagliari, Italy.
- Zänker, H.; Weiß, S.
Laserinduzierte Breakdown-Detektion (LIBD)
Seminar on particle measurement in ultrapure waters of semiconductor industry, Infineon Technologies Dresden GmbH, March 20, 2007, Dresden, Germany.

► Posters

- Baumann, N.; Arnold, T.; Foerstendorf, H.;
Read, D.; Black, S.; Massanek, A.
**Fingerprinting of a thin secondary mineral
film on DU**
*17th Annual V.M. Goldschmidt Conference 2007,
August 19-24, 2007, Cologne, Germany.*
- Brendler, V.; Trepte, P.; Křepelová, A.;
Baumann, N.
**TRLFS fingerprinting for uranyl(VI) surface
species on clay model substances**
*Migration 2007, 11th Conference on the
Chemistry and Migration Behaviour of Actinides
and Fission Products in the Geosphere, August
26-31, 2007, Munich, Germany.*
- Funke, H.; Chukalina, M.; Scheinost, A. C.;
Voegelin, A.
**EXAFS studies of Zn/Al and Ni/Al Layered
Double Hydroxides**
*17th ESRF User's Meeting 2007, February 07-
09, 2007, Grenoble, France.*
- Geissler, A.; Reitz, T.; Selenska-Pobell, S.
**Bacterial response to sodium and uranyl
nitrate treatments of uranium mining waste
samples**
*VAAM-Jahrestagung, April 01-04, 2007,
Osnabrück, Germany.*
- Glorius, M.; Moll, H.; Geipel, G.; Bernhard, G.
**Uranium(VI) complexation studies with
selected aromatic acids - A comparison of
different spectroscopic techniques**
*Migration 2007, 11th Conference on the
Chemistry and Migration Behaviour of Actinides
and Fission Products in the Geosphere, August
26-31, 2007, Munich, Germany.*
- Gonzalez-Munoz, M.; de Linares, C.; Martinez-
Ruiz, F.; Morcillo, F.; Merroun, M.; Arias, J.
**Characterization of a novel *Idiomarina*
loihiensis strain isolated from the
westernmost Mediterranean: Heavy-metal
resistance and biomineralization capability**
*BAGECO 9 – 9th Symposium on Bacterial
Genetics and Ecology, June 23-27, 2007,
Wernigerode, Germany.*
- Großmann, K.; Arnold, T.; Krawczyk-Bärsch, E.;
Diessner, S.; Wobus, A.; Bernhard, G.;
Krawietz, R.
**Identification of fluorescent U(V) and U(VI)
microparticles in a multispecies biofilm by
confocal laser scanning microscopy and
fluorescence spectroscopy**
*ISEB 2007, Environmental Biogeochemistry at
the Extremes, November 11-16, 2007, Taupo,
New Zealand.*
- Hennig, C.
**Double-electron excitations in L₃-edge X-ray
absorption spectra of Actinides**
*17th ESRF User's Meeting 2007, February 07-
09, 2007, Grenoble, France.*
- Hofmann, S.; Wobus, A.; Rosenlöcher, J.;
Großmann, K.; Arnold, T.; Krawczyk-
Bärsch, E.; Röske I.
**Phylogenetic analysis and in situ
identification of bacteria community
composition in uranium contaminated soil**
*ISEB 2007, Environmental Biogeochemistry at
the Extremes, November 11-16, 2007, Taupo,
New Zealand.*
- Ikeda, A.; Hennig, C.; Rossberg, A.; Tsushima, S.;
Scheinost, A. C.; Bernhard, G.
**Complexation of uranium(VI) with nitrate in
nonaqueous and aqueous solutions:
Speciation and structural studies**
*Migration 2007, 11th Conference on the
Chemistry and Migration Behaviour of Actinides
and Fission Products in the Geosphere, August
26-31, 2007, Munich, Germany.*
- Ikeda, A.; Hennig, C.; Tsushima, S.; Rossberg, A.;
Scheinost, A. C.; Bernhard, G.
**XAFS study of uranyl carbonate complexes in
aqueous solution**
*17th ESRF User's Meeting 2007, February 07-
09, 2007, Grenoble, France.*
- Krawczyk-Bärsch, E.; Arnold, T.; Großmann, K.;
Wobus, A.; Hoffmann, S.
**Increased metabolic activity in biofilms
caused by uranium: A microsensor study**
*ISEB 2007, Environmental Biogeochemistry at
the Extremes, November 11-16, 2007, Taupo,
New Zealand.*

- Krawczyk-Bärsch, E.; Großmann, K.; Arnold, T.; Diessner, S.; Wobus, A.
Uranium as a stress factor in well aerated multispecies biofilms – A microsensor study of the O₂ concentrations
International Symposium on Microbial Adaptation in Stress and Environment, April 12-14, 2007, Marburg, Germany.
- Krawczyk-Bärsch, E.; Großmann, K.; Arnold, T.; Diessner, S.; Wobus, A.
A microsensor study on the O₂ consumption in a U(VI) contaminated multispecies biofilm
6. Jenaer Sanierungskolloquium „Mikroben-Mineral Wechselwirkungen an Schwermetallbelasteten Standorten“, October 04-05, 2007, Jena, Germany.
- Křepelová, A.; Sachs, S.; Geipel, G.; Bernhard, G.
Influence of humic acid on the Am(III) sorption onto kaolinite
Migration 2007, 11th Conference on the Chemistry and Migration Behaviour of Actinides and Fission Products in the Geosphere, August 26-31, 2007, Munich, Germany.
- Lehmann, S.; Geipel, G.; Bernhard, G.
Aqueous uranium(IV) fluoride complexes: determination of fluorescence properties by means of TRLFS
Migration 2007, 11th Conference on the Chemistry and Migration Behaviour of Actinides and Fission Products in the Geosphere, August 26-31, 2007, Munich, Germany.
- Li, B.; Foerstendorf, H.; Raff, J.; Bernhard, G.
FT-IR investigation of the uranium S-layer interaction in aqueous solutions
17th Annual V.M. Goldschmidt Conference 2007, August 19-24, 2007, Cologne, Germany.
- Matys, S.; Raff, J.; Soltmann, U.; Selenska-Pobell, S.; Böttcher, H.; Pompe, W.
Germination pathway of long-time storable biocer layers with immobilized bacterial endospores
XIVth International Sol-Gel Conference, September 02-07, 2007, Montpellier, France.
- Merroun, M.; Geissler, A.; Nedelkova, M.; Selenska-Pobell, S.
Interactions of U(VI) and Eu(III) with natural bacterial isolates
17th Annual V.M. Goldschmidt Conference 2007, August 19-24, 2007, Cologne, Germany.
- Merroun, M.; Geissler, A.; Raff, J.; Hennig, C.; Selenska-Pobell, S.
Interaction mechanisms of bacterial strains isolated from uranium mining waste piles with U and Pb
VAAM-Jahrestagung, April 01-04, 2007, Osnabrück, Germany.
- Missana, T.; Alonso, U.; Scheinost, A. C.; Granizo, N.; García-Gutiérrez, M.
Selenite retention by iron oxy-hydroxides: Role of adsorption, reduction and dissolution/co-precipitation
Migration 2007, 11th Conference on the Chemistry and Migration Behaviour of Actinides and Fission Products in the Geosphere, August 26-31, 2007, Munich, Germany.
- Moll, H.; Johnsson, A.; Schäfer, M.; Glorius, M.; Pedersen, K.; Budzikiewicz, H.; Bernhard, G.
Complexation of actinides with bioligands secreted by a subsurface strain of *Pseudomonas fluorescens*
Migration 2007, 11th Conference on the Chemistry and Migration Behaviour of Actinides and Fission Products in the Geosphere, August 26-31, 2007, Munich, Germany.
- Morcillo, F.; Merroun, M.; Bueno, J. D.; Gonzalez-Munoz, M. T.; Arias, J. M.
Tolerancia y fijación de uranio por *Idiomarina loihiensis* MAH1
XXI Congreso Nacional de Microbiología, September 17-20, 2007, Sevilla, Spain.
- Müller, K.; Foerstendorf, H.
Hydrolysis of U(VI). An infrared spectroscopic verification of uranyl species
Migration 2007, 11th Conference on the Chemistry and Migration Behaviour of Actinides and Fission Products in the Geosphere, August 26-31, 2007, Munich, Germany.
- Müller, K.; Foerstendorf, H.; Bernhard, G.
Speciation of Np(V) in aqueous solution investigated by FT-IR spectroscopy.
Migration 2007, 11th Conference on the Chemistry and Migration Behaviour of Actinides and Fission Products in the Geosphere, August 26-31, 2007, Munich, Germany.
- Pollmann, K.; Raff, J.; Merroun, M.; Selenska-Pobell, S.; Herrmannsdörfer, T.
Selbstorganisierende bakterielle Hüllproteine als Grundlage für die Entwicklung neuartiger Nanomaterialien
6. Präsentation BMBF BioFuture, January 29.-30, 2007, Berlin, Germany.

- Raditzky, B.; Stephan, H.; Weiß, S.; Geipel, G.; Polkowska, J.; Klärner, F.-G.
Binding properties of a phosphonate substituted clip towards nucleosides
COST D31 3rd Workshop, March 28-31, 2007, Athens, Greece.
- Raff, J.; Pollmann, K.; Scholz, A.
Novel photocatalytic nanomaterials for environmental purposes based on bacterial cells and S-layer proteins.
1st International Workshop Aquatic Nanosciences and Nanotechnology, December 09-11, 2007, Wien, Austria
- Reitz, T.; Geissler, A.; Merroun, M.; Selenska-Pobell, S.
Crenarchaeota 1.1b and Firmicutes consortium recovered from a uranyl nitrate treated uranium waste sample and its possible role against the toxicity of uranium
VAAM-Jahrestagung, April 01-04, 2007, Osnabrück, Germany.
- Rossberg, A.; Tsushima, S.; Ulrich, K.-U.; Scheinost, A. C.
Carbonate effects on surface speciation of uranyl at the ferrihydrite-water interface: New insights from advanced EXAFS data analysis
Migration 2007, 11th Conference on the Chemistry and Migration Behaviour of Actinides and Fission Products in the Geosphere, August 26-31, 2007, Munich, Germany.
- Tsushima, S.; Rossberg, A.; Hennig, C.; Moll, H.; Scheinost, A. C.
The structure of trimeric uranyl hydroxo complexes in aqueous solution
Migration 2007, 11th Conference on the Chemistry and Migration Behaviour of Actinides and Fission Products in the Geosphere, August 26-31, 2007, Munich, Germany.
- Viehweger, K.; Geipel, G.
Interactions of uranium with *Brassica Bt'07*
Annual Meeting of the German Botanical Society, September 03-09, 2007, Hamburg, Germany.
- Wenzel, M.; Gloe, Ke.; Gloe, K.; Bernhard, G.; Clegg, J. K.; Ji, X.-K.; Lindoy, L. F.
Cation and anion binding studies of a large N,O-donor macrocycle: Single ion extraction and synergistic enhancement
II. International Symposium on Macrocyclic and Supramolecular Chemistry, June 24-28, 2007, Salice Terme, Italy.
- Wenzel, M.; Antonioli, B.; Gloe, Ke.; Gloe, K.; Bernhard, G.; Sanchez, M. G.; Bray, D. J.; Clegg, J. K.; Lindoy, L. F.
Tripodal polyamines as anion receptors: Extraction and structural studies
II. International Symposium on Macrocyclic and Supramolecular Chemistry, June 24-28, 2007, Salice Terme, Italy.
- Zänker, H.; Opel, K.; Weiß, S.; Hübener, S.; Bernhard, G.
Formation of uranium(IV) colloids
43th Meeting of the German Colloid Society, October 08-10, 2007, Mainz, Germany.

▶ Awards / Research fellowships

Geipel, G.

Fellow

School of Engineering, The University of Tokyo, Tokyo, Japan (2007).

Raff, J.

BIOREM-business idea honored as "Die Beste Geschäftsidee" in the category bio- and nanotechnology in phase I of the business plan competition Saxony

FutureSAX 2007, Dresden, Germany (2007).

Raff, J.

Winner of the BIOREM-business plan in the business plan seminar of the SAP endowed chair of entrepreneurship and innovation

Dresden University of Technology, Dresden, Germany (2007).

Selenska-Pobell, S.

Ehrenmedaille der Bulgarischen Akademie der Wissenschaften

Bulgarian Academy of Sciences, Sofia, Bulgaria (2007).

▶ Patent

Arnold, T.; Großmann, K.; Krawczyk-Bärsch, E.

Messsensor

Patent No. 10 2005 051 4057

▶ Theses

Geissler, A.

Characterization of microbial communities in a uranium mining waste pile and investigation of their interactions with heavy metals and uranium

Dresden University of Technology, Dresden, Germany (2007).

Schierz, A.

Anwendung von kolloidaler Aktivkohle zur in-situ-Grundwasserreinigung

Universität Leipzig, Leipzig, Germany (2007).

Křepelová, A.

Influence of humic acid on the sorption of uranium(VI) and americium(III) onto kaolinite

Dresden University of Technology, Dresden, Germany (2007).

► Diploma

Ihlau, A.

Architektur und Administration einer web-basierten chemischen Stoffdatenbank. Konzept und Prototyp

University of Applied Sciences, Dresden, Germany (2007).

Jähnigen, P.

Simultanbestimmung von Betastrahlern in Nuklidgemischen mittels Flüssigszintillations-spektrometrie

Dresden University of Technology, Dresden, Germany (2007).

Jankowski, U.

Spectroscopic characterization of Au and Pt complexation and nanocluster formation on S-layer

TU Bergakademie Freiberg (2007).

Klinger, M.

Radiogene Färbung natürlicher Zirkone EPR- und Lumineszenzuntersuchungen
TU Bergakademie Freiberg (2007).

Münzberg, M.

Konzeptioneller Entwurf und prototypische Realisierung einer Datenbanklösung für chemische Risikoanalysen

University of Applied Sciences, Dresden, Germany (2007).

► Work placements

Gründig, I.

Reduktion von Uran(VI) durch Glucose

University of Applied Sciences, Dresden, Germany (2007).

Weinert, U.

Isolierung und Charakterisierung bakterieller Hüllproteine (S-Layer)

University of Applied Sciences, Dresden, Germany (2007).

Rentzsch, M.

Schwingungsspektroskopische Untersuchungen der molekularen Wechselwirkung von Actiniden an mineralischen Eisenphasen in wässriger Lösung

University of Applied Sciences, Dresden, Germany (2007).

- ▶ Seminars (talks of visitors)
- ▶ Workshops
- ▶ Teaching activities

► Seminars

Dr. Udo Gerstmann

*Institut für Strahlenschutz, Deutsches
Forschungszentrum für Gesundheit und Umwelt,
Munich, Germany*

**Untersuchungen zur Gesundheitsgefährdung
durch DU-Munition**

January 23, 2007

Prof. Dr. Karsten Pedersen

*Department of Cell and Molecular Biology,
Göteborg University, Sweden*

**The significance of biogeochemical processes
in geological disposal of high level radioactive
waste**

May 10, 2007

Dr. Dorothea Schumann

*Laboratory for Radiochemistry and
Environmental Chemistry, Paul Scherrer
Institute, Villigen, Switzerland*

**ERAWAST – A new production route for
exotic long-lived radionuclides**

July 13, 2007

Prof. Dr. Ingo Klimant

*Institute of Analytical Chemistry and
Radiochemistry, Graz University of Technology,
Graz, Austria*

**Entwicklung und Anwendung von
optochemischen Sensoren**

July 20, 2007

Anna Moritz, Jonas Wiebke

*Institut für Theoretische Chemie, University of
Cologne, Cologne, Germany*

**DFT-Studie zur Modellierung der Uran(VI)-
Koordination durch ausgewählte Bioliganden**

August 06, 2007

Dr. Johanna Lippmann-Pipke

*Institute of Interdisciplinary Isotope Research,
Leipzig, Germany*

**Skalenübergreifende Tracerstudien zu
Fluidtransportprozessen – Arbeitsbeispiele in
interdisziplinären Zusammenhängen**

September 10, 2007

Dr. Barbara Gouget

*Laboratoire Pierre Süe, CEA CNRS, Gif sur
Yvette, France*

**Selenium and uranium resistance in the
telluric bacteria *Cupria vidus metallidurans*
CH34 and *Deinococcus radiodurans***

October 26, 2007

Dr. Concepción Jiménez-Lopéz

*Department of Microbiology, University of
Grenada, Grenada, Spain*

**Looking for criteria to recognize the
biological origin of iron oxides: The case of
the magnetite induced by *Shewanella*
*oneidensis***

November 29, 2007

Prof. Dr. Lynne Macaskie

*Unit of Functional Bionanomaterials, School of
Sciences, University of Birmingham,
Birmingham, Great Britain*

**Novel bionanocatalysts for chemical and
sustainable energy applications**

December 12, 2007

► Workshops (organized by the IRC)

Workshop of the Institute of Radiochemistry (IRC) and the Paul Scherrer Institute (PSI), Villigen , Switzerland

*PSI, Villigen, Switzerland,
November 05 – 06, 2007.*

Baeyens, B. (PSI)

Geplante Messungen (Sorption/TRLFS/XAS) von Actiniden im Rahmen des INCA- Projektes (Maria Marques-Fernandez)

Glaus, M. (PSI)

Diffusion von Iodid/Iodat im Opalinuston

Großmann, K. (IRC)

Gegenwärtige Möglichkeiten und Grenzen des gekoppelten CLSM/TRLFS-Systems

Jakob, A. (PSI)

Die Problematik der numerischen Auswertung von Diffusionsexperimenten

Nebelung, C. (IRC)

Uranium(VI)-Sorption an natürlichem und synthetischem Sandstein

Schierz, A. (IRC)

Sorption of actinides on manufactured nanoparticles

Stuedtner, R. (IRC)

Wechselwirkung von Uran mit Glucose

Viehweger, K. (IRC)

Interactions of uranium with *Brassica*

Discussion meeting Surface reactions & EIL Experiments and models Towards a common basis

*Hotel Bristol, Opatja, Croatia
October 08 – 13, 2007.*

Organized by:

Croatia Chemical Society, Zagreb, Croatia;
Forschungszentrum Karlsruhe, Karlsruhe, Germany;
Forschungszentrum Dresden-Rossendorf, Dresden,
Germany

Participants:

Abdelmonem, A. (Egypt, Germany)
Arnold, T. (Germany)
Bickmore, B. (USA)
Blesa, A. (Argentina)
Brendler, V. (Germany)
Bourg, A. (France)
Bourg, I. (France, USA)
Chibowski, E. (Poland)
Fedoroff, M. (France)
Fitts, J. (USA)
Kallay, N. (Croatia)
Kent, D. (USA)
Kovacevic, D. (Croatia)
Kulik, D. (Ukraine, Switzerland)
van der Lee, J. (France)
Lefèvre, G. (France)
Lövgren, L. (Sweden)
Lützenkirchen, J. (Germany)
Ly, J. (France)
Martin, Ch. (France)
Piasecki, W. (Poland)
Predota, M. (Czech Republic)
Preocanin, T. (Croatia)
Rabung, T. (Germany)
Regazzoni, A. (Argentina)
Rudzinski, W. (Poland)
Rosenqvist, J. (USA)
Villalobos, M. (Mexico)

► Teaching activities

Lectures

Bernhard, G.

Radiochemistry – Radiochemical methods

*Dresden University of Technology,
Summer term 2007*

Bernhard, G.

Environmental analysis (Trace analysis)

*Dresden University of Technology,
Summer term 2007*

Bernhard, G.

**Environmental chemistry (Environment –
Substance – Energy)**

*Dresden University of Technology,
Winter term 2007/2008*

Merroun, M.

**Lixiviación y Recuperación de Metales:
Bioleaching and removal of metals**

*Centro de Enseñanzas Virtuales de la
Universidad de Granada – Fundación Empresa
Universidad de Granada & Escuela Superior de
Enseñanza Abierta
Study course: Máster de Biotecnología – Master
of Biotechnology*

Courses

The IRC provided one experiment of the laboratory course “Instrumental Analysis” held by the Institute for Analytical Chemistry, Dresden University of Technology, during winter term (wt):

– Alpha spectrometric isotope dilution analysis of uranium

Advisers:

Dr. Foerstendorf, H. (wt 07/08)

Dr. Hübener, S. (wt 06/07)

Teaching Assistants:

wt 06/07

Glorius, M.

Großmann, K.

Müller, K.

Steuertner, R.

Weiß, S.

wt 07/08

Dreissig, I.

Götz, C.

Joseph, C.

Reitz, T.

PERSONNEL

Prof. Dr. habil. G. Bernhard (Director)

Administration

Kirmes, Claudia; Kovács, Jenny; Kreusel, Gabriele

Radiation Protection Technics

Heim, Heidemarie; Falkenberg, Dirk; Henke, Steffen; Hiller, Bernd; Rumpel, Annette

D I V I S I O N S

BIOGEOCHEMISTRY

Dr. Geipel, Gerhard

Dr. Arnold, Thuro
Dr. Barkleit, Astrid
Dr. Günther, Alix
Dr. Ikeda, Atsushi
Dr. Krawczyk-Bärsch, Evelyn
Dr. Merroun, Mohamed L.
Dr. Moll, Henry
Dr. Pollmann, Katrin
Dr. Raff, Johannes
Dr. Sachs, Susanne
Dr. Schmeide, Katja
Dr. Selenska-Pobell, Sonja
Dr. Viehweger, Katrin

Technical Staff

Dudek, Monika
Eilzer, Manuela
Flemming, Katrin
Grambole, Genia
Heller, Sylvia
Ritter, Aline
Seidel, Annett

MIGRATION

Dr. Brendler, Vinzenz

Dr. Baumann, Nils
Dr. Foerstendorf, Harald
Gester, Sven
Dr. Hübener, Siegfried
Nebelung, Cordula
Dr. Richter, Anke
Dr. Schierz, Ariette
Dr. Zänker, Harald

Technical Staff

Bruder, Mandy
Eckardt, Carola
Eidner, Irmgard
Fröhlich, Christine
Heim, Karsten
Müller, Christa
Neubert, Heidrun
Schaefer, Ursula
Weiß, Stephan

MOLECULAR STRUCTURES

(ROBL, ESRF, Grenoble, France)

Dr. habil. Scheinost, Andreas C.

Dr. Banerjee, Dipanjan
Dr. Funke, Harald
Dr. Hennig, Christoph
Dr. Roßberg, André
Prof. Dr. Tsushima, Satoru

Strauch, M.
Glückert, Marion
(Administration)

Technical Staff

Hesse, Marco
Strauch, Udo

PH. D. STUDENTS

Dreissig, Isabell
Glorius, Maja
Götz, Christian
Großmann, Kay
Heller, Anne
Joseph, Claudia
Kirsch, Regina
Křepelová, Adela
Lehmann, Sandra

Li, Bo
Müller, Katharina
Raditzky, Bianca
Reitz, Thomas
Schreppel, Katja
Steudtner, Robin
Tanh Jeazet, Harold B.
Vogel, Manja

DIPLOMA STUDENTS

Ihlau, Alexander
Jaehnigen, Peggy
Jankowski, Ulrike
Klinger, Mathias
Lederer, Franziska
Münzberg, Marco
Weinert, Ulrike

GRADUATE ASSISTANTS, STUDENT ASSISTANTS, TRAINEES

| | | | |
|--------------------------|-------------------|-------------------|------------------|
| Bernhard, Jörg | Heinitz, Stephan | Pietzsch, Doreen | Semjank, Laura |
| Brockmann, Sina | Heller, Tina | Rentzsch, Michael | Trepte, Paul |
| Fajardo Uribe, Carlos H. | Henke, Franziska | Rieck, Carolin | Weinert, Kareen |
| Gründig, Ines | Husar, Richard | Schleith, Kathrin | Weinert, Ulrike |
| Hänsch, Samuel | Krause, Martin | Schott, Juliane | Wenzel, Marco |
| Haferkorn, Ulrike | Müller, Christian | Schwiebs, Melanie | Wimmer, Christin |

GUEST SCIENTISTS

- Prof. Dr. M. Fedoroff *Laboratoire d'Electrochimie et de Chimie Analytique,
École Nationale Supérieure de Chimie de Paris, Paris, France*
- Prof. Dr. E. Golovinsky *Institute of Molecular Biology,
Bulgarian Academy of Sciences, Sofia, Bulgaria*
- J. Harrison *Institute for Environmental Research,
Australian Nuclear Science and Technology Organisation, Menai, Australia*
- Dr. C. Jiménez-López *Departamento de Microbiología,
Universidad de Granada, Granada, Spain*
- Dr. G. Lefevre *Laboratoire d'Electrochimie et de Chimie Analytique,
École Nationale Supérieure de Chimie de Paris, Paris, France*
- Prof. Dr. S. Nagasaki *Tokyo Institute of Technology,
Tokyo, Japan*
- Dr. G. Radeva *Institute of Molecular Biology,
Bulgarian Academy of Sciences, Sofia, Bulgaria*
- Prof. Dr. D. Strawn *Department of Plant, Soil and Entomological Sciences,
University of Idaho, Moscow, U.S.A.*
- Dr. J. Tits *Laboratory for Waste Management
Paul Scherrer Institute (PSI), Villigen, Switzerland*

ACKNOWLEDGEMENTS

The Institute of Radiochemistry is part of the Forschungszentrum Dresden-Rossendorf e. V. (FZD) which is financed in equal parts by the **Federal Republic of Germany** and the **Free State of Saxony**.

The Commission of the European Communities (EU) supported the following projects:

- ACTINET – Network for Actinide Sciences:
Contract No.: FIRI-2002-20211
Contract No.: FI6W-CT-2004-508836
- ACTINET-6 – Joint projects:
 - Actinide selective recognition by bio mimetic molecules*
Contract No.: JRP 05-01
 - Actinides and lanthanides solution chemistry in water stable room temperature ionic liquids (RTILs) – Part II*
Contract No.: JRP 05-26
 - Batch experiments and spectroscopic studies of Np(V) sorption on montmorillonite*
Contract No.: JRP 05-22
 - Combining XAS at variable energy and theoretical calculations to investigate bonding in actinide molecules*
Contract No.: JRP 07-06
 - Complexation of U, Np, and Pu ions with organic ligands: Combined quantum chemical and EXAFS study*
Contract No.: JRP 05-10
 - Coupling variable energy X-ray absorption spectroscopy and quantum chemistry: A new tool to investigate actinide molecules*
Contract No.: JRP 04-02
 - Development of advanced EXAFS analysis methods for speciation of radionuclides in natural systems*
Contract No.: JRP 03-08
 - Free and silica-gel-bound tetraazamacrocycles as complexing agents of actinide cations: investigation of the solid-state and solution coordination scheme*
Contract No.: JRP 07-05
 - Influence of carbonate on actinides sorption on clay minerals*
Contract No.: JRP 06-02
 - Microscale investigations of the speciation and mobility of uranium in cementitious materials*
Contract No.: JRP 06-13
 - Physico-chemical and redox properties of protactinium*
Contract No.: JRP 07-20
 - Probing the interaction of actinides with the functional species of mineral/electrolyte interfaces by sum frequency vibrational spectroscopy*
Contract No.: JRP 05-11
 - Reduction of uranium(VI) by adsorbed Fe(II) on several clays and by structural Fe(II) in smectite in O₂, CO₂ free atmosphere*
Contract No.: JRP 06-08
Contract No.: JRP 07-21
 - Speciation of actinides and fission products nanoparticles embedded into the mesoporous matrices*
Contract No.: JRP 07-16
 - Studies of the chemical forms of actinides and fission products adsorbed on nanocrystalline magnetite*
Contract No.: JRP 04-08
 - Understanding the electronic structure of actinyl complexes (part II)*
Contract No.: JRP 05-15

- ACTINET – Sorption Board:
 - Knowledge infrastructure and education*
Contract No.: JRP 02-23
 - Managing experiments, models and data*
Contract No.: JRP 02-24
- Integrated project NF-Pro:
 - Understanding and physical and numerical modelling of the key processes in the near-field and their coupling for different host rocks and repository strategies*
Contract No.: FI6W-CT-2003-002389
- Integrated project FUNMIG:
 - Fundamental processes of radionuclide migration*
Contract No.: 516514

Six projects were supported by the **Bundesministerium für Wirtschaft und Technologie (BMW)** and by the **Bundesministerium für Bildung und Forschung (BMBF)**:

- Mobilisierung von Actiniden durch mikrobiell produzierte Liganden unter Berücksichtigung der Endlagerung von radioaktivem Abfall
Contract No.: BMW 02E9985
- Integriertes Sorptionsdatenbanksystem für Wechselwirkungen chemisch-toxischer und radioaktiver Kontaminanten mit mineralischen Systemen in geologischen Formationen (ISDA-FZR)
Contract No.: BMBF 02C1144
- Thermodynamische Referenzdatenbasis THEREDA, Teilvorhaben FZR, gefördert durch das BMBF
Contract No.: 02C1436
- Thermodynamische Referenzdatenbasis THEREDA, Teilvorhaben FZR, gefördert durch das BMWi
Contract No.: 02E10136
- Verbundprojekt: Actinidenmigration im natürlichen Tongestein: Charakterisierung und Quantifizierung des Einflusses von Tonorganika auf die Wechselwirkung von U und Am im Ton
Contract No.: BMW 02E10156
- NanoFoto – Neue Wege zur verwertungsorientierten Netzwerkbildung in der Nanobiotechnologie
Contract No.: BMBF 01SF0717

The supported through the **Bundesamt für Strahlenschutz (BfS)** one project:

- Entwicklung einer thermodynamischen Referenzdatenbasis (Teilprojekt Spaltprodukte und Zement: THEREDA-SZ)
Contract-No.: VA3252 - AN550550 - UA2671

Five projects were supported by the **Deutsche Forschungsgemeinschaft (DFG)**:

- Fluoreszenzspektroskopie von gelösten Uran(IV)-Komplexen – Aufklärung der Speziation im umweltrelevanten Konzentrationsbereich
Contract No.: GE 1011/4-1
- Kolloidgetragener Transport von Uran und anderen radiotoxischen Schwermetallen in toxischen Bergwerkswässern
Contract No.: ZA 238/2-2
- In-situ Speziation von Uran in Biofilmen
Contract No.: AR 584/1-1
- Sorptionsprozesse von Np(V) an Alumosilikaten. Schwingungsspektroskopische Untersuchungen
Contract No.: FO 619/1-1
- In situ-Strukturuntersuchungen von Neptunium-Spezies in wässriger Lösung unter reduzierenden Bedingungen
Contract No.: HE 2297/2-1
- Bindungsform von Cm(III) und Eu(III) in menschlichen Biofluiden (Speichel, Urin)
Contract No.: BE 2234/10-1
- Strukturbestimmung von ternären aquatischen U(VI)-Sorptionskomplexen mittels neuester entwickelter kombinierter EXAFS-Auswertemethoden (ITFA, MCTFA)
Contract No.: RO 2254/3-1

The **University of Manchester, Department of Chemistry**, Great Britain supported one project:

- Access to beamtime at Rossendorf Beamline at ESRF in the frame of a scientific collaboration

The **University of Jena** supported one project:

- Uranaufnahme
Contract-No.: 02S8517

The **Verein für Kernverfahrenstechnik und Analytik e.V. (VKTA)**, Dresden, supported one project:

- Modellierung der Freisetzungprozesse von Radionukliden im Aquifer einer geothermischen Anlage
Contract-No.: FZD-Reg.-No.: 21/2007

INDEX OF AUTHORS

| AUTHOR | PAGE | AUTHOR | PAGE |
|-----------------------|--|--------------------------|----------------------------|
| Arnold, T. | 13, 23, 44 | Klinger, C. | 49 |
| Barkleit, A. | 28, 35 | Köhler, M. | 61 |
| Baumann, N. | 50, 51 | Kraus, W. | 11 |
| Bernhard, G. | 9, 15, 18, 19, 20, 26, 27, 28, 29, 30, 31, 35, 37, 38, 56, 57, 59, 60 | Krawczyk-Bärsch, E. | 44 |
| Brasser, T. | 49 | Křepelová, A. | 51 |
| Brendler, V. | 11, 16, 25, 49, 51, 52, 53, 61 | Lederer, F. | 39 |
| Büchner, B. | 30 | Li, B. | 36, 42 |
| Charlet, L. | 54 | Merroun, M. | 41, 43 |
| Claußner, J. | 11 | Moll, H. | 15, 18, 21, 26, 27, 35, 59 |
| Degering, D. | 61 | Moritz, A. | 21 |
| Dreissig, I. | 57 | Müller, K. | 12, 25 |
| Eilzer, M. | 15 | Nebelung, C. | 52, 53, 60 |
| Emmerling, F. | 11 | Pedersen, K. | 27 |
| Fahmy, K. | 43 | Pollmann, K. | 39 |
| Flemming, K. | 39 | Raditzky, B. | 20 |
| Foerstendorf, H. | 25, 36, 42 | Raff, J. | 36, 39, 40, 42, 45 |
| Funke, H. | 54, 55 | Raff, T. | 39 |
| Geipel, G. | 13, 14, 15, 19, 20, 22, 24, 29, 30, 31, 46 | Reitz, T. | 41 |
| Gester, S. | 61 | Richter, A. | 49, 52 |
| Gloe, K. | 29, 30, 31, 37, 38 | Rossberg, A. | 9, 10, 12, 18 |
| Gloe, Ke. | 29, 30, 31 | Scheinost, A. C. | 9, 10, 11, 12, 54, 55 |
| Glorius, M. | 15, 18, 21, 26 | Scherschel, C. | 49 |
| Götz, C. | 24 | Schierz, A. | 56 |
| Großmann, K. | 13, 23, 44 | Schmeide, K. | 11, 16, 17, 19, 20 |
| Gründig, I. | 22 | Schreppel, K. | 37, 38 |
| Günther, A. | 17, 45 | Selenska-Pobell, S. | 43 |
| Heine, A. | 31 | Stedtner, R. | 13, 17, 22 |
| Heller, A. | 28 | Tanh Jeazet, H. B. | 29, 30, 31 |
| Henle, T. | 37, 38 | Trepte, P. | 51 |
| Hennig, C. | 9, 11, 43 | Tsushima, S. | 9, 10, 12 |
| Hofmann, S. | 44 | Veerhoff, M. | 49 |
| Ikeda, A. | 9, 11, 12, 13 | Viehweger, K. | 46 |
| Jäger, A. | 30, 31 | Vogel, M. | 40 |
| Jähnigen, P. | 60 | Vogel, Manja. | 45 |
| Jankowski, U. | 43 | Weinert, U. | 39, 40, 42 |
| Johnsson, A. | 27 | Weiß, S. | 37, 38, 57, 58 |
| Joseph, C. | 19 | Wenzel, M. | 29, 31 |
| Kataeva, O. | 30 | Wiebke, J. | 21 |
| Kirsch, R. | 54 | Wobus, A. | 44 |
| | | Zänker, H. | 37, 38, 56, 57, 58 |



Forschungszentrum Dresden - Rossendorf
Institute of Radiochemistry
P.O. Box 51 01 19 · 01314 Dresden/Germany
Phone +49 351 260-3210
Fax +49 351 260-3553
Email contact.radiochemistry@fzd.de
www.fzd.de

Member of the Leibniz Association